Theoretical and Experimental Investigation of Switch-Like Responses Arising from Multisite Protein Phosphorylation

by

Seyedeh Marjan Varedi Kolaei

A dissertation submitted in partial fulfillment
of the requirements for the degree of
Doctor of Philosophy
(Chemical Engineering)
in The University of Michigan
2011

Doctoral Committee:

Assistant Professor Xiaoxia Nina Lin, Chair
Professor Jennifer J. Linderman
Professor Sofia D. Merajver
Associate Professor Kristina I. Håkansson
Peter J. Woolf

To the Memory of My Beloved Sister

Nadereh Varedi (1973–2010)

ACKNOWLEDGEMENTS

I would first like to express my deepest gratitude to my advisor, Professor Nina Lin, for her support and guidance throughout my graduate studies. She is a great advisor and I truly appreciate her effort in providing an instructive, active, and happy environment for the research group. Her enthusiasm and dedication to high quality research have been a source of inspiration to me and I hope I have inherited these and all her other wonderful qualities.

I would like to extend my appreciation to my committee members: Professor Kristina Håkansson, Professor Jennifer Linderman, Professor Sofia Merajver, and Doctor Peter Woolf. To Professor Håkansson and her students, Hangtian Song and Wendi Hale, I say thank you for their collaboration with mass spectrometry analysis. To Professor Linderman and Professor Merajver, I express gratitude for their helpful discussions and advice. To Doctor Woolf, I offer my profound indebtedness for his wonderful ideas and comments that not only shaped the fourth chapter of this thesis, but also helped me in winning a post-doctoral fellowship.

Thanks to being a part of an active research group my knowledge on synthetic biology and biotechnology is much broader than the knowledge that I gained directly from working on my thesis. I would therefore like to thank all the members of the Lin research group: Minsheng Liu (past member), Jeremy Minty, Jihyang Park, Alissa Kerner, Marc Singer, Mike Nelson, Fengming Lin, and Yu Chen. I sincerely wish them success in their graduate studies and careers. I would also like to thank my undergraduate assistant, Elisa Cauley, for helping me with the project presented in

Chapter 5. Additionally, I would like to thank Gulari research lab members Trinh Pham, Saadet Albayrak, and Yusuf Murgha, for sharing their lab space, reagents, and equipment.

At the Department of Chemical Engineering at the University of Michigan, I have become acquainted with a number of great faculty and staff. Professor Ronald Larson, Professor Robert Ziff, and Doctor Susan Montgomery helped me far beyond their responsibilities on multiple occasions and I am so grateful to them. I would also like to thank the staff, particularly Mike Africa, Pablo Lavalle, Susan Hamlin, and Shelly Fellers for their technical and administrative assistance.

It was my pleasure to befriend many fun, bright, and supportive individuals in the Department of Chemical Engineering (Amir, Mohammad, Tanawan, Nasim, Ploy, Ida, Adam, Tom, and Geeta) and many more outside the academic environment. I can not list all their names here, but I would nonetheless like to express my feelings. I am so grateful to them for their moral support and the good times we spent together. I wish them all the best in their lives.

Finally, I would like to thank my extended family: my parents, siblings, in-laws, and husband. I would like to specially thank my precious older sister, Nadia, for her love and encouragement that have been with me always. My beloved sister, Nadereh, is tragically gone and not with me today; but I will never forget her influential role on shaping my current life and achievements. Words can not express the gratitude that I feel for my husband, Mehdi Abarham. His love, positive energy, sense of humor, and consistent support absolutely played an integral role in keeping my sanity and courage through the hard times of the last four years. I am so fortunate to have him in my life.

TABLE OF CONTENTS

LIST OF FIGURES

Figure

LIST OF TABLES

Table

LIST OF APPENDICES

Appendix

ABSTRACT

Theoretical and Experimental Investigation of Switch-Like Responses Arising from Multisite Protein Phosphorylation

by

Seyedeh Marjan Varedi Kolaei

Chair: Xiaoxia Nina Lin

Switch-like responses are important regulatory features of biological processes involving binary decisions such as cell division. Multisite protein phosphorylation is a proposed mechanism for achieving switch-like behaviors. For example, it is conjectured that the G1/S transition of the yeast cell cycle occurs in a switch-like fashion due to multisite phosphorylation-triggered degradation of the Sic1 protein. The objective of this dissertation is first to acquire a quantitative and predictive understanding of switch-like behaviors arising from multisite phosphorylation in natural systems, and second to employ this knowledge for the design of synthetic protein devices.

We first developed a mathematical model to investigate systematically the role of multisite phosphorylation in the phosphorylation-triggered degradation process of a protein like Sic1. We found that as the number of sites increases, a more switch-like temporal profile can be generated. The steepness is determined synergistically by various factors, including the total number of sites and kinetic parameters. To test our theoretical predictions, we examined the steady-state response of wild-type and mutant Sic1 with various numbers of phosphorylation sites. It was observed that

the response of Sic1, measured by its binding to a downstream protein Cdc4 in the degradation pathway, to the Cln2-Cdc28 kinase *in vitro* is switch-like. Furthermore, the ultrasensitivity decreases as the number of sites decreases.

We next showed, through computational analysis, that a multisite protein can exhibit sustainable and tunable oscillations when embedded in a negative feedback loop, formed via inhibition of the first phosphorylation step. We also designed a protein degradation device based on multiple protein binding domains and carried out preliminary study of its implementation. Our work demonstrates the potential of utilizing multisite proteins or the broader design principle of intramolecular multiple interaction modules, which provides an effective and flexible means for generating high nonlinearity, in creating a wide range of synthetic biological devices.

This dissertation suggests quantitative design principles for switch-like stimulus-response relationships arising from multisite protein phosphorylation, which might be a widespread mechanism in cellular regulation. In addition, our results provide intriguing hypotheses to be investigated experimentally in future work, such as the critical effect of multi-step phosphorylation kinetics.

CHAPTER I

Motivation and Background

"Men love to wonder, and that is the seed of science."

Ralph Waldo Emerson (1803–1882)

1.1 Summary

Cells have biochemical switches within their intracellular signaling networks to make binary decisions. Multisite phosphorylation, one of the most frequent protein modifications in living organisms, has been proposed as a mechanism for generating switch-like responses. To investigate switch-like behaviors arising from multiple phosphorylation sites, I employed a combined theoretical/experimental approach.

In this chapter, I summarize previous theoretical and experimental studies at the interface of switch-like stimulus-response relationships and multisite phosphorylation. I briefly review examples of multisite proteins involved in cell cycle regulation, previously proposed mechanisms for switch-like responses, and current methods for quantification of protein phosphorylation. I also discuss current state-of-the-art of modular protein design in synthetic biology with special attention to tandem repeats of protein interaction modules. I conclude by stating the scope of this dissertation and providing a brief summary of each chapter.

1.2 Switch-Like Responses in Biological Systems

The term "switch-like", also termed "ultrasensitive" in the steady-state domain, is applied to a system that is more sensitive to changes of stimuli in the intermediate regime than a hyperbolic (Michaelis-Menten) one [1]. Such a system filters out small stimuli and reaches to saturated level sharply (Figure 1.1). Signaling cascades with ultrasensitive stimulus-response curves convert continuous inputs to discrete outputs and thereby are crucial for the regulation of processes involving binary decisions such as cell fate decision and cell division.

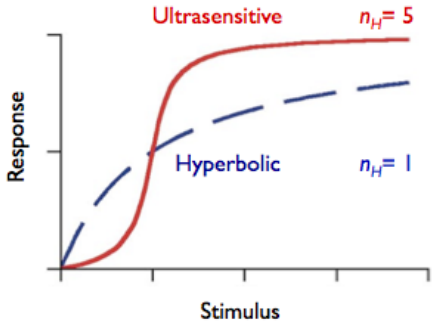

Figure 1.1: Ultrasensitive versus hyperbolic stimulus-response curve. Ultrasensitivity is quantified by Hill coefficient, n_H. The more ultrasensitive the response is, the larger n_H is in a sigmoidal stimulus-response curve.

1.2.1 Mechanisms of Ultrasensitivity

In 1903, the Danish physiologist Christian Bohr reported the sigmoidal binding curve of hemoglobin to oxygen and called it the Bohr effect [2]. The Bohr effect is caused by cooperative interactions between the four subunits of the hemoglobin tetramer: the binding of an oxygen ligand molecule to one subunit increases the affinity of other subunits for oxygen due to changes in their tertiary structure. This explanation is supported by the fact that myoglobin, a monomer with no cooperativity, does not exhibit the Bohr effect. Ligand cooperativity, also called "allostery", is one of the first and well known mechanisms for ultrasensitivity.

In 1910, Hill formulated the Hill equation to describe the sigmoidal binding of oxygen to hemoglobin, and generally cooperative ligand binding [3]. In this system, n molecules of ligand (L) bind to a receptor (R) with infinite cooperativity, $R + nL \rightleftarrows RL_n$, $\frac{Bound}{Total} = \frac{[RL_n]}{[R]+[RL_n]} = \frac{[L]^n}{K_d+[L]^n}$, where K_d is the dissociation constant. The response curve defined by the Hill equation is sigmoidal when $n > 1$, and the steepness of the curve increases as n increases. The Hill coefficient, n, is 1 for a standard hyperbolic stimulus-response curve. The Hill coefficient is 2.8 for the hemoglobin system, not 4, because the cooperativity is not infinite.

The Hill equation has been used routinely to fit sigmoidal response curves resulting from other mechanisms and the Hill coefficient, denoted by n_H, has been accepted as a standard measurement of ultrasensitivity for sigmoidal stimulus-response curves in the literature. The term "allostery" has also been extended and is defined as "the regulation of protein function, structure, and/or flexibility induced by binding of a ligand or another protein, covalent modification or mutation at a distant site" [4]. It is worthy to note that by this definition, if phosphorylation causes conformational changes in the protein, multisite phosphorylation falls in the category of allosteric effects.

Another well characterized mechanism of ultrasensitivity is enzyme saturation by substrate, which is called the "zero-order ultrasensitivity effect" [1, 5]. When a converter enzyme is saturated by its protein substrate, it operates in or near the "zero-order" region, the amount of modified substrate changes in an ultrasensitive fashion.

Other mechanisms of ultrasensitivity include positive feedback loops [6], substrate competition [7], and multi-level cascade [8–10]. Multi-level cascade can cause high sensitivity by passing of ultrasensitivity from one level to the next and the accumulation of sensitivity along the cascade. The response can be further amplified if an effector acts at more than one step in a cascade of covalent modification [11]. An

example of such systems is the mitogen-activated protein kinase (MAPK) cascade. The ultrasensitivity arises in part from the fact that MAPK requires the phosphorylation of two sites for activation [9, 12], and it increases nearly multiplicatively as the cascade is descended [10].

1.2.2 Ultrasensitivity Arising from Multisite Protein Phosphorylation

Analysis of dual phosphorylation of MAPK cascade proteins indicated for the first time that distributive phosphorylation causes the steady state proportion of doubly phosphorylated substrate to depend ultrasensitively on kinase concentration [12]. *In vitro* assays revealed that human MAPKK-1 R4F phosphorylates two sites of Xenopus p42 MAPK by a distributive mechanism rather than a processive mechanism, and thus causes p42 MAPK to exhibit a sharp, sigmoidal stimulus-response curve [13]. *In vivo* assays also demonstrated that the dual distributive phosphorylation of p42 MAPK, combined with a positive feedback loop, underlies the very ultrasensitive response of *Xenopus oocytes* to progesterone (Hill coefficient of at least 35) [14].

These results led to the emergence of the idea that more phosphorylation sites could create a more switch-like response, as proposed for substrates like cyclin-dependent kinase inhibitor Sic1 and cyclin E. Sic1 is phosphorylated on nine Ser/Thr-Pro residues by Cln-Cdc28 kinase complex in *Saccharomyces cerevisiae* [15]. This protein provides correct timing for the G1 to S transition by specifically inhibiting Clb-Cdc28 [16]. Phosphorylation of six sites is sufficient for Sic1 degradation and release of Clb-Cdc28 for DNA synthesis [17] (Figure 1.2). Nash and colleagues [17] proposed that multisite phosphorylation would lead to a switch-like degradation: Sic1 destruction will be slow at first, but as soon as phosphorylation happens on five sites, degradation increases more rapidly. Therefore, there will be a temporal threshold for Sic1 destruction. If the degradation of Sic1 is governed by a single phosphorylation site, there would have been a gradual decrease of Sic1 with increasing activity of

kinase. A similar discussion was presented by Welcker and colleagues [21] about the multisite phosphorylation of cyclin E by Cdk2 and GSK3. At least four phosphorylation sites contribute to phosphorylation-triggered degradation of Cyclin E. However, no experiments have been conducted on Sic1 or cyclin E to verify the ultrasensitivity of the response to the corresponding kinases.

Figure 1.2: The role of Sic1 in the cell cycle. At G1 phase, Sic1 binds to Clb-Cdc28 that is necessary for entering S phase. With increasing Cln1/2-Cdc28 activity, Sic1 becomes phosphorylated and releases Clb-Cdc28, hence the cell enters into the S phase. Phosphorylated Sic1 is specifically recognized by SCF^{Cdc4} ubiquitin ligase and undergoes ubiquitination and eventually degradation [18–20]. Picture from Tyers Lab (http://www.mshri.on.ca/tyers).

Salazar and Hofer [22] examined the NFAT transcription factor (with at least 13 serine residues) which is activated through dephosphorylation by the phosphatase calcineurin. The main NFAT members, NFAT1-4, reside in the cytoplasm in a phosphorylated (inactive) form and are imported into the nucleus after dephosphorylation by calcineurin (activation). Mathematical analysis showed that multiple phosphorylation sites result in a threshold for protein activation. The sharpness of the threshold increases with the number of phosphorylation sites, and thus NFAT proteins can exhibit a switch-like response to calcineurin activity.

Gunawardena [23] accentuated the distinction of thresholding from switching. He considered a hypothetical protein with an arbitrary number of sites which become phosphorylated in an ordered distributive manner. The input is the ratio of kinase

concentration over the phosphatase concentration, and the output is the fraction of fully phosphorylated protein. He argued that this system exhibits good thresholding feature but not necessarily good switching. Specifically, the fraction of fully phosphorylated substrate does not change appreciably when the ratio of kinase to phosphatase activity is below a certain threshold (strong buffering at relatively low levels of input), and this threshold becomes more strict as the number of sites increases. However, above this threshold, the fraction of fully phosphorylated substrate changes only gradually in response to the ratio of kinase to phosphatase activity (weak buffering effect at relatively high levels of input).

More recently, Lin and colleagues [24] extended Gunawardena's study and demonstrated under what conditions multisite phosphorylation can be a good switch. Their model is based on distributive phosphorylation and dephosphorylation. However, the substrate with n phosphorylation sites becomes functional when m sites become phosphorylated and m can be any number from 1 to n. The input is again the ratio of the kinase concentration over the phosphatase concentration, but the output is the fraction of functional proteins. The resulted stimulus-response curve is the most sigmoidal (i.e. switch-like) when $m \sim \frac{n}{2}$ and this characteristic is more significant for large values of n (Figure 1.3). The effects of various factors, the kinetics parameters of the phosphorylation/dephosphorylation reactions, the changes of "activity"of the substrate along the phosphorylation reactions, and the order of phosphorylation on ultrasensitivity were also examined.

In many regulatory systems, multisite phosphorylation regulates dynamic processes. For example, Sic1 degrades when multiple sites become phosphorylated. However, none of the previous theoretical work has examined the role of multisite phosphorylation in temporal responses. Hence, we proposed to employ systematic modeling to investigate switch-like temporal responses, where elimination of the substrate protein is triggered by multisite phosphorylation (Chapter 2). The number of

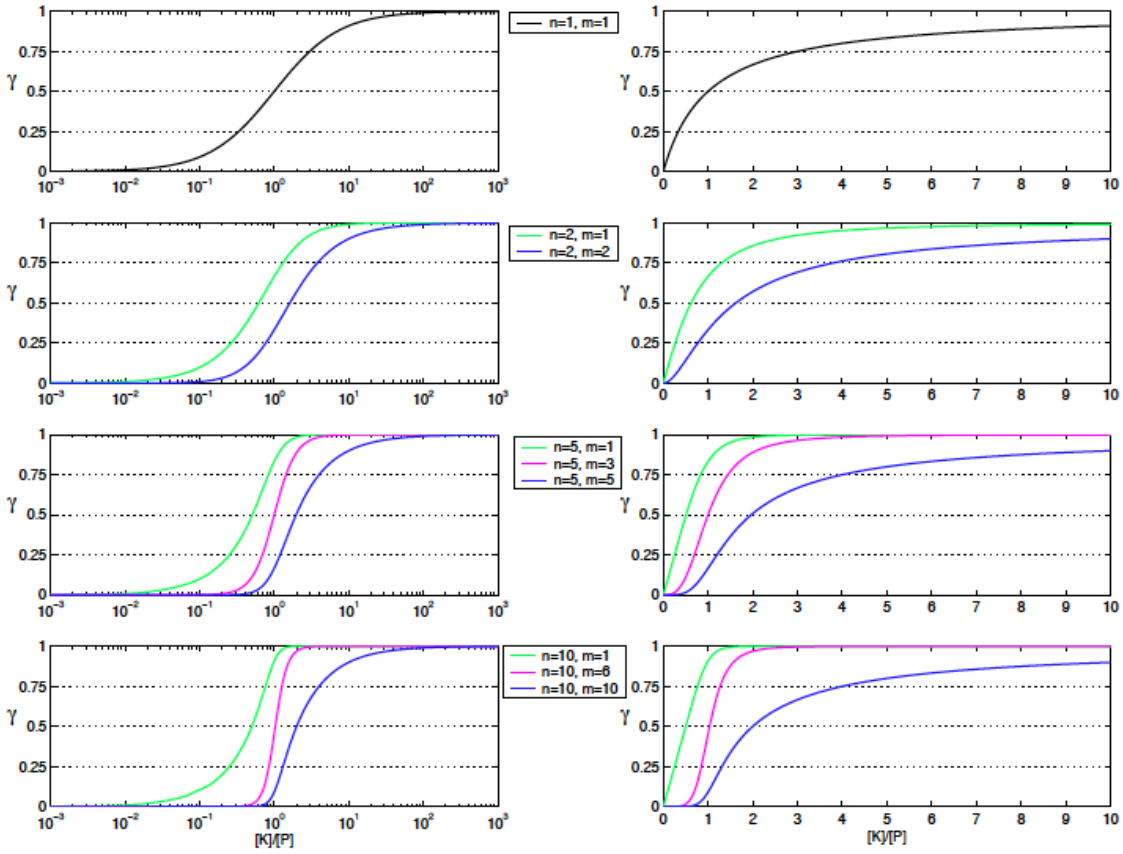

Figure 1.3: Steady-state stimulus-response curve. Substrate protein S has n phosphorylation sites and becomes "functional" when more than m sites are phosphorylated. γ represents the fraction of functional protein. The input is the ratio of the kinase concentration over the phosphatase concentration ([K]/[P]) [24].

phosphorylation sites, phosphorylation ordering, temporal profiles of the kinase have been investigated as well.

On the experiment side, we aimed to closely examine the steady-state response of the wild-type Sic1 protein and mutants with a varying number of phosphosites (Chapter 3). Protein Sic1 has been chosen because Sic1 is a relatively well-studied protein and yeast is a simple organism compared to other eukaryotes. Furthermore, Sic1 as a cyclin-dependent kinase inhibitor plays an important role in the cell cycle regulation which is well conserved in all eukaryotes. A particularly fascinating example of proteins evolutionarily related to Sic1 is its functional homolog in mammalian

cells, p27 [25–27]. The misfunction of p27 has been observed in a number of human tumor types [28]. Reduced nuclear p27 is observed in up to 60% of primary human breast cancers, which has been correlated with increased activity of the Src kinase family which phosphorylates p27 [29]. Despite this protein's biological significance, little is known regarding its phosphorylation sites and potential ultrasensitivity property. Fundamental insights obtained from the Sic1 phosphorylation system might be possible to apply to other multisite proteins and have important implications for the treatment of related diseases and for designing anti-cancer drugs.

1.2.3 Analytical Methods for Quantification of Multisite Phosphorylation

In order to test the theoretical predictions discussed above, it is essential to identify and quantify phosphorylation states of the substrate protein. Current methods for the detection of phosphorylation can be categorized into radioactive-based and radioactive-free strategies.

Protein phosphorylation is usually studied by labeling with ^{32}P-labeled inorganic phosphate [30, 31]. Although this technique is very simple and sensitive, particularly for high-throughput proteomic analysis, it suffers from two drawbacks. The main problem is the danger of radioactive exposure and safety issues involved. Secondly, this technique might not always be suitable for *in vivo* studies due to several reasons: (i) Incorporation of radioactive phosphorus isotopes into proteins *in vivo* might be very inefficient due to the presence of the endogenous unlabeled ATP, (ii) The rate of ^{32}P- incorporation into proteins depends heavily on the rate of turnover of phosphate in the protein, (iii) High levels of radioactive phosphate incorporation may cause cellular damage and alteration of phosphorylation states.

Alternative non-radioactive strategies are based on antibodies, electrophoresis, and some mass spectrometry methods. Once the amino acid sequence around a phosphorylation site has been determined, it is possible to make antibodies against

synthetic phosphopeptides modeled on these phosphorylation sites [32]. Such anti-phosphopeptide antibodies are very useful tools for monitoring the phosphorylation of the protein at specific sites. However, it is very difficult to generate antibodies specific to all sites, particularly when the substrate protein like Sic1 has multiple phosphorylation sites. Moreover, it can not be used as a high-throughput method.

Each phosphate group is 80 Da and carries negative charge. Thereby, phosphorylation alters the mobility of a protein during polyacrylamide gel electrophoresis and decreases its isoelectric point. The presence of phosphorylated residues in an unlabeled protein can be deduced from altered gel mobility. However, no information on which sites are phosphorylated can be deduced and the resolution is not high. We have checked the activity of our kinase and phosphatase sources on Sic1 by monitoring the band shift on the SDS polyacrylamide gel.

Mass spectrometry is another method that has become widely used in the identification and quantification of protein phosphorylation. This method is based on the measurement of mass-to-charge (m/z) ratios and can be used for fast, sensitive and high-throughput measurements. Several specific approaches have been developed.

The most common one is based on labeling proteins or peptides with different isotopes by chemical or metabolic means [33, 34]. In this approach, the sample is split, both halves are differentially isotopically labeled, and one of the samples might be dephosphorylated chemically or enzymatically before pooling of the two fractions and MS analysis. The degree of phosphorylation can then be determined by comparison of the signal intensity of the two differentially labeled unphosphorylated species, assuming that the increase in signal intensity of one species is due to dephosphorylation [35–37].

Recently, a stable isotope-free MS approach for relative and absolute quantification of protein phosphorylation stoichiometry was reported [38]. The proposed approach is based on the assumption that the ion currents of a particular phosphopeptide

and its unmodified cognate are correlated. Thereby, by monitoring the normalized ion currents absolute concentration of phosphopeptides will be measured. We are collaborating with Dr. Kristina Håkansson's lab in the Chemistry Department of the University of Michigan to develop MS methods for analyzing Sic1 phosphorylation. Initial exploration of the above approach was not successful. Nevertheless, we have developed and are applying new MS assays that suit our specific needs for the study of Sic1 (Chapter 6).

1.3 Protein-Based Synthetic Devices

The field of synthetic biology is currently dominated by manipulation of gene regulatory networks [39–41]. Nevertheless, regulation at the protein level is often faster, more precise, and more efficient for the cell compared to regulation at the transcription level. Analysis of natural proteins often employ the approach of decomposition into multiple domains. Fusing proteins with various tags have been extensively used for various purposes such as purification or fluorescence imaging [42]. In recent years, it has become more and more common to recombine regulatory and catalytic domains of multiple proteins to build synthetic proteins with novel functions for reprogramming signaling networks or constructing synthetic devices [43–45].

1.3.1 Recombination of Protein Domains

A domain is defined as an evolutionarily and structurally separable unit within a protein [45]. A domain in isolation may not be folded into its natural structure, and furthermore folding of one domain may prevent correct folding of other domain(s) in a synthetic protein [43]. In contrast, a module is defined as a functionally minimal unit that is transferable from one protein context to another and hence are frequently used in biological devices [46].

A "device" is a collection of one or more building blocks that operate together

and exhibit a defined function [47]. A biological device consists of an input module, an output module, and a mechanism through which the changes in the input module are translated to changes in the output function. The input and output functions can be part of a single protein domain or separate domains, fused end-to-end in a single protein or multiple proteins. The construction of a hybrid protein or device starts with *de novo* design, exploring existing parts (motifs, domains, modules), or a combination of the above, and is implemented through efficient DNA exchange and assembly [42].

Due to the difficulty in predicting protein folding, stability, and dynamics, synthetic biologists tend to work with well-behaved and characterized parts. Examples of commonly used parts are Src homology 2 (SH2) and 3 (SH3) domains [48–50]. The domains are usually connected through glycine-based peptides long enough to allow the required configurations and interactions [51].

Small molecules have often been used as the input to a synthetic device. For instance, rapamycin, a natural dimerizing molecule, has been shown to bind with high affinity to the protein Fpr1, and this complex in turn binds to Tor1 [52]. Rapamycin has been used commonly in synthetic devices to heterodimerize two proteins of interest for inactivation, translocation, or changing the stability of a cellular protein [53–55].

An example of such synthetic devices was constructed for protein degradation by George Church's lab at Harvard Medical School. Janse and colleagues [56] fused the Rpn10 subunit of *S. cerevisiae*'s 26S proteasome with Fpr1 tag, and a target protein His3 with the ligand-binding domain of Tor (Figure 1.4). Addition of rapamycin to the cell culture medium leads to association of Fpr1 and Tor, and thus localization of Tor-His3 to the proteasome and thereby its destruction. Tor-His3 degrades with a half-life of about 20 min.

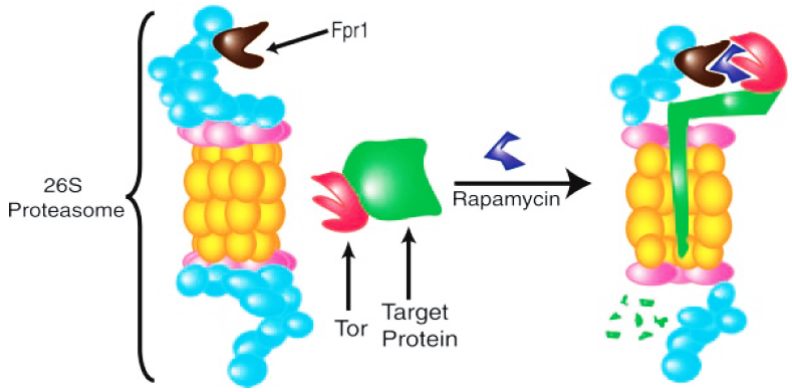

Figure 1.4: Design and fusion constructs for artificial localization of a target protein to proteasome. One part of the heterodimerizing pair (Fpr1) is fused to a proteasome subunit. The other part (Tor) is fused to a target protein. Dimerization of the two parts occurs upon addition of the small molecule rapamycin. This strategy localize the target protein to the proteasome upon introduction of rapamycin [56].

1.3.2 Repeats of Interaction Modules

In principle, multiple regulatory domains can potentially lead to ultrasensitive interactions if binding of one input ligand enhances the binding of subsequent ligands [57]. This is analogous to the mechanism underlying classical cooperative switches such as hemoglobin as described earlier in this chapter. As the number of interacting modules increases, the response to increasing concentration of ligands becomes more ultrasensitive.

An interesting example of ultrasensitive protein devices based on this concept was reported by Wandell Lim's lab at the University of California San Francisco. Dueber and colleagues [57] designed and built a modular protein switch by recombining the catalytic domain of the actin regulatory protein N-WASP and the autoinhibitory SH3 interaction module. In absence of SH3-binding peptide, the activity of the N-WASP catalytic output domain is inhibited due to interaction with the heterologous autoinhibitory SH3 domain. An exogenous SH3-binding peptide (stimulus) binds to SH3 domains, removes the inhibitory effect and activates the catalytic activity of N-WASP (response).

Through a combination of modeling and systematically varying the number and strength of the autoinhibitory interactions, Dueber and colleagues [57] demonstrated that ultrasensitivity is dramatically altered by the number of autoinhibitory interactions, even with no inter-domain cooperativity. A single SH3 module yielded a protein that was activated in a linear fashion by SH3-binding peptide. Increasing the number of SH3 domains increased ultrasensitivity, and the most ultrasensitive response (n_H of 3.9) was achieved by using five identical SH3 domains. Furthermore, they showed that changes in individual affinities largely affect the EC50 but not the overall shape of the input/output transfer function.

Inspired by this work, we decided to improve the performance of the protein degradation device previously developed in the Church lab [56] by adding extra binding domains (Chapter 5). We expected to see faster degradation by increasing the number of Tor domains fused to the target protein.

1.4 Dissertation Overview

The objective of this thesis is first to obtain fundamental knowledge of switch-like responses arising from multisite phosphorylation in natural systems; and second to employ this knowledge for design of synthetic biological switches. The organization of the dissertation is as follows:

In Chapter 2, phosphorylation-triggered protein degradation, a common regulatory mechanism in signaling processes, was modeled and systematically analyzed. The model closely examined the role of multisite phosphorylation in affecting the shape and particularly the sharpness of the temporal profile of the substrate protein.

In Chapter 3, we examined the response of a model protein Sic1 to the increasing activity of the kinase. We observed ultrasensitive steady-state responses and dissected the role of multiple phosphorylation sites through analysis of various Sic1 mutants. Experimental results were combined with modeling, which led to new predictions of

characteristics of the Sic1 phosphorylation system.

In Chapter 4, we discussed the application of multisite phosphorylation in the design of protein-based oscillators. We showed theoretically how oscillatory behavior can be generated in a broader space of parameters by increasing the number of phosphorylation sites.

In Chapter 5, we studied ligand-induced protein degradation in a synthetic degradation device. The effect of multiple protein binding domains was explored with a target protein in *S. cerevisiae*.

Finally, in Chapter 6, the major conclusions derived from this thesis and our contributions to the field are stated. Possible areas for future investigation are discussed as well.

CHAPTER II

Theoretical Investigation of Multisite Phosphorylation-Triggered Degradation

2.1 Summary

Phosphorylation-triggered degradation is a common strategy for elimination of regulatory proteins in many important cell signaling processes. Interesting examples include cyclin-dependent kinase inhibitors such as p27 in human and Sic1 in yeast, which play crucial roles during the G1/S transition in the cell cycle. In this work, we have modeled and analyzed the dynamics of multisite-phosphorylation-triggered protein degradation. Inspired by experimental observations on the Sic1 protein and a previous intriguing theoretical conjecture, we develop a model to examine in detail the degradation dynamics of a protein featuring multiple phosphorylation sites and a threshold site number for elimination in response to a kinase signal. Our model explains the role of multiple phosphorylation sites, compared to a single site, in the regulation of protein degradation. A single-site protein cannot convert a graded input of kinase increase to much sharper output; whereas multisite phosphorylation is capable of generating a highly switch-like temporal profile of the substrate protein with two characteristics: a temporal threshold; and rapid decrease beyond the threshold. We introduce a measure termed temporal response coefficient to quantify the extent

to which a response in the time domain is switch-like and further investigate how this property is determined by various factors including the kinase input, the total number of sites, the threshold site number for elimination, the order of phosphorylation, the kinetic parameters, and site preference. Some interesting and experimentally verifiable predictions include that the non-degradable fraction of the substrate protein exhibits a more switch-like temporal profile; a sequential system is more switch-like, while a random system has the advantage of increased robustness; all the parameters, including the total number of sites, the threshold site number for elimination, and the kinetic parameters synergistically determine the extent to which the degradation profile is switch-like. Our results suggest design principles for protein degradation switches which might be a widespread mechanism for precise regulation of cellular processes such as cell cycle progression.

2.2 Introduction

One third of all proteins in eukaryotic cells are phosphorylated at any time [58]. Phosphorylation profile has been interpreted as a "molecular barcode" [59] to direct protein for other processes such as activation, inactivation, translocation, and degradation. In particular, three major transitions in the cell cycle, namely, entry into the S phase, separation of sister chromatids, and exit from mitosis, involve degradation of certain proteins after phosphorylation-dependent ubiquitination [60–62]. Phosphorylation-driven ubiquitination through the SCF pathway and subsequent proteasomal degradation have been considered as a biochemical switch crucial for coordinating phase changes during the cell cycle [63, 64]. For instance, the ubiquitination and degradation of Sic1, a cyclin-dependent kinase inhibitor in yeast, and its functional homolog in mammalian cells, p27, are triggered by phosphorylation [15, 17, 25, 26]. Degradation of Sic1 and p27 leads to the release of cyclins required for DNA synthesis in the S phase. Reduced nuclear p27 is observed in up

to 60% of primary human breast cancers, which has been correlated with increased activity of the Src kinase family [29].

The number of phosphorylation sites observed in one protein can vary from 1 to over 100 [65]. It has become increasingly apparent that multisite phosphorylation is a widespread phenomenon among regulatory proteins in eukaryotic cells. Multisite protein phosphorylation potentially provides a precise tool for dynamic regulation of the downstream process. Different phosphorylation profiles of a single protein might be linked to different functions.

For example, the retinoblastoma protein (Rb) has 16 Ser/Thr-Pro phosphorylation sites and interacts with different proteins during various cell cycle phases depending upon its phosphorylation profile [66, 67]. Most notably, in early G1, Rb is hypophosphorylated and sequesters the E2F family of transcription factors, thereby preventing the transcription of genes required for S-phase entry; while in late G1, Rb becomes hyperphosphorylated and thus inactive in repressing G1/S transition [68].

As another example, two sites in *Xenopus* protein Wee1A are responsible for the mitotic inactivation of this protein, while at least two others regulate its proteolysis during interphase [69]. Intriguingly, as far as protein stability is concerned, an alternative property of multisite phosphorylation, the degree of phosphorylation (i.e. the number of phosphate groups on a protein), instead of the exact pattern, might determine the protein's fate.

A well-studied example is protein Sic1, which plays a key role in regulating the G1/S transition in the cell cycle of *Saccharomyces cerevisiae*. Sic1 inhibits Clb5,6-Cdc28 kinase required for DNA replication and is believed to provide precise timing for the G1 to S transition by undergoing switch-like proteasome-mediated degradation upon phosphorylation by the Cln2-Cdc28 kinase complex. Yeast strains lacking Sic1 initiate DNA replication earlier and show extended S phase [70, 71]. On the other hand, in mutant strains that are resistant to Sic1 degradation, cells experience

lengthened G1 phase in an otherwise wild-type genetic background [72] or G1 phase arrest in more complex situations [18]. Sic1 is phosphorylated by the Cln2-Cdc28 kinase complex on nine Ser/Thr-Pro residues [15]. Nash *et al.* [17] investigated how multisite phosphorylation of Sic 1 regulates its ubiquitination and degradation. They began with the Sic1 mutant which lacks all the nine phosphorylation sites and restored the sites one by one in the order of their importance measured by the degree to which elimination of a single site affects the Sic1 turnover. Serial reintroduction of five sites failed to reestablish Sic1 binding to Cdc4, a subunit in the ubiquitin ligase SCF^{Cdc4} that determines the target specificity, or cell viability. Astonishingly, readdition of a sixth seemingly insignificant site abruptly restored Sic1's binding with Cdc4 *in vitro* and revived the cells *in vivo*. These experiments clearly revealed that there is a threshold number of phosphorylated sites required to render binding of Sic1 with Cdc4. The "counting" mechanism underlying this multisite-dependent digital interaction between phosphorylated Sic1 and Cdc4 has been studied both theoretically and experimentally. Mathematical modeling suggested that cooperative interactions between a disordered multi-phosphorylated Sic1 and a single-site receptor Cdc4 can explain the observed phosphorylation threshold [73]. Furthermore, cumulative electrostatic forces resulted from negatively charged phosphate groups were proposed as the physical basis for the digital interaction between Sic1 and Cdc4 [74]. Recently, NMR analysis showed that Sic1 indeed exists in an intrinsically disordered state and its multiple phosphorylated sites interact with the single receptor site of Cdc4 in dynamic equilibrium [75, 76].

Upon their remarkable discovery that Sic1 requires at least six sites phosphorylated to bind to Cdc4 for subsequent ubiquitination and degradation, Nash *et al.* hypothesized that this phosphorylation threshold eventually causes Sic1 to degrade in a switch-like manner during the G1/S transition [17]. Reviewing the above seminal work, Deshaies and Ferrell conjectured more specifically that multisite phosphory-

lation can create temporal thresholds [20]. They calculated time courses for Sic1 destruction in three scenarios: Sic1 destruction triggered by one fast, one slow, or six fast phosphorylations. It was suggested that when six distributive and equivalent phosphorylations are required, Sic1 destruction is initially very slow when the first five sites are getting phosphorylated, then after a lag period, degradation dramatically speeds up. In another word, a temporal threshold is created for Sic1 destruction from the onset of Cln-CDK activation. Alternatively, if the degradation of Sic1 is governed by a single phosphorylation, there would have been a gradual decrease of Sic1 amount without time delay. The modeling framework presented by Deshaies and Ferrell in this review, albeit primitive, represents a very intriguing idea aiming to make the key connection between Sic1's observed phosphorylation threshold number to its ultimate function of regulating the G1/S transition. However, there remained several caveats. First, six phosphorylations were considered, while Sic1 has a total of nine sites. Do the remaining sites play any role? Second, it can be anticipated that exactly how the kinase is activated, i.e. the temporal profile of the kinase signal, affects the degradation of the substrate protein, and this aspect was not discussed. Finally, it was not clear what determined quantitatively the temporal threshold and speed of degradation. In this work, we will attempt to address the above issues, by carrying out systematic and detailed mathematical modeling to examine how multisite phosphorylation might lead to switch-like protein degradation.

Switch-like behaviors have been studied extensively in the steady state domain, where the response of a biological system (e.g. the amount of oxygen bound by the hemoglobin protein in response to the change of oxygen concentration) exhibits the very intriguing property of buffering fluctuations in the stimulus below a threshold and amplifying drastically the change of stimulus above the threshold. This type of switch-like response in the steady state domain has been termed "ultrasensitivity" in the literature and a number of mechanisms have been proposed to account

for its sources, including ligand cooperativity [3], multi-step effect [8, 11, 77], enzyme saturation (i.e. zero-order ultrasensitivity) [1, 78], positive feedback [79–82], multi-level cascade [10, 13, 83], multisite phosphorylation [17, 22, 23, 78, 84–86], and substrate competition [7]. These studies have generated important insights concerning steady-state responses, which often correspond to *in vitro* experimental assays, on how switch-like behaviors arise. Nevertheless, what is crucial for many systems, particularly *in vivo* processes, is the transient stimulus-response curve such as the temporal profile of Sic1 during the G1/S transition, whereas switch-like responses in the temporal domain have been investigated very limitedly. It should be noted that the cell cycle signaling network in yeast has been examined very extensively through mathematical modeling [87–90]; however, degradation of macromolecules such as Sic1 has been modeled with a single phosphorylation reaction without taking into account the multiple phosphorylation steps.

Lin and colleagues [24] showed that multisite phosphorylation is a potential source of switch-like steady-state responses; most importantly, a large number of total sites combined with an intermediate threshold number of sites for changing substrate functionality account for the switch-like behavior. Here, extending our previous studies, we investigate switch-like responses in the time domain when protein stability depends on the degree of phosphorylation. We will present a model to analyze phosphorylation-triggered elimination of the substrate protein in response to the rise of kinase activity. We will show quantitatively how different parameters affect the protein elimination dynamics when degradation occurs above a threshold number of phosphorylations. In particular, we will explore how the extent to which the degradation dynamics is switch-like is affected by the type of kinase stimuli, the number of phosphorylation sites, the order of phosphorylation reactions, and kinetic parameters. We have developed the model mainly based on the Sic1 system to reveal the role of its existing multiple sites in regulating the protein's switch-like destruction during

the G1/S transition. However, multisite phosphorylation is potentially a widespread source of switch-like protein degradation and the design principles revealed by our model might be applicable to many other multisite regulatory proteins.

2.3 Methods

Systems of ordinary differential equations (described in the following section) were formulated and solved with MATLAB 7.1. The codes are available at our website http://www.engin.umich.edu/dept/che/research/lin/downloads.html.

The events integrated in k_i include: binding of ATP and phosphospecies i to the kinase, dissociation of phosphospecies i from the kinase, the chemical reaction of phosphorylation and dissociation of the product from the kinase. The events integrated in k_i^{-1} include: binding of ADP and phosphospecies i to the phosphatase, dissociation of phosphospecies i from the phosphatase, the chemical reaction of dephosphorylation and dissociation of the product from the phosphatase. k_i^d includes all events after phosphorylation to proteolysis. The ODE system is non-dimensionalized as described in Appendix A and an unitless time unit is used through this chapter.

2.4 Results

2.4.1 Model Description

Figure 2.1A illustrates the phosphorylation-dephosphorylation-degradation reaction network of a hypothetical protein with n phosphorylation sites. We consider a single kinase and a single phosphatase acting on the substrate. We assume that each phosphorylation or dephosphorylation reaction involves an independent collision between the enzyme and the substrate; i.e., reactions proceed distributively. The number of distinguishable phosphorylated species depends on the order of the phosphorylation and dephosphorylation reactions. Due to the lack of data in multi-step

phosphorylation/dephosphorylation kinetics, currently, it is not clear whether there are specific major patterns across different systems. Therefore, in this chapter, we consider the most general case in which the reactions happen in a random manner. In another word, any unphosphorylated (or phosphorylated) site can be phosphorylated (or dephosphorylated) at any time regardless of the states of other sites. Existing data on half-lives of Sic1 mutants suggested that phosphorylation on most of this protein's sites (eight out of nine) might be largely random. We term such a system a random one, in which there are 2^n differently phosphorylated species and there exist $n!$ distinct pathways to move from the completely unphosphorylated state to the fully phosphorylated one. An important special case arises when the kinase/phosphatase chooses a specific site with 100% bias over the other sites at any time. In this case, the phosphorylation/dephosphorylation reactions proceed in an entirely ordered manner, as shown in Figure 2.1B. There are evidences that certain proteins undergo phosphorylation in such a sequential manner. For instance, β-catenin, a cadherin associated protein in *Mammalia*, is phosphorylated by kinase Gsk3 on three sites sequentially during the G2/M-G1 transition [91]. Such systems are termed sequential here, which simplifies into $n+1$ differently phosphorylated species and a single straight-line pathway from the unphosphorylated state to the fully phosphorylated one.

During proteolysis, once a substrate protein is phosphorylated properly, it is then ubiquitinated by a constitutively active SCF ubiquitin ligase [63] and thereafter degraded by the proteasome. In this work, for simplicity we modeled the degradation as a single elimination reaction. As mentioned previously, the protein Sic1 undergoes ubiquitination and proteolysis if it is phosphorylated on at least six sites [17]. In our model, we introduced a second parameter, m, and generalized that once m or more sites are phosphorylated, the substrate protein is recognized by the SCF complex and goes through degradation.

Our interest is to investigate the temporal change of the substrate protein as

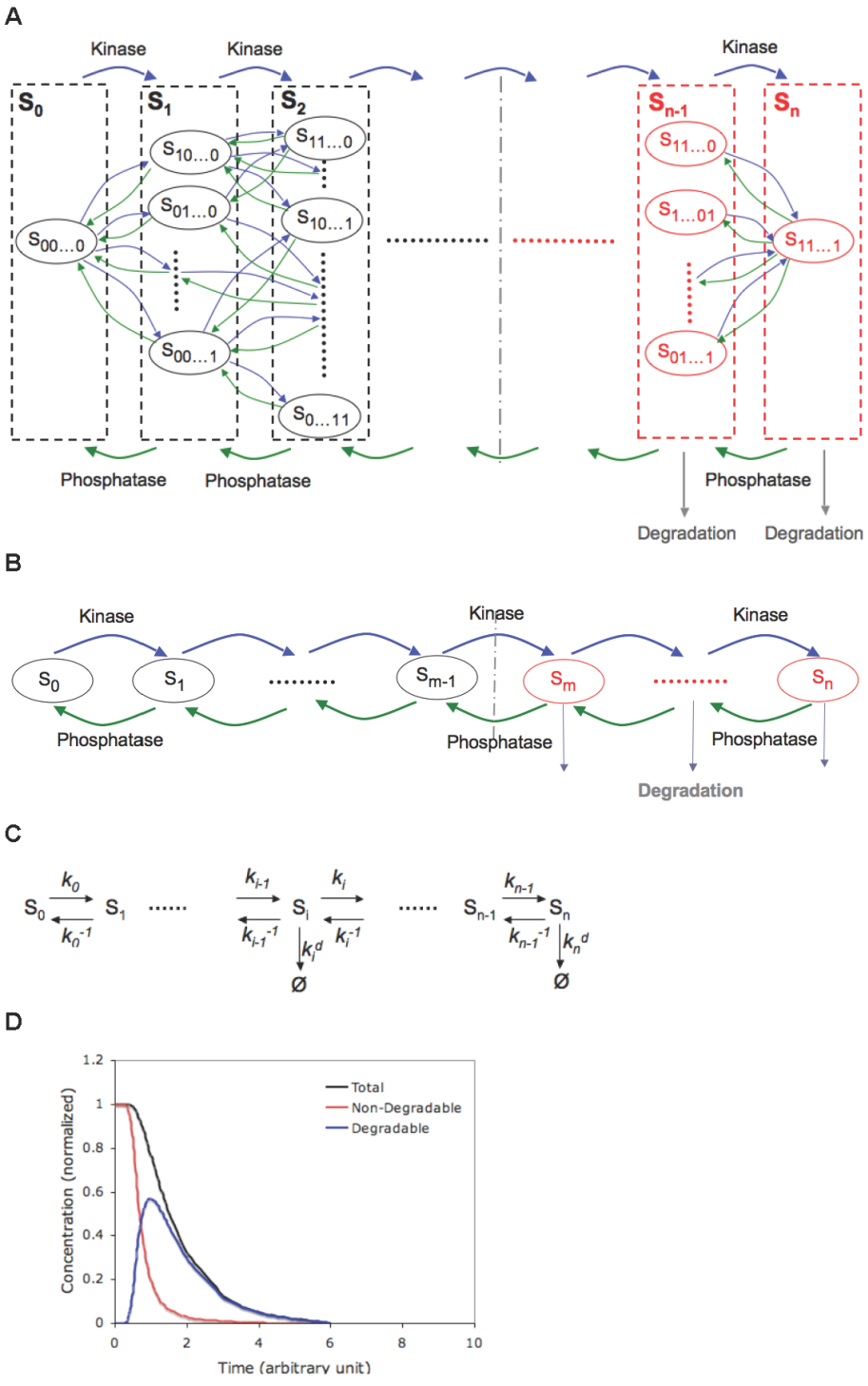

Figure 2.1: Phosphorylation-triggered degradation of a multisite protein. The kinase and phosphatase act on an n-site protein randomly (A) or sequentially (B). The protein becomes degradable (highlighted in red) if m or more sites are phosphorylated. (C) Kinetic parameters for sequential system: k_i, k_i^{-1} and k_i^d stand for kinetic rate constants of phosphorylation, dephosphorylation and degradation, respectively. $k_i^d = 0$ for $i = 0, ..., m-1$ and $k_i^d > 0$ for $i = m, ..., n$. (D) The output of the model is shown for a random system: $n = 9$, $m = 6$, $k = 10$, $k^{-1} = 10$, $k_i^d = 1$ for $i = 6 - 9$, $[pho] = 1$, $[kin] = 5\frac{t^2}{1+t^2}$.

the kinase level increases converting the substrate to degradable forms and causing it to be eliminated from the system. An ordinary differential equation (ODE) based approach was employed to examine this dynamic process. According to the Michaelis-Menten formalism for enzymatic reactions, the substrate reacts with the kinase to form a substrate-kinase complex that can in turn dissociate to form either the enzyme and substrate, or the enzyme and a product which has one more site phosphorylated. Similarly, the phosphorylated protein and the phosphatase react to form the substrate-phosphatase complex, which dissociates to form either the phosphatase and phosphorylated protein or the phosphatase and a product that has one less site phosphorylated. A complete mechanistic model with these elementary steps would consist of $3 \times 2^n - 2$ ODEs for all the substrate related species in the random system described above. It is possible, fortunately, to make substantial simplifications when i) the concentrations of both enzymes are much lower than the initial concentration of the substrate protein, or ii) the enzyme-substrate association and dissociation rate constants are much larger than the catalysis rate constants. The first condition holds readily for *in vitro* experiments. For *in vivo* systems, we do not know to what extent these two conditions would cover all circumstances, because of scarce kinetic information of multi-step phosphorylation/dephosphorylation reactions. Nevertheless, considering what is generally believed with regard to the rate-limiting step in enzymatic reactions, we believe that either of these conditions can be satisfied for a wide range of systems. Hence the model presented here potentially represents a phosphorylation-triggered degradation process that captures common features of many multisite proteins. Under the aforementioned two conditions, the enzyme-substrate complexes evolve in a much faster time scale compared with the free substrates and can be assumed to operate at quasi steady states. Consequently, they can be neglected in the model and the governing ODEs reduce to simplified forms as described below.

With the assumption that ATP is abundant, the concentration of each specific substrate state with a unique combination of phosphorylated and nonphosphorylated sites (termed phospho-state in this work) depends on the concentration of other phospho-states that are upstream or downstream in the phosphorylation-dephosphorylation network, the concentration of the kinase and phosphatase, as well as the kinetic parameters. For easiness of understanding, we illustrate first the equations for a sequential system which involves $n+1$ phospho-states in a straight-line pathway (see Figure 2.1B for reaction scheme and Figure 2.1C for kinetic parameter notations).

First phospho-state:

$$\frac{d[S_0]}{dt} = k_0^{-1}[pho][S_1] - k_0[kin][S_0] - k_0^d[S_0] \tag{2.1a}$$

Intermediate phospho-states: $i = 1, ..., n-1$

$$\frac{d[S_i]}{dt} = k_{i-1}[kin][S_{i-1}] + k_i^{-1}[pho][S_{i+1}] - k_i[kin][S_i] - k_{i-1}^{-1}[pho][S_i] - k_i^d[S_i] \tag{2.1b}$$

Last phospho-state:

$$\frac{d[S_n]}{dt} = k_{n-1}[kin][S_{n-1}] - k_{n-1}^{-1}[pho][S_n] - k_n^d[S_n] \tag{2.1c}$$

where k_i, k_i^{-1} and k_i^d stand for kinetic rate constants of phosphorylation, dephosphorylation and degradation, respectively. $[kin]$, $[pho]$ and $[S_i]$ represent the concentration of the kinase, phosphatase and substrate state with i phosphorylated sites, respectively. It should be noted that first-order kinetics is used to describe the aggregated degradation reaction; $k_i^d = 0$ for $i = 0, ..., m-1$ and $k_i^d > 0$ for $i = m, ..., n$. In this work, we further assume that k_i^d is the same for all phospho-states with m or more sites phosphorylated.

For a random system, there are 2^n dependent variables representing concentrations of all the possible phospho-states. Each of them is determined by up-

stream/downstream reactions that produce/consume it, which can be mathematically described in a similar manner as in Eq. (2.1b) for the sequential system:

$$\frac{d[S_x]}{dt} = \sum_{S_y \in U_x} k_{yx}[kin][S_y] + \sum_{S_y \in D_x} k_{yx}^{-1}[pho][S_y] - \sum_{S_y \in D_x} k_{xy}[kin][S_x] - \sum_{S_y \in U_x} k_{xy}^{-1}[pho][S_x] - k_x^d[S_x] \tag{2.2}$$

where S_x is any phospho-state in the phosphorylation-dephosphorylation-degradation network shown in Figure 2.1A; U_x and D_x represent all the phospho-states upstream and downstream of S_x, respectively. For example, for S_{10100}, the set of upstream phospho-states with one less site phosphorylated $U_{10100} = \{S_{00100}, S_{10000}\}$ and the set of downstream phospho-states with one more site phosphorylated $D_{10100} = \{S_{11100}, S_{10110}, S_{10101}\}$. k_{xy} denotes the rate constant of the phosphorylation reaction converting S_x to S_y; while k_{xy}^{-1} is that for the dephosphorylation reaction converting S_x to S_y. k_x^d represent the degradation rate constant for S_x. Despite exhibiting a seemingly more complicated form, Eq. (2.2) is structurally identical to Eq. (2.1b) and describes five types of reaction determining the change of each phospho-state: the first two positive terms represent increases due to phosphorylation of upstream phospho-state(s) and dephosphorylation of downstream phospho-state(s); the next two negative terms represent decreases due to phosphorylation to downstream phospho-state(s) and dephosphorylation to upstream phospho-state(s); the last negative term depicts degradation.

To simulate phosphorylation-triggered proteolysis, we assume that a basal activity of the phosphatase is always present in the system and the substrate exists in the unphosphorylated state initially. The kinase is then introduced into the system and increases gradually (detailed discussions will follow in the next section), converting the substrate to more and more phosphorylated states. As the substrate becomes sufficiently phosphorylated (i.e. on at least m of the n sites), it is eliminated through the

degradation reaction, which causes the overall amount of the substrate to decreases continuously as proteolysis occurs. Figure 2.1D illustrates a typical simulation result, where the total, degradable and non-degradable amounts of the substrate are depicted.

Inspired by a previous conjecture that multisite phosphorylation enables temporal thresholds [20], we hypothesize that precise timing of concentration decreases is crucial for certain proteins such as those regulating cell cycle transitions. Accordingly, our main interest in this work centers on the shape of the response curve representing concentration changes of the substrate. By applying standard non-dimensionalization techniques (Appendix A), we can reduce all the parameters to two sets, specifically $\frac{k_i}{k^d}[kin]$ and $\frac{k_i^{-1}}{k^d}[pho]$, where k^d is the rate constant for the degradable states. Subsequently, we focus on examining the normalized concentrations of the substrate versus dimensionless time (i.e. in some properly selected time scale). Available experimental data on various proteins such as p42 MAPK [13], Pho4 [92], and Sic1 (see Section 6.2.3.1), indicate that the phosphorylation reactions proceed in minutes to a few hours. Whereas, it remains unclear what the time scale of dephosphorylation is.

By "precise timing of concentration decrease", we mean two features: i) starting from the time the kinase concentration increases, there is no appreciable change in the substrate concentration until a critical moment (i.e. temporal thresholding), and ii) the substrate concentration decreases immediately after passing the temporal threshold. Such a switch-like degradation process essentially enables the substrate protein to exist at two distinct levels separated in time, which might be a fundamental component in the mechanism of discrete and often irreversible cellular decisions. Graphically, these response curves exhibit the characteristic reverse-sigmoid shape, as illustrated by the red curve for the non-degradable substrate in Figure 2.1D.

2.4.2 Response Coefficient

To what extent the degradation is switch-like can be quantified by the steepness of the response curve. Borrowing the basic idea of response coefficients used in measuring ultrasensitivity in steady state responses [1], here we define a response coefficient in the time domain to characterize the steepness of the response curve for phosphorylation-triggered protein degradation:

$$R_{0.1/0.9} = \frac{t_{0.1}}{t_{0.9}} \tag{2.3}$$

where $t_{0.9}$ and $t_{0.1}$ represent the times at which the substrate concentration decreases to 90% and 10% of the initial amount, since the kinase level starts increasing. The closer this value is to one, the steeper the reverse-sigmoid response curve appears and the more switch-like the degradation is. We can further extend this index to examine related local properties of the response curve. More specifically, the following two partial response coefficients can be used to indicate how steep the decrease of the substrate is during the first and second halves of the degradation process, respectively.

$$R_{0.5/0.9} = \frac{t_{0.5}}{t_{0.9}}; \qquad R_{0.1/0.5} = \frac{t_{0.1}}{t_{0.5}} \tag{2.4}$$

where a middle time point $t_{0.5}$, the time at which the substrate reaches exactly half of the original concentration, is incorporated. It is worth noting that the overall response coefficient, $R_{0.1/0.9}$, is the product of these two partial response coefficients. It means that the overall process is switch-like if and only if the response curve is highly nonlinear both in the early and in the late phases.

2.4.3 Stimulus Profile

The stimulus in our model is the increase of kinase level, but very little is known concerning exactly how a kinase rises in phosphorylation-triggered protein degradation. We started out by considering three types of stimuli that differ in how the level of active kinase changes from zero to the same maximum value within the same period of time: step-function increase; linear increase; and nonlinear increase. Figure 2.2 illustrates these three types of kinase stimuli and how a nine-site substrate gets eliminated in response to each of them.

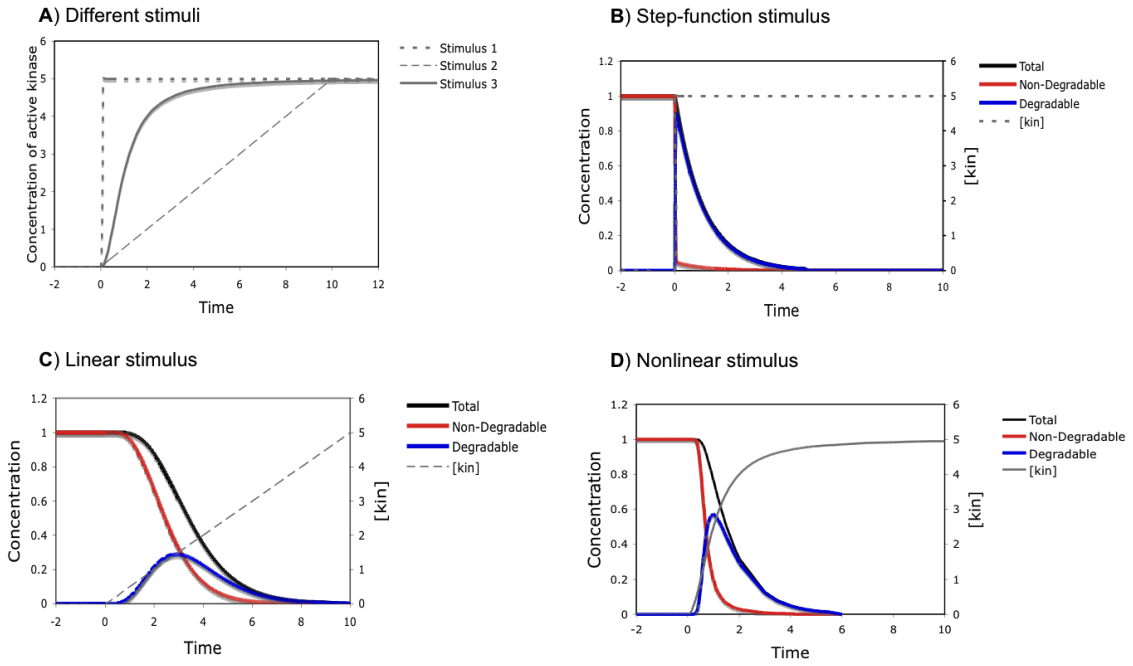

Figure 2.2: Responses of a nine-site protein to three types of kinase stimuli. (A) The concentration of active kinase increases from zero to a maximum value in three different manners: a step function (Stimulus 1, $[kin] = 5, t \geq 0$); a linear function (Stimulus 2, $[kin] = 0.5t$); and a nonlinear function (Stimulus 3, e.g. $[kin] = \frac{5t^2}{1+t^2}$). (B-D) Responses of a random system to the three stimuli with the following parameters: $n = 9$, $m = 6$, $k = 10$, $k^{-1} = 10$, and $k_i^d = 1, i = 6 - 9$, $[pho] = 1$.

It is very clear that the kinase profile greatly affects when and how rapidly the substrate disappears. As shown in Figure 2.2B, when the kinase is sharply increased like a step function, the substrate level decreases immediately in an exponential man-

ner, which could be very rapid. This type of stimuli is an ideal case and is likely to be valid only for *in vitro* experiments when the kinase is added instantaneously to a phosphorylation-dependent degradation system. Under *in vivo* conditions, the rise of the kinase can only occur gradually, either in a linear or nonlinear fashion. For nonlinear stimuli, we use a sigmoid function with the general formula of $kin^{max}\frac{t^n}{1+t^n}$, the sharpness of which can be tuned by parameter n. As exemplified in Figure 2.2C&D, now the substrate disappears at slower rates, compared with that in response to a step-function kinase increase, and we can observe temporal delays in the substrate decrease. Both the total and non-degradable amounts of the substrate follow a reverse-sigmoid curve, hence we can quantify to what extent the response is switch-like (i.e. combining temporal thresholding and rapid decrease after the threshold) using the response coefficients introduced above. Not surprisingly, the sharper the kinase profile is, the faster and more switch-like the degradation is. For example, a sharper (nonlinear) increase of the kinase in Figure 2.2D leads to steeper response curves of the total and non-degradable substrate, compared to the linear kinase increase in Figure 2.2C. Therefore, the exact response of a multisite protein in such a phosphorylation-triggered degradation process is determined by both the molecular properties of the substrate and the kinase stimulus.

Our main focus, in this work, is to examine whether and how various properties of a multisite protein can enable it to behave like a molecular switch, converting graded inputs to discrete outputs. Consequently, for further investigation, we chose to continue with the sigmoid function for specifying the kinase stimulus, which exhibits flexible shapes and may capture well many temporal profiles in real systems. For sigmoid kinase stimuli, we examined the effect of the sharpness of the stimulus profile on the steepness of the response curve, particularly of the non-degradable substrate. As illustrated in Table 2.1, for $n = 9$ and $m = 5$, increasing the nonlinearity of the sigmoid stimulus does not lead to significant improvement of the steepness of the

response curve when the exponent of t is greater than two.

Table 2.1: Effect of the sharpness of the stimulus profile. Response coefficients for the non-degradable amount of the substrate ($n = 9$)† is tabulated.

	$m = 1$			$m = 5$			$m = 9$		
$Kin(t)$	$R_{0.5/0.9}$	$R_{0.1/0.5}$	$R_{0.1/0.9}$	$R_{0.5/0.9}$	$R_{0.1/0.5}$	$R_{0.1/0.9}$	$R_{0.5/0.9}$	$R_{0.1/0.5}$	$R_{0.1/0.9}$
5	7.00	3.71	26.00	2.00	1.82	3.64	1.70	2.08	3.54
$5t$	2.90	2.00	5.80	1.48	1.35	2.00	1.31	1.60	2.10
$5\frac{t}{1+t}$	3.00	2.13	6.40	1.54	1.44	2.21	1.40	2.13	2.98
$5\frac{t^2}{1+t^2}$	2.00	1.68	3.35	1.31	1.27	1.67	1.27	1.62	2.05
$5\frac{t^4}{1+t^4}$	1.53	1.32	2.02	1.18	1.16	1.37	1.15	1.34	1.54
$5\frac{t^{10}}{1+t^{10}}$	1.20	1.14	1.38	1.07	1.08	1.16	1.07	1.15	1.24
$5\frac{t^{20}}{1+t^{20}}$	1.10	1.07	1.19	1.05	1.06	1.11	1.05	1.11	1.16

†All phosphorylation and dephosphorylation rate constants are 10 and 20, respectively. The degradation rate constant is 1 for all degradable phospho-states.

Thus, as sharper and sharper stimulus curves are specified (by increasing parameter n), improvement of the response coefficient becomes less and less significant. Accordingly, we use the sigmoid stimulus with $n = 2$ as a standard in most of our work. Within this context, we call a response curve representing the temporal profile of the substrate "switch-like" if its steepness is higher than that of the stimulus curve of the kinase, which can be determined quantitatively by comparison of the response coefficient and its counterpart for the stimulus curve.

Another relevant property of the stimulus is its duration. It is very likely that the kinase concentration will not be maintained permanently after it reaches the maximum. Instead, it will decrease gradually in a period of time because of degradation or other reasons. This is the case for many cyclin-dependent kinases, which rise and fall periodically during the cell cycle. For example, in the Sic1 system, the concentration of Cln2, which activates the Cdc28 kinase for Sic1 phosphorylation, increases gradually in the G1 phase, reaches its maximum before budding (beginning of the S phase), and then decreases [72, 93]. We investigated the effect of stimulus duration and our simulation revealed a tradeoff between stimulus duration and strength.

Figure 2.3 compares the response curves resulted from a weak stimulus and a strong one with three durations. As shown in Figure 2.3A-C, when the stimulus strength, determined by the maximum kinase level, is low, the substrate decreases slowly and a substantial amount still remains when the kinase level reaches the maximum. In this case, the duration of the kinase is important and affects to what extent the substrate can be eliminated. For example, the duration of the kinase in Figure 2.3A is not sufficient to remove 90% of the substrate. In turn, if it is required (e.g. for achieving an associated cellular regulation) to reduce the substrate to at most 10% of its initial level, the kinase would need to be maintained for a longer period of time such as the one in Figure 2.3B. However, when the stimulus strength is above certain critical level, the substrate has been largely eliminated by the time the kinase reaches the maximum and hence whether the kinase is maintained afterwards does not matter, as demonstrated in Figure 2.3D-F. This apparent tradeoff between kinase strength and duration is part of the challenge in resource allocation a cell constantly faces. We hypothesize that for certain protein degradation processes associated with critical regulations such as those in cell cycle progression, it is more desirable for the cell to generate a strong while short stimulus to achieve fast and robust degradation. Accordingly, for the rest of this chapter, we will consider stimulus strength above the critical level, sufficient to eliminate the majority of the substrate during the rise of the kinase.

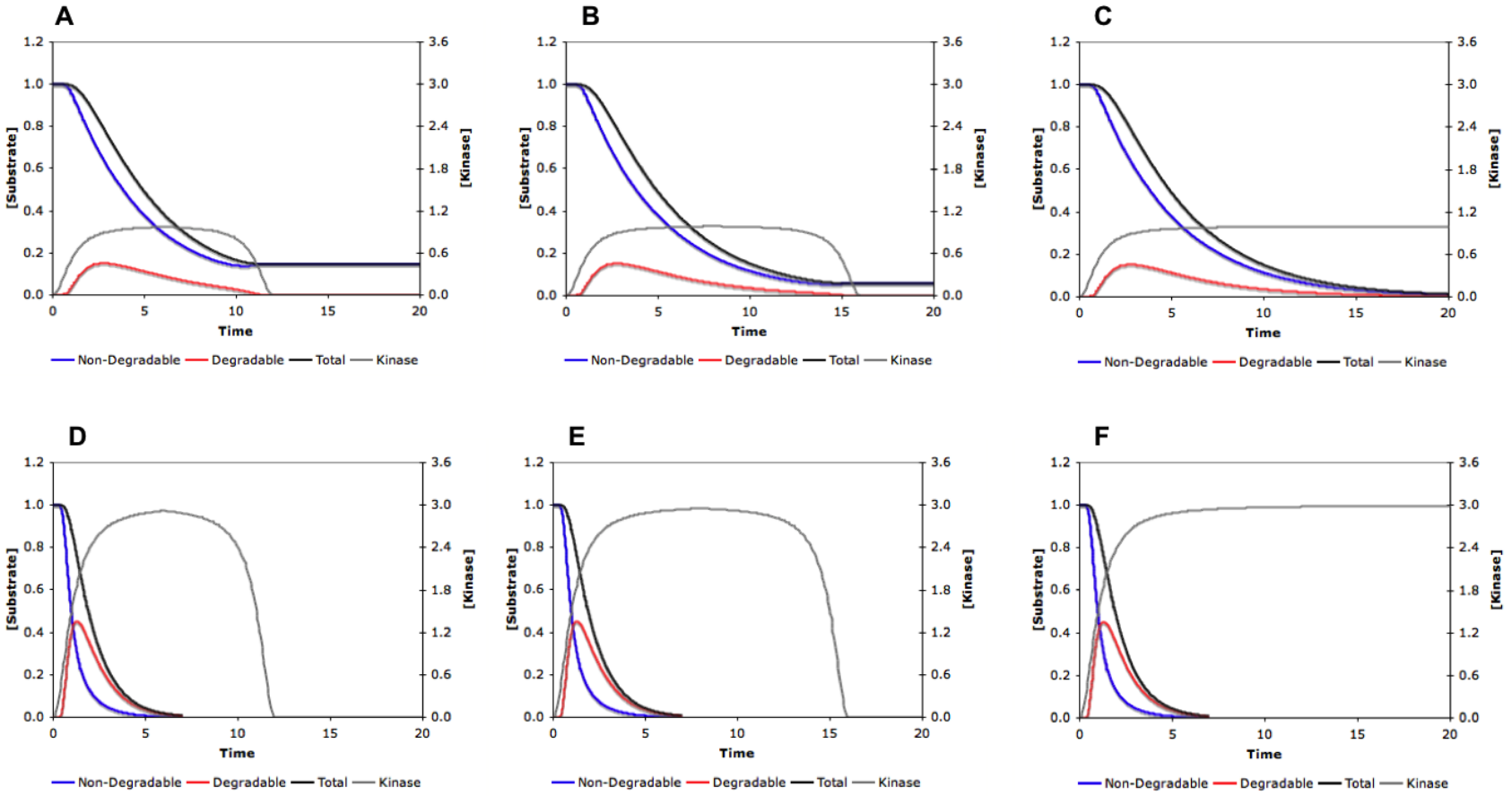

Figure 2.3: Effect of stimulus strength and duration. (A-C) A weak stimulus with three durations. (D-F) A strong stimulus with the same three durations. The shortest duration is 12 in (A) & (D): $[kin] = kin^{max}\frac{t^2}{1+t^2}$ for $t < 6$, $[kin] = kin^{max}\frac{(12-t)^2}{1+(12-t)^2}$ for $6 \leq t < 12$, and $[kin] = 0$ for $t \geq 12$. The intermediate duration is 16 in (B) & (E). Parameters: random system, $n = 9$, $m = 6$, $k = 10$, $k^{-1} = 10$, $k_i^d = 1, i = 6 - 9$, $[pho] = 1$. With this set of parameters, the minimum value of kin^{max} that leads to removal of at least 99% of the substrate during the rising phase of the kinase is 1.7.

2.4.4 Number of Phosphorylation Sites and Threshold

With well-defined kinase stimulus, we now turn to the main puzzle of whether a multisite protein is switch-like in its degradation, and most importantly, why multiple sites may help to achieve this property. In addition, we want to address the question of how the extent to which the degradation dynamics is switch-like is determined.

As described above, it is assumed that a protein with n phosphorylation sites is degradable when it is phosphorylated on at least m sites. As a case study, different values of m have been examined for $n = 9$ to model the Sic1 degradation. A question that one may raise here is which kind of Sic1 matters for the cell, the non-degradable fraction or the total protein (including the degradable and non-degradable fractions). The answer depends on the biochemistry of how Sic1 inhibits cyclins required for DNA replication and how it gets ubiquitinated. If Sic1 releases Clb5/6 as soon as it is ubiquitinated by the SCF complex, then only the non-degradable fraction is important as the CDK inhibitor. Otherwise, if Clb5/6 is released from Sic1 only when Sic1 is destructed by the proteasome, the total amount of Sic1 should be considered. Unfortunately, it is not known which case of the above is true. Therefore, we examined the dynamic profiles of the non-degradable fraction and also the total amount of the protein during the degradation process for three different scenarios: m= 1, 5 and 9.

As shown in Figure 2.4, the temporal profile of the total protein does not change much when m is varied. However, as far as the non-degradable fraction is concerned, its temporal profiles differ significantly for different m values. Specifically, the response coefficient $R_{0.1/0.9}$ for $m = 1$, $m = 5$, and $m = 9$ is 3.8, 2.3, and 10, respectively. Clearly, $m = 5$ leads to the smallest response coefficient and thus the most switch-like degradation dynamics. In this scenario, the profile of the non-degradable fraction features both an observable temporal threshold and rapid decrease after passing the threshold. In contrast, the profile for $m = 1$ shows no temporal threshold; while for $m = 9$, even though the profile also exhibits a temporal threshold, it suffers a long

tail during the later period of the response. The highly nonlinear response of the system when $m = 5$ can be attributed to the two distinct sub-chains of phospho-states created in this case. The non-degradable sub-chain can buffer the kinase signal in the early phase, thus creating the temporal threshold. While during the later phase of the response after passing the temporal threshold, the degradable sub-chain draws the substrate protein effectively, even before the substrate undergoes final destruction, and subsequently reduces the non-degradable pool very rapidly.

We can quantify the nonlinearity of the kinase stimulus with a stimulus coefficient similar to the response coefficient: $S_{0.9/0.1}$, the ratio between the time at which the kinase reaches 90% of the maximum and the time at which it reaches 10%. The stimulus we have used corresponds to a $S_{0.9/0.1}$ of 9 and in the case of $m = 5$, this gradually increasing stimulus causes a switch-like decrease of the non-degradable forms of the protein with an $R_{0.1/0.9}$ of 2.3. In another word, a single macromolecule can increase the nonlinearity of the system by four times. These results demonstrate the potential capability of multisite proteins in creating biological switches.

The above results may explain why in *S. cerevisiae* phosphorylation on at least six out of nine sites is required for Sic1 degradation. According to our model, this design would enable the Sic1 protein to respond to the kinase signal in a highly switch-like manner: the non-degradable fraction of this CDK inhibitor does not change appreciably before a temporal threshold even though kinase has risen, then once the temporal threshold is passed, the non-degradable fraction decreases very rapidly. We hypothesize that this switch-like degradation is crucial for Sic1's regulatory function during the G1/S transition of the cell cycle. Otherwise, if Sic1 could bind to Cdc4 for ubiquitination and subsequent degradation, either as soon as it was phosphorylated on a single site (i.e. $m = 1$), or only when it was fully phosphorylated (i.e. $m = 9$), elimination of Sic1 would not have been highly switch-like and the G1/S transition could not have occurred in an yes/no manner. This hypothesis will require future ex-

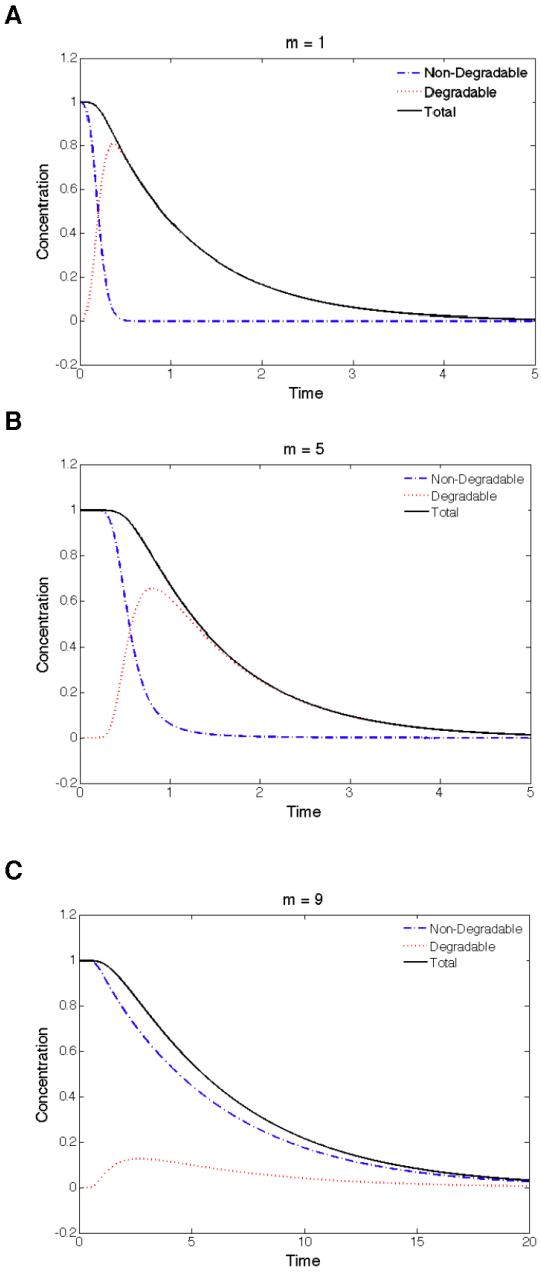

Figure 2.4: Temporal responses of a nine-site random system to different values of m. The most switch-like response takes places when $m = 5$. (A) $m = 1$, $R_{0.1/0.9} = 3.8$. (B) $m = 5$, $R_{0.1/0.9} = 2.3$. (C) $m = 9$, $R_{0.1/0.9} = 10$. System parameters: $k = 10$, $k^{-1} = 10$, $k_i^d = 0$ for $i = 0, ..., 5$ and $k_i^d = 1$ for $i = 6, ..., 9$, $[pho] = 1$, $[kin] = \frac{5t^2}{1+t^2}$.

perimental validations and specific assays can be designed to test various components of this theory. For instance, it will be interesting to examine experimentally whether or not Sic1 in a complex with Cdc4 (i.e. the degradable form of Sic1) can still inhibit Clb5/6.

In the rest of this study, we will build on the above hypothesis, i.e. we will focus on exactly how the non-degradable fraction of the substrate protein decreases in response to a rise of the kinase. Here, we first examine the effects of the total number of sites, n, and the threshold number for degradation, m. Our simulation results are summarized in Figure 2.5A for random phosphorylation/dephosphorylation and in Figure 2.5B for the sequential process. Several conclusions can be drawn based on these results. First, for both random and sequential processes, in general, the mores sites a protein has, the more switch-like it can be in its degradation dynamics. The response coefficient $R_{0.1/0.9}$ for $n = 1$ is about 7.5, which is not much smaller than the stimulus coefficient of 9. Therefore a single-site protein does not generate an output that is significantly sharper than the input. As the total number of sites, n, increases, the achievable response coefficient $R_{0.1/0.9}$ decreases, i.e. the protein can degrade in a more and more switch-like manner. Second, the threshold site number for degradation, m, plays an important role in determining the exact extent to which the response is switch-like. For random processes, the smallest response coefficient $R_{0.1/0.9}$ (i.e. the most switch-like response) is achieved when m is close to and often slightly smaller than half of n (e.g. $m = 2$ for $n = 3$, $m = 3$ for $n = 6$, and $m = 4$ for $n = 9$). In contrast, for sequential processes, an m value only slightly smaller than n delivers the most switch-like response (e.g. $m = 2$ for $n = 3$, $m = 4$ for $n = 6$, and $m = 7$ for $n = 9$). Finally, the response of a sequential system is generally more switch-like than that of a random one for given values of n and m.

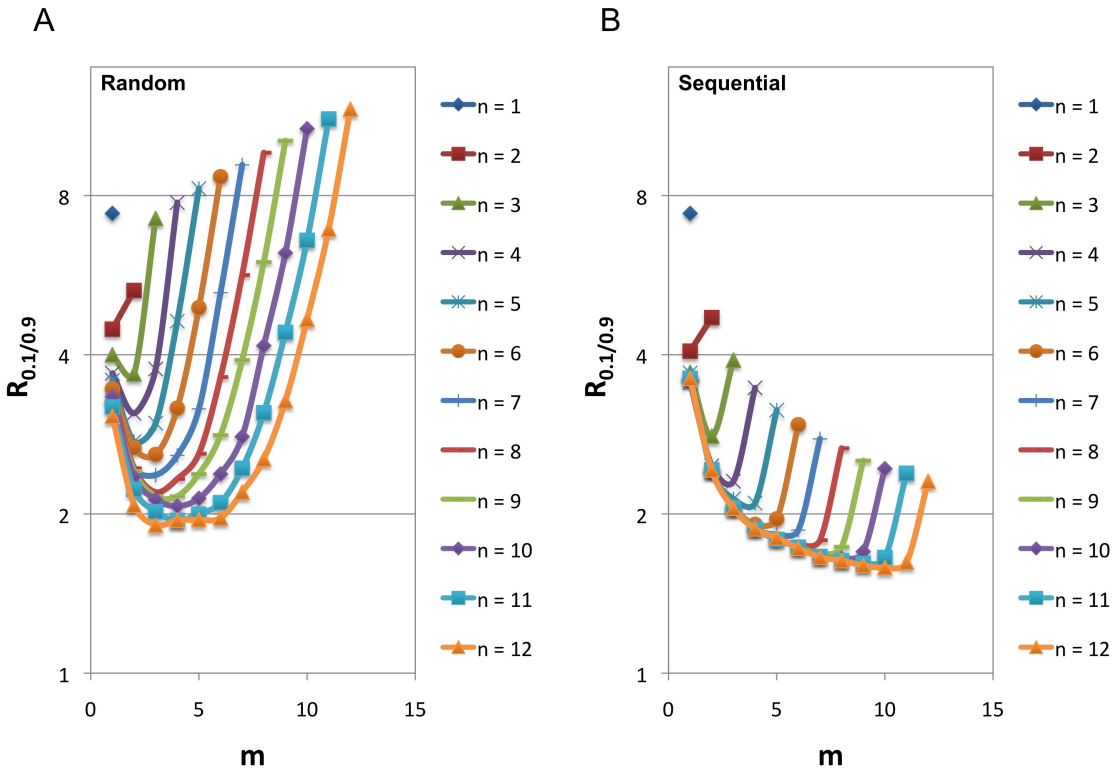

Figure 2.5: Effects of the number of phosphorylation sites (n) and the threshold for degradation (m). The response coefficient of the non-degradable fraction for different values of n and m (m varies from 1 to n) are shown for random (A) and sequential (B) processes. System parameters: $k = 10$, $k^{-1} = 10$, $k_i^d = 0$ for $i = 0, ..., m-1$ and $k_i^d = 1$ for $i = m, ..., n$, $[pho] = 1$, $[kin] = \frac{5t^2}{1+t^2}$.

2.4.5 Kinetic Parameters

Next, we will examine another important factor that affect the degradation dynamics - the kinetic parameters. In the model presented above, there are three groups of kinetic parameters, associated with phosphorylation, dephosphorylation and degradation reactions respectively. We have focused on two specific effects and conducted sensitivity analysis.

2.4.5.1 Change of Phosphorylation and Dephosphorylation Kinetics along the Chain

Phosphorylation reactions have been studied extensively, nevertheless, kinetic data of multi-step phosphorylation remain scarce. One exception is the transcription factor Pho4 in the phosphate-responsive signaling pathway in the budding yeast. Pho4 contains five phosphorylable sites for kinase Pho80-Pho85. Kinetic parameters of Pho4 phosphorylation by Pho80-Pho85 have been measured through integrating experimental data and computational modeling by Jeffery and colleagues [92]. It was found that the phosphorylation rate constants for all of the five phosphorylation steps are of the same order of magnitude ($k = \frac{k_{on}.k_{cat}}{k_{off}+k_{cat}} \sim 10\ \mu\mathrm{M}^{-1}s^{-1}$). Based on this data, we assumed in the above analysis that the rate constants of all the phosphorylation reactions are the same. In terms of dephosphorylation, even less data is presently available on its multi-step kinetics.

Given that only very limited data is available for the multi-step kinetics of phosphorylation/dephosphorylation, we would explore the possible scenario that earlier phosphorylation/dephosphorylation steps may suppress or enhance subsequent phosphorylation/dephosphorylation of remaining sites, especially if the exact phosphostate affects the substrate's configuration (e.g. enabling or disabling the binding of a downstream protein in the degradation pathway), and thus the kinetic parameters may change along the phosphorylation/dephosphorylation chain. Here, we consider the case where the phosphorylation/dephosphorylation rate constants might increase or decrease after passing the threshold for degradation. As the comparison of five cases shows in Figure 2.6, the degradation dynamics of the substrate, i.e. the temporal profile of the non-degradable fraction of the protein, does not change much if the net phosphorylation rate (i.e. phosphorylation against dephosphorylation) is faster than that of the degradation reaction (see Figure 2.6A,B,E). On the other hand, if the phosphorylation steps for the degradable part is too slow compared to the degradation

reaction, due to either slower phosphorylation (Figure 2.6C) or faster dephosphorylation (Figure 2.6D), the elimination of the non-degradable fraction of the protein becomes less switch-like, as indicated by the less rapid drop after the initial delay.

2.4.5.2 Rates of Phosphorylation/Dephosphorylation versus Degradation

As described above, our model consolidates ubiquitination and destruction by proteasome into one single degradation reaction. Relatively little is known about the kinetics of ubiquitination in general. Fortunately, a recent study has revealed the kinetics of polyubiquitylation of Sic1 [94], which is slower than the multi-step phosphorylation kinetics of Pho4. In light of this evidence, we have assumed that the degradation is slower than phosphorylation/dephosphorylation for most of the analysis presented above. Nevertheless, given the limited data currently available and the diversity that might exist in related molecular events, here we explore how the relative rates of phosphorylation/dephosphorylation versus degradation affect the degradation dynamics. Specifically, we compare the response coefficient $R_{0.1/0.9}$ of two cases: in one, the degradation is slower than phosphorylation/dephosphorylation (Figure 2.7A&C); in the other, the degradation is comparable to phosphorylation/dephosphorylation (Figure 2.7B&D). It is found that for sequential processes, if the degradation is as fast as phosphorylation/dephosphorylation, the elimination of the non-degradable substrate becomes more switch-like, as indicated by the smaller $R_{0.1/0.9}$ in Figure 2.7B compared to that in Figure 2.7A. However, the smallest $R_{0.1/0.9}$ is now achieved when $m = n$, i.e. the advantage of having a large number of sites (n) and an intermediate threshold (m) in creating a switch-like response vanishes. For random processes, faster degradation also leads to smaller $R_{0.1/0.9}$, while the most switch-like response still occurs when m is close to half of n (see Figure 2.7C&D). It remains to be seen whether nature utilizes all these different regimes in the design of protein degradation switches.

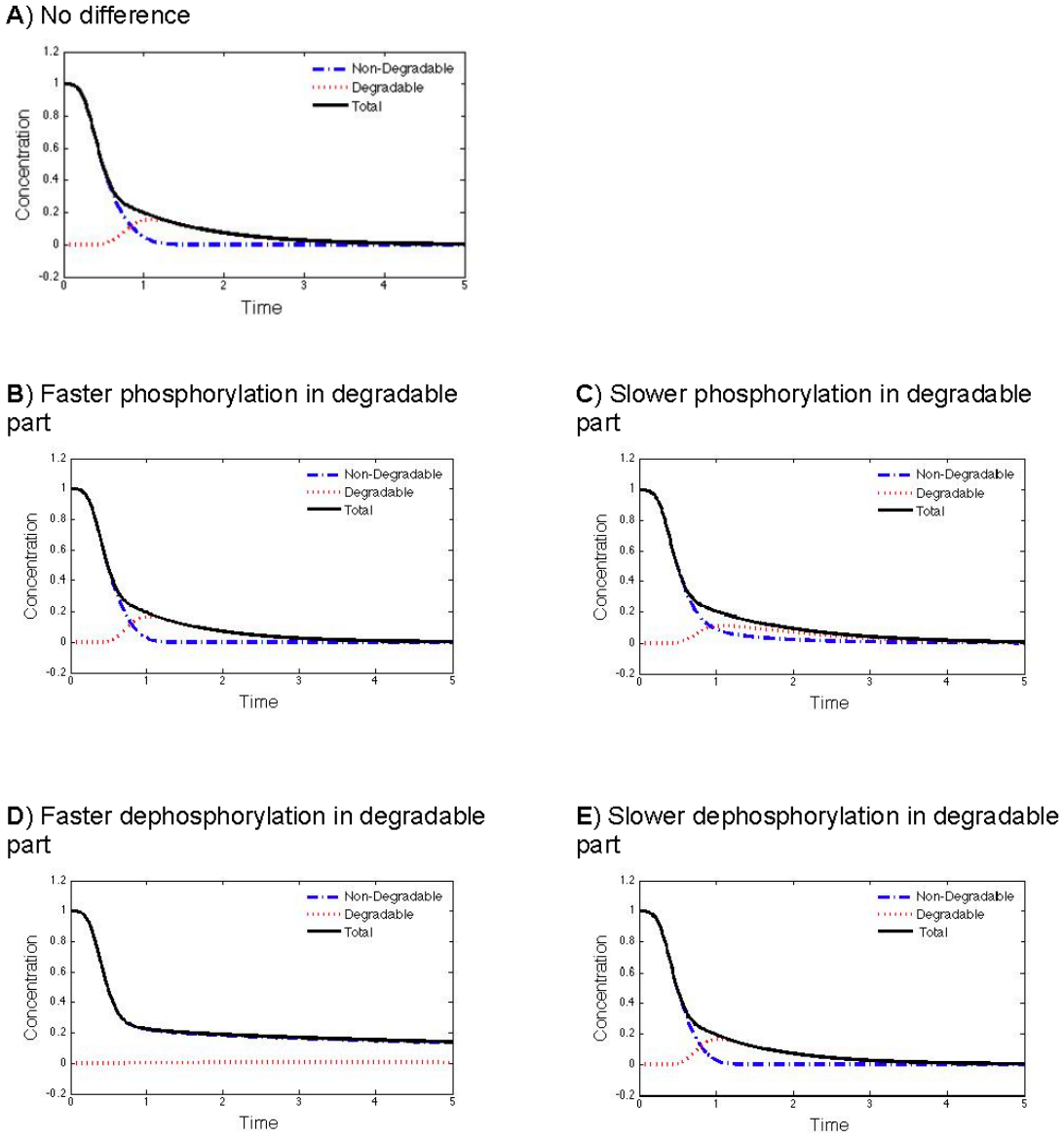

Figure 2.6: Effects of changes of phosphorylation and dephosphorylation rate constants along the chain. (A) No difference between degradable and non-degradable fraction in terms of kinetic rates of phosphorylation and dephosphorylation reactions: $k_i = 10$ and $k_i^{-1} = 10$ for $i = 0 - 8$. (B) The kinase phosphorylates the degradable fraction faster than the non-degradable fraction: $k_i = 10$ for $i = 0 - 5$ and $k_i = 1000$ for $i = 6 - 8$. (C) The kinase phosphorylates the degradable fraction slower than the non-degradable fraction: $k_i = 10$ for $i = 0 - 5$ and $k_i = 0.1$ for $i = 6 - 8$. (D) The phosphatase dephosphorylates the degradable fraction faster than the non-degradable fraction: $k_i^{-1} = 10$ for $i = 0 - 4$ and $k_i^{-1} = 1000$ for $i = 5 - 8$. (E) The phosphatase dephosphorylates the degradable fraction slower than the non-degradable fraction: $k_i^{-1} = 10$ for $i = 0 - 4$ and $k_i^{-1} = 0.1$ for $i = 5 - 8$. The outputs are shown for a sequential system with the following parameters : $n = 9$, $m = 5$, $k_i^d = 0$ for $i = 0 - 4$ and $k_i^d = 1$ for $i = 5 - 9$, $[pho] = 1$, $[kin] = \frac{5t^2}{1+t^2}$.

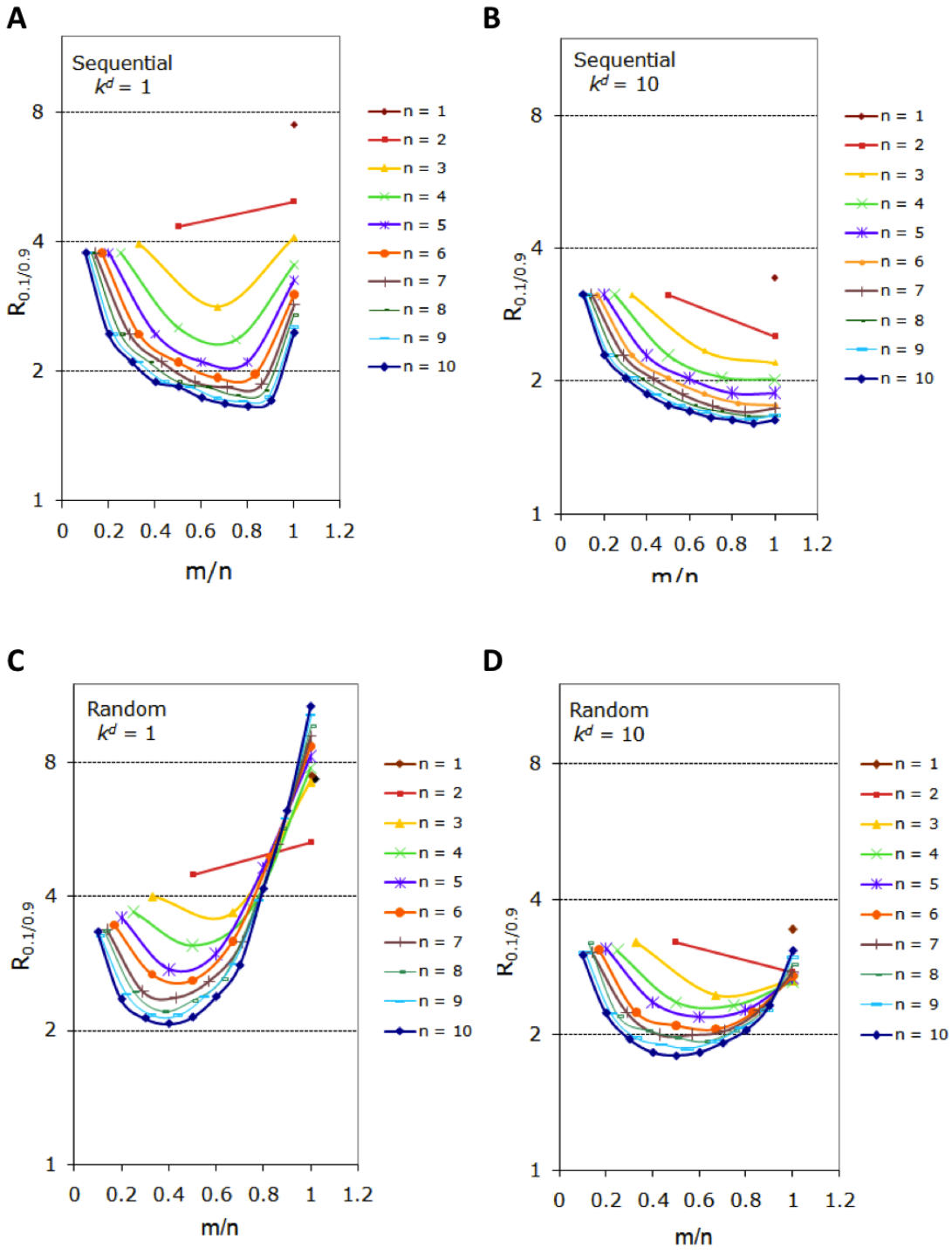

Figure 2.7: Rates of phosphorylation/dephosphorylation versus degradation. Systems with slow and fast degradation rate constants are compared in terms of sharpness of the temporal profile of the non-degradable fraction for sequential (A-B) and random (C-D) processes. The response coefficients are shown for the following parameters: $k = 10$, $k^{-1} = 10$, $[pho] = 1$, $[kin] = \frac{5t^2}{1+t^2}$.

2.4.5.3 Sensitivity Analysis

Our model of multisite phosphorylation triggered protein degradation is subject to many sources of uncertainty, including lack/inaccuracy of data and biological fluctuations. To investigate how variations in kinetic parameters affect the model output (i.e. the response coefficient of non-degradable substrate) we conducted sensitivity analysis. As a demonstration, here we focus on a sequential system with $n = 9$ and $m = 5$. There are a total of nine rate constants for phosphorylation, nine rate constants for dephosphorylation, and five non-zero rate constants for degradation.

First, we examine how perturbation of each parameter affects the model output. We choose to change the parameter within 20% of its nominal value which correspond to the base scenario discussed above ($k_i = 10$ and $k_i^{-1} = 10$ for $i = 0 - 8$, $k_i^d = 1$ for $i = 5 - 9$). It was found that such perturbations result in very insignificant changes of the response coefficient for the non-degradable substrates (less than 2%). This analysis also shows that each parameter affects the response coefficient in a monotonic manner. Specifically, increasing a phosphorylation rate constant decreases the response coefficient; increasing a dephosphorylation constant increases it; while the change of a degradation rate constant has no appreciable effect.

Then, we perturb all the parameters simultaneously while independently and examine their effect on the model output. We randomly choose the parameter values based on a normal distribution where the mean correspond to the base scenario discussed above and the standard deviation is set to be 20% of the mean. This sampling was conducted 1000 times. The mean of the model output (i.e. the response coefficient of non-degradable substrate) is 1.81 and the standard deviation is 0.04, about 2.2% of the mean. We were also interested in how each parameter correlates with the model output in this context and calculated the partial rank correlation coefficient (PRCC). PRCC is a robust measure of sensitivity for nonlinear but monotonic relationships between a certain input (a parameter in our context) and the output as long

as little or no correlation exists between the inputs [95]. As shown in Figure 2.8A, the degradation rate constants show negligible correlation with the sharpness of the temporal profile of the non-degradable substrate; while the phosphorylation and dephosphorylation parameters show significant correlations. Increasing the phosphorylation rate constants shifts the system toward the degradable fraction, which leads to faster depletion of the non-degradable substrate and thereby smaller response coefficient. Decreasing the dephosphorylation kinetic parameters has the same effect, which explains the positive correlation coefficient. Figure 2.8B-D illustrate the scatter plots for three parameters of k_5, k_3^{-1}, and k_8^d, which show the largest correlation coefficient in each set of parameters.

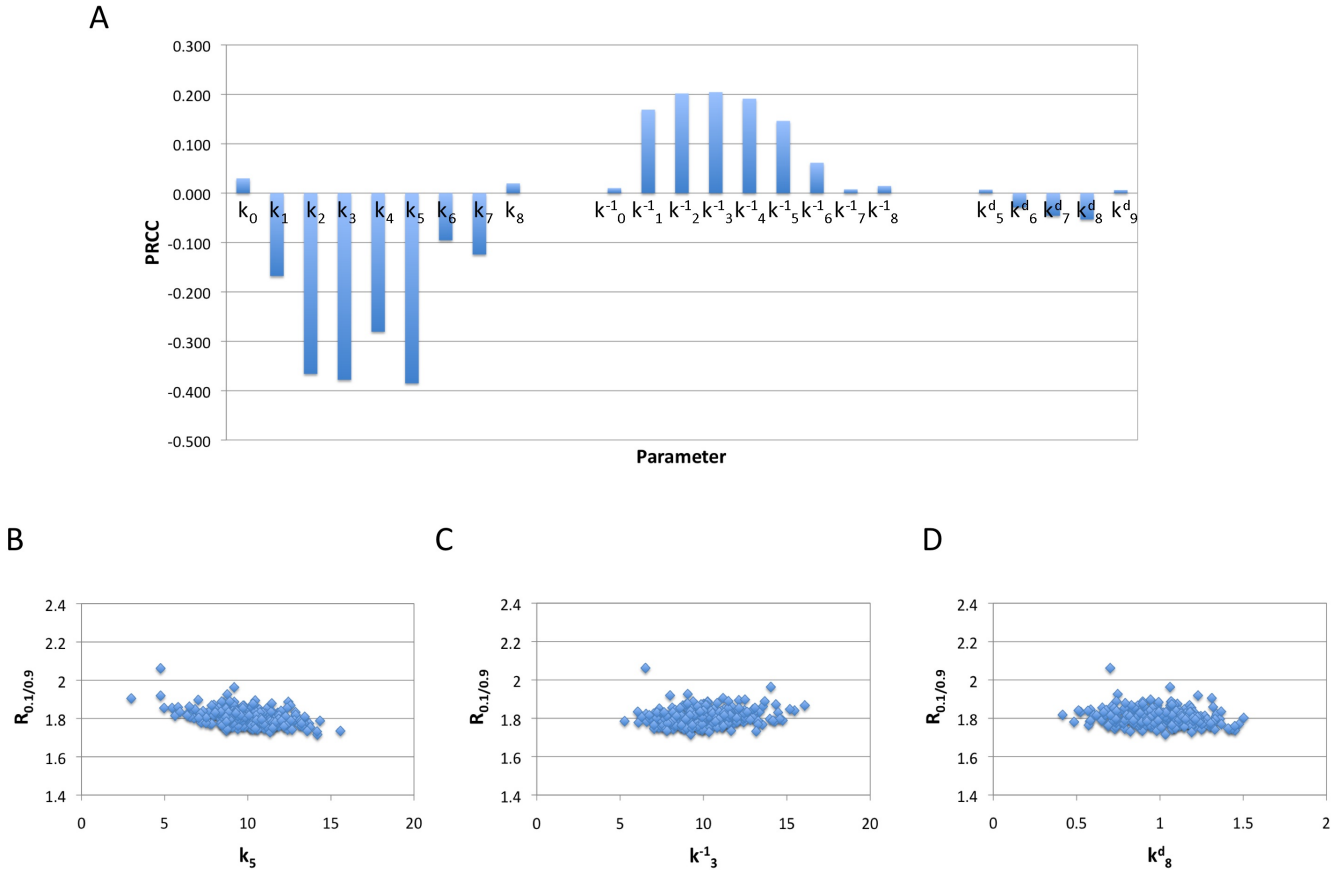

Figure 2.8: Sensitivity analysis for phosphorylation, dephosphorylation and degradation rate constants. Partial rank correlation coefficients calculated for all nine phosphorylation rate constants, nine dephosphorylation rate constants and five non-zero degradation rate constants (A). Scatter plots of the non-degradable substrate's response coefficient for k_5 (B), k_3^{-1} (C) and k_8^d $(D).Resultsarebasedon1000simulationsforasequentialsystemwith$n =9,m=5,[kin] $= 5\mathrm{t}^2\frac{}{1+t^2}$. The parameters are picked randomly from normally distributed space where the means correspond to the base scenario ($k_i = 10$ and $k_i^{-1} = 10$ for $i = 0 - 8$, $k_i^d = 1$ for $i = 5 - 9$) and the standard deviation is set to be 20% of the mean.

The above analysis assumes simultaneous and independent perturbation of all the parameters which accounts for certain types of uncertainty such as stochastic fluctuations of kinetics. There might also exist uncertainty associated with the enzymes that affects a whole set of parameters. Thus, in another analysis, we considered a total of three parameters in our model (one for all the phosphorylation reactions, one for all the dephosphorylation reactions, and one for all the degradation reactions) and then perturbed them in a similar manner. Results from 1000 samplings and simulations led to a mean response coefficient of 1.81 and a standard deviation of 0.09 (i.e. 5% of the mean).

These results clearly show that the switch-like behavior of a multisite protein's degradation is very robust against random fluctuations of kinetic parameters.

2.4.6 Site Preference

Finally, we will consider the effect of site preference on the degradation dynamics. In the completely random system described above, no site is preferred over other sites in term of the affinity for the kinase. However, for real proteins, due to effect of neighborhood amino acids, usually some sites are more likely to associate with the kinase and become phosphorylated. Consequently some pathways in the phosphorylation/dephosphorylation network are more dominant than others. A well-studied example is the extracellular-signal-regulated protein kinase ERK of the MAPK cascade. ERK contains two phosphorylable sites, Thr188 and Tyr190, for MEK kinase. The estimated kinetic parameters indicate that phosphorylation of Tyr is much faster than phosphorylation of Thr [96], with the corresponding rate constants differing by one order of magnitude. In the Sic1 system, Thr45 is preferred for phosphorylation by Cln2-Cdc28 over other sites [17]. In the Pho4 system, SP6 is preferred over other sites [92]. This property of site preference can be readily incorporated in our model by assigning a larger value of the phosphorylation rate constant for phosphorylation

of the preferred site.

When site preference exists, as expected, our model predicts that deletion of a preferred site has a stronger effect in both increasing the half-life of the protein and reducing the sharpness of the response curve, compared to deletion of ordinary sites (see Figure 2.9). However, this effect becomes less significant as the number of phosphorylation sites increases. In another word, the role of a given site, even a preferred one, in the response of the system to the kinase becomes less significant when the number of total sites increases. This result suggests that another advantage of having a larger number of sites might be enhanced robustness. If the substrate protein contains many sites, removal of one site (e.g. due to adverse mutations) is less likely to cause its function to break down, i.e. the system can tolerate better perturbations.

2.5 Discussion and Conclusion

In this chapter, we have analyzed systematically a general model for multisite-phosphorylation-triggered protein degradation processes. The model has been developed largely based on what were revealed experimentally for Sic1, a nine-site protein in *S. cerevisiae*, during its degradation at the G1/S transition of the cell cycle. Most importantly, the protein becomes degradable upon phosphorylation on a critical number of sites [17]. Inspired by subsequent theoretical conjectures concerning the role of multisite phosphorylation in regulating cellular dynamics [20], we set out to address the questions of whether and how multisite phosphorylations can cause a protein to respond to a gradually changing kinase signal and degrade in a highly switch-like manner. Here, we focus on switch-like transient responses, the characteristics of which include both temporal thresholding and rapid elimination beyond the threshold point. The temporal profile of the protein in such a process exhibits a reverse sigmoidal shape and our main interest is the steepness of the curve, which we

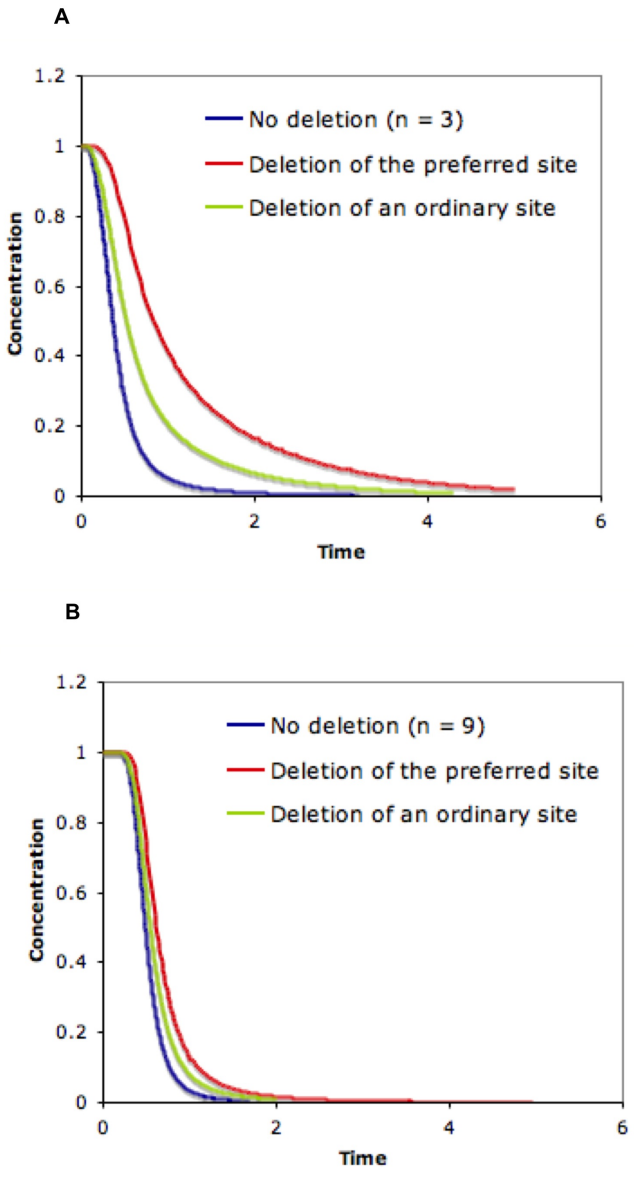

Figure 2.9: Effect of site preference. One site is preferred over other sites for the kinase. The deletion of this site is compared with deletion of an ordinary site for three-site (A) and nine-site (B) proteins in terms of sharpness of the temporal profile of the non-degradable fraction. Results are shown for a random system with the following parameters : $n = 3$, $m = 2$ for A and $n = 9$, $m = 5$ for B, $k_i^d = 1$, $[pho] = 1$, $[kin] = \frac{5t^2}{1+t^2}$. The phosphorylation rate constant for the preferred site is 100 times larger than that for the other sites.

quantify with the response coefficient $R_{0.1/0.9}$, defined as the ratio between the time taken to decrease to 10% of the original protein concentration versus that taken to reach 90%. Our extensive simulation study showed that multisite phosphorylation is indeed capable of generating a degradation switch. In addition, we examined systematically how the extent to which the degradation is switch-like is determined by various features of the system, including the total number of sites, the threshold site number for degradation, the order of phosphorylation/dephosphorylation, the kinetic parameters, and site preference in phosphorylation.

Given the mostly unknown parameters involved in our model, it remains to be tested whether the exact predictions agree with actual degradation of multisite proteins such as Sic1. On the other hand, multisite phosphorylation has emerged as a recurring theme as researchers dissect the proteasome-dependent degradation pathway of various proteins in diverse species. Table 2.2 illustrates some of these examples we were able to compile readily by conducting a literature search on multisite phosphorylation and protein degradation. It is worth noting that many of these proteins with multiple phosphorylation sites involved in degradation play important roles in the regulation of the cell cycle, which is not surprising when one considers the extreme importance of exact timings of a cascade of events required for correct cell cycle progression. For instance, the regulation of Rum1, the functional homolog of Sic1 in *Schizosaccharomyces pombe*, might also involve up to eight phosphorylation sites [97]. As an example in higher organisms, Runx1, a transcription factor associated with acute myeloblastic leukemia with maturation (M2 AML), degrades at the G2/M-G1 transition and the extent of phosphorylation on its eleven sites was suggested to play a role [98]. In addition to cell cycle control, precise protein degradation could also be critical for many other regulatory processes, such as eliminating cross-talk of mating and filamentous growth in *Saccharomyces cerevisiae* [99] and light signaling in *Arabidopsis thaliana* [100]. In light of this widespreadness of the involvement of mul-

tisite phosphorylation in regulating protein degradation, it appears plausible that the molecular mechanism described by our model might represent a common design principle utilized by nature for constructing protein degradation switches. Certain details of our model may require modifications or extensions, for example, the ability of the substrate protein to bind to ubiquitin ligase and thus undergo proteasome-dependent degradation could increase gradually instead of in a step-wise fashion. However, the overall conclusion that multisite phosphorylation provides a highly effective and flexible platform for switch-like protein degradation is likely to apply to a wide range of proteins across different eukaryotic species.

The work presented here for phosphorylation-triggered degradation also has certain limitations. First of all, we used a simplified kinetic model and the underlying assumptions regarding enzyme and substrate concentrations or kinetic parameters may not be applicable to all biological systems. Second, we considered free enzymes in our model, while in experiments, it is usually the total enzyme concentration that can be measured. It remains to be explored, perhaps with an alternative model where enzyme-substrate complexes are included explicitly, how these two quantities relate to each other. Third, we examined two extreme cases of fully random and fully sequential phosphorylation. Real biological systems might be in between. Random processes may be favored in the evolution of biology as it might provide more intermediate forms of the phosphorylated protein and allow more flexibility for protein regulation. However, phosphorylation cannot proceed fully randomly and due to neighborhood effects some sites have higher affinity for the kinase or phosphatase. Finally, we assumed only one kinase is responsible for phosphorylation while it is known that for some substrates, multiple kinases might be involved. For the Sic1 protein, different kinases are involved in different processes or at different times. Cdc28 and Pho85 apparently phosphorylate Sic1 at several sites in late G1 in the budding yeast [101, 102]. However, Ck2 phosphorylates Sic1 at Ser201 shortly after Sic1 *de novo* synthesis [103].

Ime2 is another kinase which is necessary for timely destruction of Sic1 during sporulation [104]. In addition, Hog1, a stress-activated protein kinase phosphorylates a single residue which contributes to arresting at G1 phase in response to stresses such as high osmolarity [105]. Incorporation of multiple kinases in an extended model would potentially lead to further understanding of real protein degradation switches as well as signal integration.

The biggest obstacle in theoretical studies of protein phosphorylation and dephosphorylation is that biochemical parameters are not known for most biosystems; even for well-studied systems, parameters are obtained through *in vitro* experiments and under specific conditions which may not reflect biological realities. Another difficulty is the lack of qualitative knowledge on the phosphorylation process and degradation dynamics. Even the exact number of phosphorylation sites for a given protein is usually not provided in the literature. Of the proteins listed in Table 2.2, very few have been studied carefully regarding the quantitative connection between multisite phosphorylation and degradation dynamics.

Table 2.2: Proteins regulated through phosphorylation dependent degradation.

Protein	**Species**	**Role**	**Degradation Time**	**Kinase(s)**	**No. of Sites***	**Ref.**
Sic1	*S. cerevisiae*	Cyclin-dependent kinase inhibitor	G1/S	Cln/Cdc28	9	[17]
Cdc6	*S. cerevisiae*	Replication initiator	G1/S	Clb/Cdc28	4	[106]
Cln2	*S. cerevisiae*	G1 cyclin	G1/S	Cdc28	7	[107]
Rum1	*S. pombe*	Cyclin-dependent kinase inhibitor	G1/S	Cdc2	2 (or 8?)	[97]
Cdc18	*S. pombe*	Replication initiator	G1/S	Cdc2	6	[108]
p27	*Mammalia*	Cyclin-dependent kinase inhibitor	G1/S	Cdk2, Src	4	[25, 26, 29]
Cyclin E	*Mammalia*	G1 cyclin	G1/S	Cdk2, Gsk3	4	[21, 109]
Cdc25A	*Mammalia*	Phosphatase (dephosphorylation of CDKs)	S	Chk1/2, ?	8	[110]
β-catenin	*Mammalia*	Cadherin-associated protein	G2/M-G1	Gsk3, Ckiα	4	[91]
Runx1	*Mammalia*	Transcription factor (associated with M2 AML)	G2/M-G1	Cdk1	11	[98]
Emi1	*Mammalia*	Early mitotic inhibitor (inhibit APC)	M	Cdk1, Plk1	7	[111]
Gcn4	*S. cerevisiae*	Transcription activator (biosynthesis of amino acids & purines)	-	Srb10	5	[112]
Tec1	*S. cerevisiae*	Filamentous growth regulator	In response to mating pheromone	Fus3	2	[99]
HFR1	*A. thaliana*	Transcription factor in light regulation	In darkness	CKII	5	[100]
Bim	*Mammalia*	Apoptosis signaling	In response to survival signals	MAPK, JNK	4	[113]

*: Phosphorylation sites shown to be involved in the regulation of the stability of the corresponding protein.

A main challenge in quantitative understanding of phosphorylation and dephosphorylation processes is the identification and quantification of phosphorylated protein species. Mass spectrometry (MS) is becoming widely used as a fast, sensitive and high-throughput measurement method in the identification and quantification of protein phosphorylation. For instance, Olsen and colleagues detected and quantified phosphorylation of 6,600 sites on 2,244 proteins in response to a stimulus in mammalian cells through stable isotope labeling by amino acids in cell culture [37]. In most MS approaches, the substrate protein is digested into peptides and the degree of phosphorylation at one site is calculated based on the summed abundance of the peptides containing this site. For a protein such as Sic1 which has nine phosphorylation sites, a partially phosphorylated protein solution might contain $2^9 = 512$ different phosphorylated states of the protein, whereas even in the ideal case where each peptide contains only one phosphorylation site, merely $2 \times 9 = 18$ concentrations can be measured from MS. Although results of phosphopeptide concentrations can be utilized for certain characterizations such as determining site preference, they are not sufficient for estimating kinetic parameters. New approaches are needed to address this issue. For example, one might consider making use of a set of mutants, each with a subset of the phosphorylation sites, in kinetic assays and then integrating the data systematically.

In this chapter, we investigated the capability of a single protein with multiple phosphorylation sites in converting a graded input to a switch-like output signal in the time domain. We would like to point out that besides phosphorylation, a dominant post-translational modification for regulating protein stability and activity, other types of modification such as ubiquitination, methylation and glycosylation have also been shown to be involved in tuning the stability, activity and translocation of macromolecules. The model presented here or its variations can potentially explain and predict the behavior of these multisite modification systems as well. Finally, as

have been demonstrated by a synthetic single-molecule signaling switch using multiple autoinhibitory domains [57], the multisite design principle revealed by our model can help guide the engineering of synthetic protein degradation switches, which may have diverse biomedical applications.

CHAPTER III

Ultrasensitive Binding of Sic1 to Cdc4 in Response to Cln2-Cdc28

3.1 Summary

Sic1 is a cyclin-dependent kinase inhibitor that regulates DNA replication in the budding yeast *Saccharomyces cerevisiae* by inhibiting Clb-Cdc28 complexes required for DNA replication in the S phase. Sic1 degrades and releases S cyclins upon phosphorylation on multiple sites by Cln-Cdc28 kinase complex at late G1 phase. Computational studies suggest that multisite phosphorylation can lead to an ultrasensitive response to the kinase and ultimately a switch-like G1/S transition. Here, we demonstrate experimentally that the binding of phosphorylated Sic1 to Cdc4, the subunit of SCF^{Cdc4} that recruits Sic1 for ubiquitination and degradation, in response to the increasing activity of the Cln2-Cdc28 kinase is indeed ultrasensitive (Hill coefficient $n_H \simeq 3.2$); and the ultrasensitivity decreases as the number of phosphorylation sites decreases to five ($n_H \simeq 1.0$). Mutant Sic1 proteins with less than five phosphorylation sites are not recognized by Cdc4 and as the number of phosphorylation sites increases, more Sic1 binds to Cdc4 at the saturated level of Cln2-Cdc28. In parallel, mass spectrometry analysis shows that the wild-type Sic1 is phosphorylated mostly on less than five sites in the initial lag phase of the binding curve. Interestingly,

the distribution shifts dramatically toward six and higher orders of phosphorylated states as the concentration of Cln2-Cdc28 increases. We hypothesize that the multi-step phosphorylation reaction of Sic1 proceeds in a cooperative manner in order to explain the Sic1-Cdc4 binding data. This study highlights the potential of multisite protein phosphorylation in converting a graded input (Cln2-Cdc28 activity) to an ultrasensitive output (binding to Cdc4) and thereby generating a switch-like cellular behavior such as the G1/S transition.

3.2 Introduction

Sic1 is a cyclin-dependent kinase inhibitor that plays a key role in regulating the G1/S transition in the cell cycle of *Saccharomyces cerevisiae*. Sic1 inhibits Clb5,6-Cdc28 kinase complexes which are the primary regulators of the initiation of DNA replication [15, 18, 72, 114]. Entry into the S phase requires elimination of Sic1 which is triggered by phosphorylation by Cdc28 kinase in complex with G1 cyclins. The concentration of Cdc28 is constant over the *S. cerevisiae* cell cycle, but the concentration of G1 cyclins (Cln1, Cln2, and Cln3) changes periodically [72, 115]. In late G1 phase, the concentration of G1 cyclins increases, leading to higher activity of the Cln-Cdc28 activity. The activated complex phosphorylates Sic1 at multiple sites which causes its ubiquitination by the constitutively active SCF^{Cdc4} ubiquitin ligase complex and subsequently its proteolysis by the 26S proteasome [17]. This leads to emancipation of the active Clb-Cdc28 complex which stimulates DNA replication in the S phase (Figure 3.1). Yeast strains lacking Sic1 initiate DNA replication earlier and show extended S phase [70, 71]. On the other hand, in mutant strains that are resistant to Sic1 degradation, cells experience lengthened G1 phase in an otherwise wild-type genetic background [72] or G1 phase arrest in more complex situations [15, 18].

The Sic1 protein contains nine Ser/Thr-Pro phosphorylatable sites for proline-

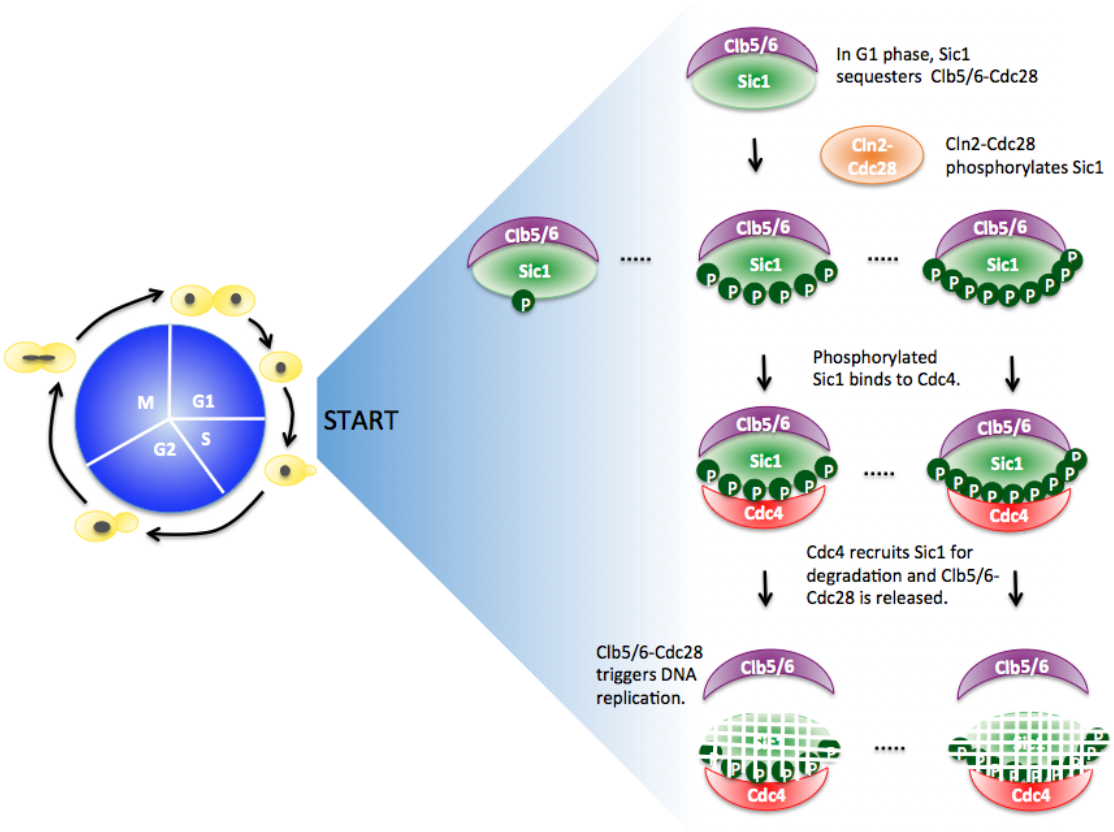

Figure 3.1: The role of Sic1 in the cell cycle and its multiple phosphorylation sites. At the G1 phase, Sic1 is bound to Clb5/6-Cdc28, which is required for the onset of DNA replication in the S phase. With increasing the activity of Cln2-Cdc28 kinase, Sic1 becomes phosphorylated on multiple sites and releases Clb5/6-Cdc28, hence the cell enters into the S phase. Phosphorylated Sic1 is recruited by Cdc4 for ubiquitination and eventually degradation through the SCF^{Cdc4} pathway.

directed kinases including the Cln-Cdc28 kinase. The C-terminal 70 amino acids of Sic1 is required for *in vivo* and *in vitro* Clb5-Cdc28 inhibition [72, 116]. The N-terminal fragment is required and sufficient for targeting of Sic1 to Cdc4 as demonstrated by *in vitro* binding and ubiquitination assays and *in vivo* mutational studies [16, 17]. Nash *et al.* investigated how multisite phosphorylation of Sic 1 regulates its ubiquitination and degradation [17]. They began with the Sic1 mutant which lacks all the nine phosphorylation sites and restored the sites one by one in the order of their importance measured by the degree to which elimination of a single site affects the Sic1 turnover. Serial reintroduction of five sites failed to reestablish Sic1 binding

to Cdc4 or cell viability. Re-addition of a sixth seemingly insignificant site abruptly restored Sic1's binding with Cdc4 *in vitro* and revived the cells *in vivo*. These experiments clearly revealed that there is a threshold number of phosphorylated sites required to render binding of Sic1 with Cdc4.

Substrate recognition of Cdc4 is based on its interaction with consensus binding motifs, the so-called Cdc4 phospho-degrons (CPD), on the surface of the phosphorylated Sic1. Phosphorylation affects certain hydrophilic and charged contacts, which probably releases transient structures involving the CPDs and facilitates their interactions with Cdc4 [76]. The optimal consensus sequence for Cdc4 binding is a phosphorylated serine or threonine followed by a proline and a basic amino acid. However, none of the CPDs on the surface of the Sic1 show such a composition. Therefore, multiple phosphorylation of Sic1 is needed to generate high-affinity binding to Cdc4. Recent structural analysis shows that Sic1 exists in an intrinsically disordered state and its multiple phosphorylated sites interact with the single receptor site of Cdc4 in dynamic equilibrium [76, 117]. Phosphorylation of multiple CPD motifs increases the local concentration of these sites around Cdc4 once the first CPD site is bound, to the extent that diffusion-limited escape from the receptor is overwhelmed by the higher probability of rebinding of any CPD site [118].

It has been proposed that multisite phosphorylation can lead to "ultrasensitive" responses [17, 20, 23, 119]. The term "ultrasensitive" is applied to a system that is more sensitive to changes of stimuli in the intermediate regime than a standard hyperbolic (Michaelis-Menten) one, and is measured by the Hill coefficient, n_H, for sigmoidal curves. The Hill coefficient of a stimulus-response curve can be estimated by fitting the data to the Hill equation [3]: $Response = \frac{Stimulus^{n_H}}{EC_{50}^{n_H} + Stimulus^{n_H}}$, where EC_{50}, the half maximal effective concentration, refers to the concentration of stimulus which induces a response halfway between the baseline and maximum. For a standard hyperbolic response curve, $n_H = 1$, and as the steepness of the curve increases, n_H

becomes larger.

Previous theoretical studies suggested that ultrasensitivity can arise from a combination of multistep phosphorylation and changes of functionality along the phosphorylation chain [24]. In particular, high degree of ultrasensitivity is believed if there exists a threshold site number of phosphorylation sites that abruptly changes the substrate activity from zero to maximum and this threshold number is about half of the total number of sites. In the case of Sic1, there are a total of nine sites and the threshold site number, according to Nash's study [17], is six.

In this work we examine experimentally how the number of phosphorylation sites of Sic1 affects the shape and specifically the steepness of the steady-state Sic1-Cdc4 binding curve. We measure the fraction of Sic1 that binds to Cdc4 in response to the increasing activity of Cln2-Cdc28 kinase *in vitro*. We utilized a panel of Sic1 variants that contain different numbers of phosphorylation sites and noted the profound role of multiple phosphorylation in Sic1's ultrasensitivity property. Combined with mathematical modeling, these experimental results provide new insights as well as testable hypothesis about the underlying mechanism of ultrasensitivity arising from multisite phosphorylation in the Sic1 system.

3.3 Methods

3.3.1 Recombinant Protein Expression and Purification

N-6xHis-tagged *S. cerevisiae* Sic1, including the wild type and various mutants, were cloned into the pMCSG7 vector. Proteins were expressed in *E. coli* with IPTG induction, and purified using nickel-NTA columns according to manufacturer's protocol (Qiagen). The Cln2-Cdc28 kinase was expressed in Hi5 cells at the Protein Expression Center of CalTech using baculoviruses encoding GST-Cdc28-HA, Cln2, Cak1, and Cks1-6xHi [120]. The Cln2-Cdc28 kinase was purified using glutathione-

sepharose beads (GE Healthcare). Since the subunits of the kinase complex are co-expressed in the same cell, no assembly step was required. The N-Flag-tagged Cdc4 was purified using anti-FLAG M2 Affinity gel (Sigma-Alderich), from baculovirus infected Hi5 cells as previously described [17]. For binding assays, Flag-tagged Cdc4 was immobilized on anti-FLAG M2 Affinity Gel after re-suspending cell pellets in lysis buffer (50 mM HEPES, 100 mM NaCl, 0.1% NP-40, 5 mM NaF, 10% Glycerol, 5 mM EDTA) and brief sonication. The size and identity of all recombinant proteins were confirmed by SDS-polyacrylamide electrophoresis and immunoblotting.

3.3.2 Yeast Extract Preparation

α-factor was used to arrest the yeast cells at the G1 phase. The α-factor pheromone (a short peptide of 13 residues) is produced by MAT-α cells and arrest MAT-a cells at START, the G1/S boundary, by inhibiting Cln-Cdc28 activity. ATCC 201388 (MATa his3Δ1 leu2Δ0 met15Δ0 ura3Δ0) cells were grown in YPD at 30°C to early log phase and then α-factor (Sigma-Aldrich) was added at two times with one hour interval to a final concentration of 10 μg/ml. At the time of adding α-factor, pH was lowered to 3.9. The cells were harvested after two hours. Because α-factor is a Cdc28 inhibitor, to avoid its effect on our phosphorylation assay, the cells were washed twice with YPD medium prior to the lysis step. The cells were lyzed in CelLytic Y Cell Lysis reagent (Sigma-Aldrich) according to manufacturer's protocol. DTT was added to the lysis buffer before use at a final concentration of 10 mM to increase the total protein yield. In addition, a protease inhibitor cocktail (Sigma P8215) was added to inhibit endogenous proteases. The phosphatase activity of the G1 yeast extract on phosphorylated Sic1 was confirmed by observing a shift in the position of Sic1 band on the SDS-polyacrylamide gel.

3.3.3 Kinase and Binding Assays

All phosphorylation reactions were carried out in kinase buffer (Cell Signaling) and ATP (Cell Signaling) at 30°C for three hours to reach steady state. Various amounts of purified Cln2-Cdc28, from zero to approximately 25 nM, was added. Concentrations of Sic1 in the reactions were approximately 2.5 μM, in the range of the estimated 1 μM concentration of Sic1 in the yeast nucleus [20]. Flag-Cdc4 was immobilized on anti-FLAG M2 affinity gel (Sigma-Alderich) for one hour at room temperature. After two times washing of Flag gel with TBS, the Sic1 mix (containing a mixed population of Sic1 phosphospecies) was incubated with Flag-captured Cdc4 at 4°C with gentle shaking for one hour. At low temperature, the phosphorylation and dephosphorylation reactions are probably slowed, thus the equilibrium does not change after binding a fraction of phosphorylated Sic1 to Cdc4. Then the Flag gel was washed twice with TBS. The Cdc4-Sic1 complex was eluted using 0.1 mM glycine hydrochloride. The eluted fraction was mixed with SDS Laemmli sample buffer (Bio-Rad) for SDS-PAGE and immunoblotting with the C-terminus Sic1 antibody (Santa-Cruz). Before choosing the current set up for binding assay for the His-tagged Sic1 and Flag-immobilized Cdc4, we had explored other protein fusions of Sic1 and Cdc4 using various binding set ups. These explored but ineffective approaches are described in Appendix B.

3.3.4 Mass Spectrometry

Phosphorylated proteins were purified by an Agilent 1100 HPLC system (Agilent Technologies) with an Agilent Zorbax XBD C8 reverse phase column. The fractions containing proteins were concentrated by an Eppendorf Vacufuge (Eppendorf North America) and reconstituted in 1:1 (v/v) water/acetonitrile with 0.1% formic acid. Samples were electrosprayed via an Apollo II (Bruker Daltonics) electrospray source. Mass spectra were acquired on a Bruker 7-T SolariX ESI-Q-FT-ICR mass spectrom-

eter at broad band mode. Spectra were processed by DataAnalysis software (Bruker Daltonics) and an in-house software which deconvoluted based on charge state distribution.

3.3.5 Data Analysis and Curve Fitting

The data points for each binding curve were collected from several independent experiments. Each independent experiment included about eight various levels of Cln2-Cdc28 kinase concentration in duplicate and one control sample to check variability from experiment to experiment. Calibration curves correlating Sic1 amount and band size were generated and the linear range was utilized in quantification (Appendix C). The amount of Cdc4-bound Sic1 was estimated by measuring the band size of Sic1 blot using the ImageJ package. To combine data from different experiments, we normalized the amount of Sic1 with respect to the saturated value in each experiment and then we pooled the normalized data. We used the same stocks of Sic1, Cln2-Cdc28, yeast extract, and Cdc4 to minimize variation across different experiments. The pooled data were fitted to a three-parameter Hill equation: $y = \frac{ax^{n_H}}{K+x^{n_H}}$, where y was the amount of Cdc4 bound fraction (normalized to 1 at saturation level) and x was the percentage of Cln2-Cdc28 in the phosphorylation reaction buffer.

3.3.6 Modeling and Simulation

Systems of ordinary differential equations were formulated and solved with MATLAB 7.1. ATP was assumed to be held constant and its effect was included into the corresponding rate constants. Mass action kinetics were applied for phosphorylation, dephosphorylation, and binding reactions.

3.4 Results

3.4.1 Ultrasensitive Binding of Sic1 to Cdc4 in Response to Cln2-Cdc28

To experimentally determine whether the steady-state response of Sic1 to kinase Cln2-Cdc28 is ultrasensitive, as previously hypothesized, we began by developing an *in vitro* phosphorylation/dephosphorylation/binding assay and measured the response curve of wild-type Sic1. Our assay requires four proteins or protein complexes: (i) the Sic1 substrate; (ii) the kinase Cln2-Cdc28; (iii) the phosphatase; and (iv) the downstream protein Cdc4, the subunit of ubiquitin-ligase SCF^{Cdc4} that binds to phosphorylated Sic1 and thereby recruits it for proteasomal degradation.

We used bacterially expressed His-tagged Sic1, and purified the Cln2-Cdc28 kinase and Flag-tagged Cdc4 expressed in insect cells. For phosphatase activity, the exact identity of the phosphatase for Sic1 during G1/S transition is not clear. We initially attempted to use Cdc14, a phosphatase that has been reported to dephosphorylate Sic1 during mitotic exit [121, 122]. However, we did not observe appreciable dephosphorylation activity of this phosphatase on Sic1 in our *in vitro* assay (data not shown). Comprehensive screening has suggested that multiple phosphatases are involved in the dephosphorylation of Sic1 (Mike Tyers, personal communications). We thus prepared protein extract of yeast cells arrested at G1 phase and used it to provide phosphatase activity. Similar approaches using *Xenopus* egg extracts were employed previously to effectively provide phosphatase background in studies of steady-state ultrasensitive response of Wee1 and Cdc25c in *Xenopus* [7, 123]. As shown in Figure 3.2, the yeast extract we collected from G1 phase clearly has phosphatase activity on phosphorylated Sic1.

Our phosphorylation/dephosphorylation/binding assay aims to quantify how the amount of Sic1 that can bind to Cdc4 changes in response to increase of kinase activity. As illustrated in Figure 3.3, the assay starts with incubating unphosphorylated Sic1

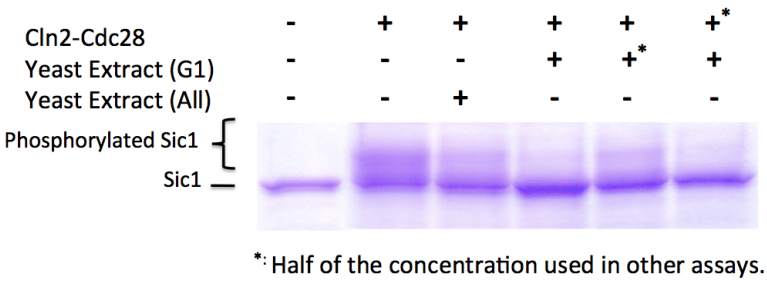

Figure 3.2: The protein extract of yeast cells arrested at the G1 phase shows phosphatase activity on phosphorylated Sic1.

with the mixture of Cln2-Cdc28 and G1 cell extract for three hours to allow the phosphorylation to reach a steady state. Then the mixed population of Sic1 with different phosphorylation states is incubated with immobilized Cdc4 for one hour to allow binding of sufficiently phosphorylated Sic1 and Cdc4. After washing to remove Sic1 molecules that do not bind to Cdc4, we elute pSic1-Cdc4 complexes from the Flag resin and the amount of Sic1 is quantified through immunoblotting with a C-terminus Sic1 antibody.

We carried out this assay on wild-type Sic1 with various amounts of Cln2-Cdc28 kinase and the same level of G1 extract. Up to eight kinase concentrations were examined in duplicates in each experiment, as illustrated in Figure 3.4A. The amount of Sic1 bound to Cdc4 is normalized with the saturation level (i.e. maximum level) in each experiment and plotted against the amount of Cln2-Cdc28. Data from seven experiments were pooled and fitted to a three-parameter Hill function (Figure 3.4B). The Hill coefficient was determined to be 3.2 with an standard error of 0.5. Thus, the steady-state response of Sic1 to kinase Cln2-Cdc28, as measured by its fraction that can bind to Cdc4, is ultrasensitive.

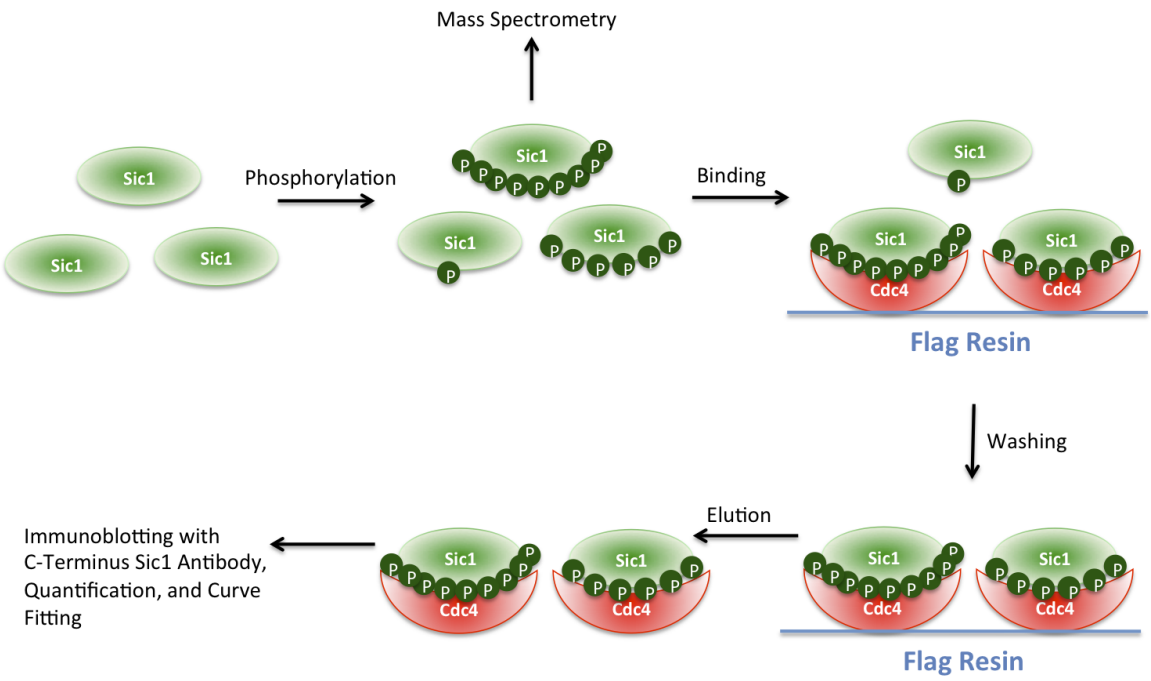

Figure 3.3: Experimental procedure for the phosphorylation and binding assays in this study. Sic1 is phosphorylated and then part of it is incubated with Flag-immobilized Cdc4 for the binding assay. Another part of it is used for mass spectrometry analysis.

3.4.2 Ultrasensitivity Decreased in Sic1 Mutants with Reduced Numbers of Phosphosites

Nash *et al.* [17] reported the importance of each Ser/Thr site of Sic1 according to the degree to which elimination of a single site affects the Sic1 turnover. Thr45, Ser76, Thr5 and Thr33 seemed to have a larger contribution to Sic1 instability compared to other sites and thus were considered the most important sites [17]. They constructed a panel of Sic1 mutants containing various combinations of the phosphorylation sites. They began with the Sic1 mutant which lacks all the nine phosphorylation sites and restored the sites one by one in the order of their relative importance. In their investigation, serial reintroduction of five sites failed to reestablish Sic1 binding to Cdc4, however, re-addition of a sixth seemingly insignificant site abruptly restored Sic1's binding with Cdc4 *in vitro*. We used the same panel of mutants, except that

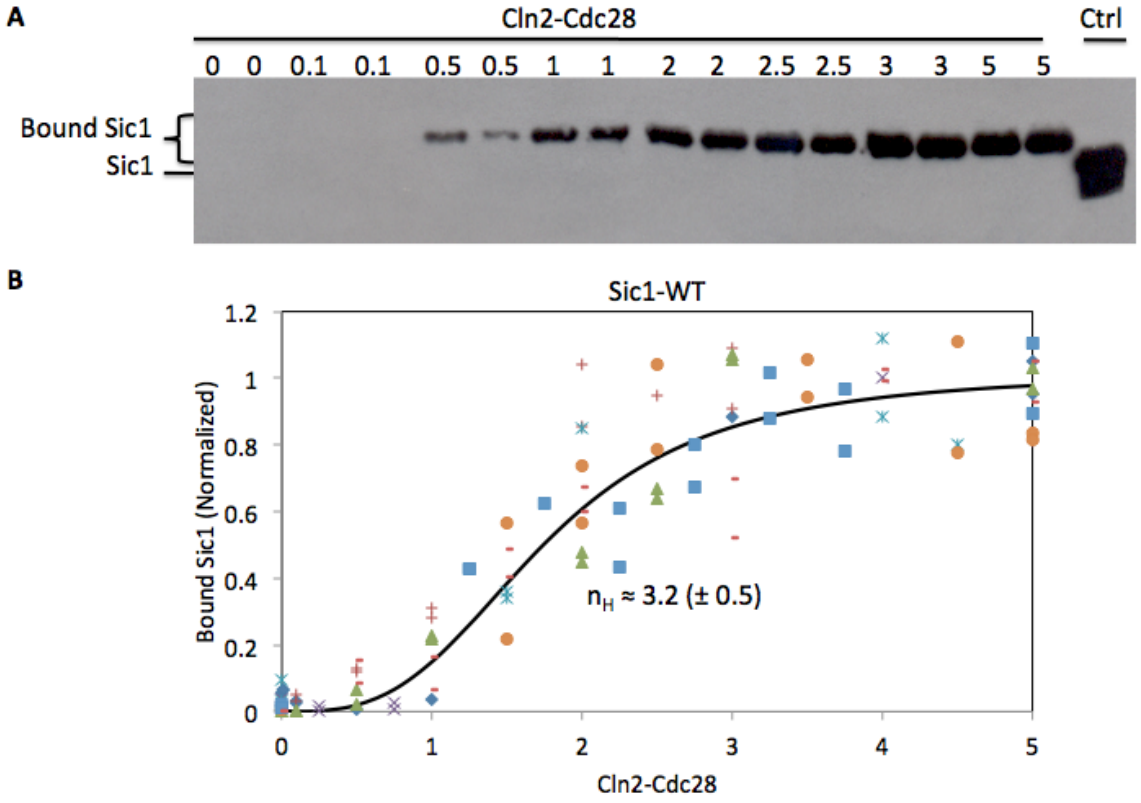

Figure 3.4: Response of wild-type Sic1 to Cln2-Cdc28 in binding to Cdc4. (A) Western blot from a representative experiment to measure Cdc4-bound Sic1 at various activities of Cln2-Cdc28 kinase complex.The Cdc4-bound fraction of Sic1 is visualized by immunoblotting using the C-terminus Sic1 antibody (Santa Cruz). (B) Ultrasensitive binding of Sic1 to Cdc4 in response to Cln2-Cdc28 based on 100 data points we observed from seven experiments. The Cdc4-bound fraction of Sic1 is quantified using ImageJ, normalized, pooled from seven experiments, and plotted against the amount of Cdc28 kinase complex and fitted to a three-parameter Hill function. The range of kinase activities was generated by 0-5 μl of purified Cln2-Cdc28 which roughly led to 0-25 nM of the enzyme.

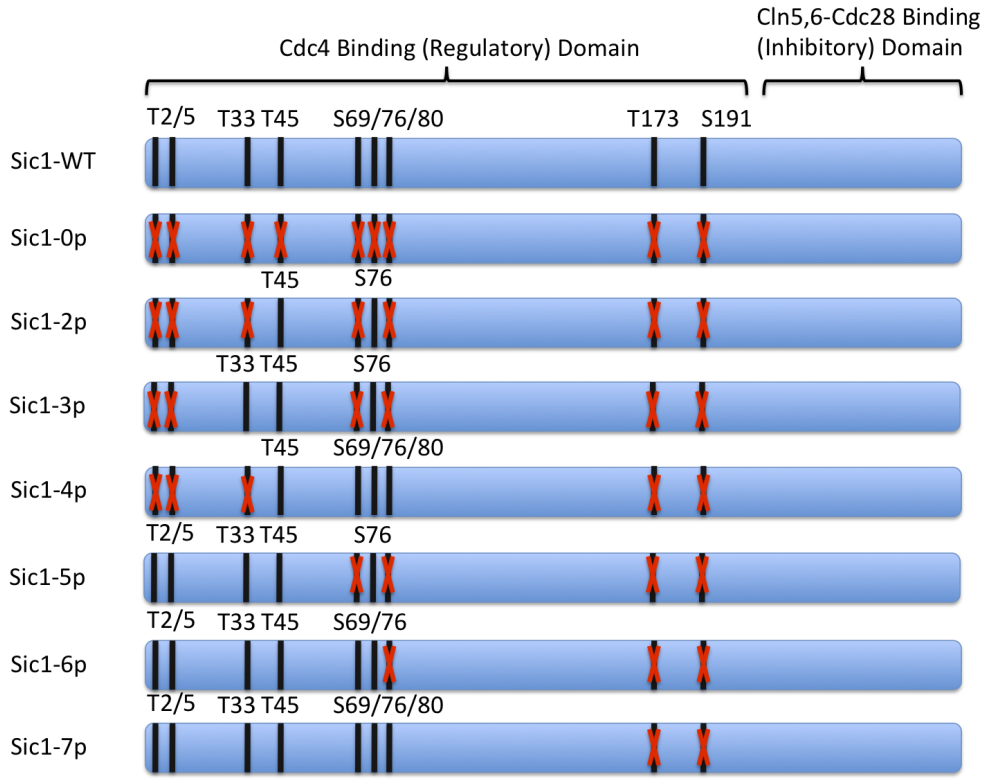

Figure 3.5: Sic1 wild-type and mutants used in this study. The wild-type Sic1 has nine Ser/Thr phosphorylatable sites for Cln2-Cdc28. In mutants, the indicated sites are mutated to Alanine.

we changed the fused Gst tag to a much shorter His tag suitable for top-down mass spectrometry analysis (Figure 3.5).

We observed that the Sic1 proteins with no available phosphosites, with two phosphosites (Thr45, Ser76), three phosphosites (Thr45, Ser76, Thr33), and four sites (Thr45, Ser69, Ser76, Ser80) did not show appreciable binding affinity for Cdc4 (Figure 3.6). Note that the sample results shown in Figure 3.6 may not be very convincing for Sic1-2p. We have conducted more binding experiments and Western blot analysis that confirm Sic1-2p does not bind appreciably to Cdc4. These were consistent with Nash's previous studies. However, the Sic1 protein with five available phosphosites (Thr45, Ser76, Thr33, Thr2, Thr5) binds Cdc4 *in vitro*. We believe this discrepancy is mainly due to differences in assay sensitivities. The six-(Thr45, Ser76, Thr33, Thr2,

Thr5, Ser69) and seven-(Thr45, Ser76, Thr33, Thr2, Thr5, Ser69, Ser80) phosphosite Sic1 proteins bind well.

We then measured the steady-state response of the five-, six-, and seven-site Sic1 to Cln2-Cdc28. Very intriguingly, the response curves of Sic1-5p and Sic1-6p are largely hyperbolic, with an equivalent Hill coefficient of 1.0 ± 0.2 and 1.2 ± 0.3, respectively (Figure 3.7 A and B). Whereas when another site is restored into Sic1-7p, the response curve becomes ultrasensitive and the Hill coefficient dramatically increases to 3.5 ± 0.5, a level comparable to that of the wild-type Sic1 (Figure 3.7C). Note that the exact values of the fitted Hill coefficients are not reliable and and the difference between 3.2 for the Sic1-WT and 3.5 for the Sic1-7p may not be meaningful.

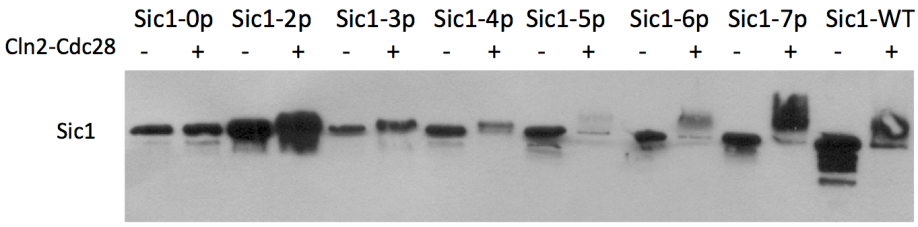

Figure 3.6: Binding of Sic1 variants to Cdc4 at the presence and absence of the Cln2-Cdc28 kinase. Mutants with four or less phosphorylatable sites do not show appreciable binding affinity.

3.4.3 The Saturated Level of Cdc4-Bound Sic1 Increases with the Number of Phosphosites

We also noted that the number of phosphosites affects not only the shape of Sic1's response curve, but also the saturated level of Cdc4-bound Sic1. The measured Cdc4-bound fraction at the plateau of the binding curve was larger for Sic1 proteins with more phosphosites available: about 2%, 6%, 8% and 10% for Sic-5p, Sic1-6p, Sic1-7p, and Sic1-WT, respectively. This phenomenon occurs if the binding to Cdc4 becomes stronger as the number of phosphorylated sites increases (i.e., phosphostates with more phosphorylates have higher affinity for Cdc4), as will be discussed later.

3.4.4 Mass Spectrometry Characterization of the Distribution of Phosphorylation States

To examine closely the phosphorylation state of Sic1 at different levels of kinase activity, we analyzed various Sic1 samples using a top-down mass spectrometry approach. Here we call Sic1 that is phosphorylated once phosphoform 1, Sic1 that is phosphorylated twice phosphoform 2, etc., without distinguishing exactly which sites are phosphorylated. As shown in Figure 3.4B, the binding curve of wild-type Sic1 is steepest between 1 and 2 μl, corresponding to a concentration of 5–10 nM. When the Sic1 samples treated with different levels of Cln2-Cdc28 were analyzed by mass spectrometry, we observed that the wild-type Sic1 was phosphorylated mostly on four or less sites in the initial lag phase of the binding curve, where the amount of Cln2-Cdc28 is less than 1 μl. However, the distribution shifts dramatically toward seven and higher orders of phosphorylated states as the amount of Cln2-Cdc28 increases to 5 μl (Figure 3.8A). Note that even at the saturated level, the protein was not fully phosphorylated and existed as a mixture of seven- to ten-site phosphoforms. The existence of a phosphoform with ten sites indicated another site in addition to the nine Ser/The-Pro residues described earlier. This could be one of the non-Ser/Thr-Pro sites previously described [16].

We also examined the distribution of phosphoforms at the saturated level for three Sic1 mutants, of which we measured the steady-state binding curves. As shown in Figure 3.8B-D, maximally phosphorylated Sic1 exists as a mixture of all possible phosphoforms with up to six or seven phosphorylated sites in mutants Sic1-5p and Sic1-6p, whereas Sic1-7p exhibits a narrow distribution of 7p–9p phosphoforms. Here we again observed the presence of other non-Ser/Thr-Pro sites, which will require further investigation in our future work. These different distributions of phosphoforms in the Sic1 variants underlie their different ultrasensitivity properties.

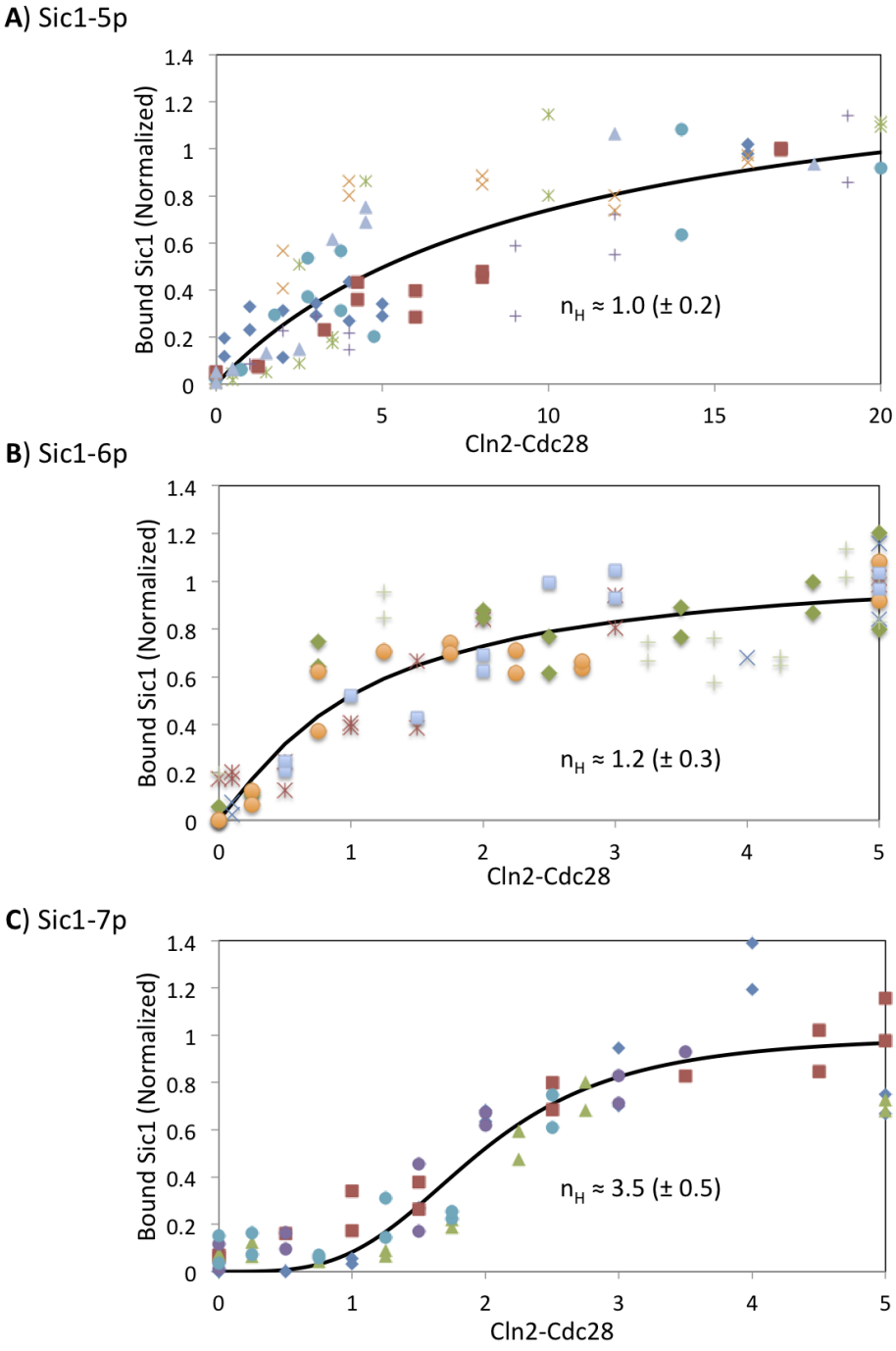

Figure 3.7: Response of Sic1 mutants to Cln2-Cdc28 in binding to Cdc4. The normalized bound fraction of five-site Sic1 (A), six-site Sic1 (B), and seven-site Sic1 (C) is plotted against the increasing activity of Cln2-Cdc28.

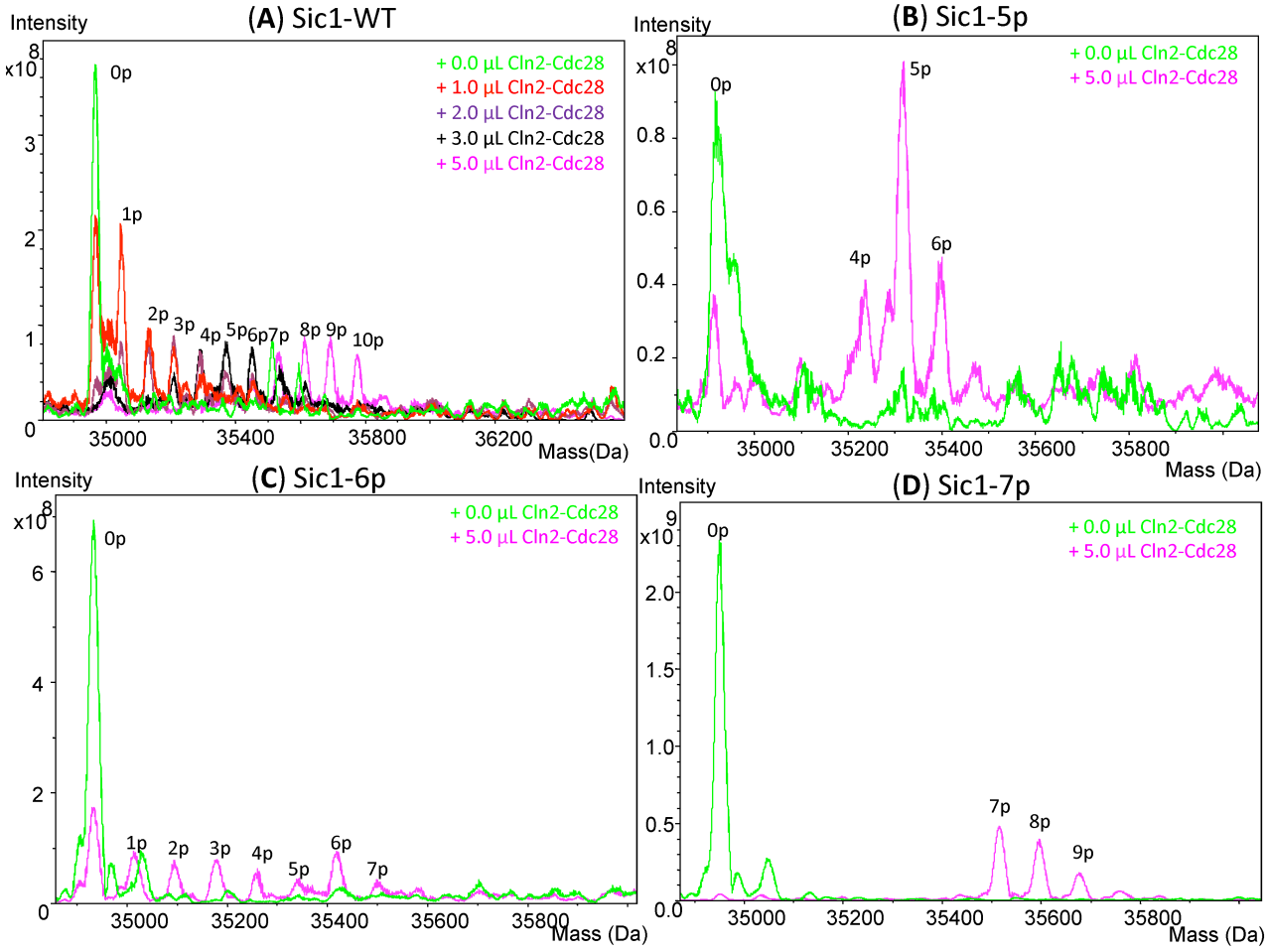

Figure 3.8: Distribution of phosphoforms obtained from mass spectrometry top-down analysis. Mass spectra show the relative distribution of phosphoforms at various levels of Cln2-Cdc28 in wild-type Sic1 (A), five-site Sic1 (B), six-site Sic1 (C), and seven-site Sic1 (D). (These data are produced in collaboration with Håkansson Lab.)

3.5 Discussion and Conclusion

To unravel the mechanism underlying the observed ultrasensitivity behavior of Sic1, we set out to investigate theoretically how ultrasensitivity can arise in such a system from multisite phosphorylation. We consider protein Sic1 containing n phosphorylation sites and assume the protein is "functional" when more than m sites are phosphorylated. Here by "functional" we mean affinity for binding to Cdc4; i.e., Sic1 phosphoforms phosphorylated on four or less sites are inactive and the higher-order of phosphoforms are considered active. The phosphorylation reaction is distributive and proceeds in a random order; the dephosphorylation reaction is also distributive and proceeds randomly too. The total amount of Cdc4 protein is constant and we assume it is about twice the amount of Sic1 based on our experimental study. Such a system can be modeled by a series of ordinary differential equations (ODEs) and be solved to steady states numerically with MATLAB. There are three important sets of parameters: the phosphorylation rate constants, the dephosphorylation rate constants, and the Sic1-Cdc4 association/dissociation rate constants. We explored this large parameter space to investigate exactly how the steady-state response curves of Sic1 can exhibit the following observed features:(i) "shape", and (ii) "saturation".

Upon extensive search in the parameter space, we noted that the experimentally observed Sic1-Cdc4 binding curves could be reproduced theoretically (Figures 3.9 and 3.10) under the following conditions: (i) the ratio of phosphorylation to dephosphorylation becomes larger as phosphorylation proceeds, and (ii) the Sic1-Cdc4 binding rate constant becomes as stronger as phosphorylation proceeds. The first condition enhances ultrasensitivity by promoting the multistep phosphorylation reaction as it proceeds. This type of cooperativity between phosphorylation sites was also suggested previously for Cdc25C [123] and Ste5 [124]. The second condition is necessary to achieve different levels of saturation for different mutants and wild-type.

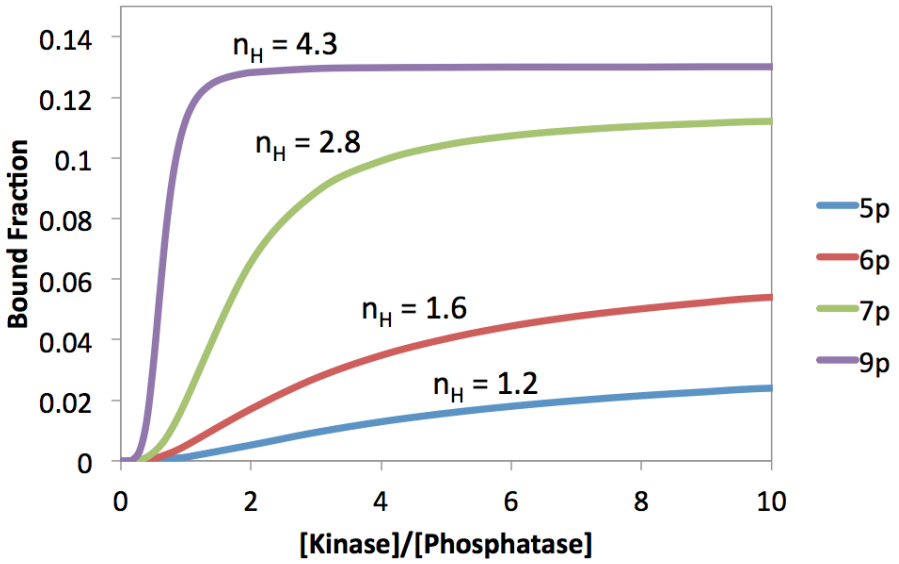

Figure 3.9: Modeling results for substrate protein with various number of sites. The threshold site number for binding is set at five. The total normalized amount of multisite substrate protein, the binding partner, and the phosphatase is set at 1, 2, and 1, respectively. The phosphorylation rate constant of phosphoforms with more than five phosphate groups is set four times greater than that of phosphoforms with zero to five phosphate groups (4 and 1, respectively). The association rate constant for the binding reaction from phosphoform-0 to phosphoform-9 is 0, 0, 0, 0, 0, 0.02, 0.04, 0.07, 0.08, 0.08 in order. All the dissociation and dephosphorylation rate constants are set at 1.

We hypothesize that ultrasensitive binding of Sic1 to Cdc4 in response to Cln2-Cdc28 we have observed *in vitro* is inherently related to its switch-like degradation *in vivo* and ultimately leads to the precise G1/S transition. Nevertheless, additional factors may also contribute to the switch-like Sic1 elimination process *in vivo*. The most important one is believed to be the positive feedback exerted by liberated Clb5,6-Cdc28. Clb5,6-Cdc28 is released from Sic1 while the 26S proteasome actively extracts, unfolds, and degrades ubiquitinated Sic1 [125]. Clb5,6-Cdc28 can phosphorylate Sic1 subsequently [60]. This positive feedback further enhances Sic1's ultrasensitivity. Another factor might be the involvement of kinases other than Cln2-Cdc28. Sic1 is phosphorylated by multiple kinases, which can differentially affect the stability of Sic1 and consequently the progression through G1. In our experiment, we used

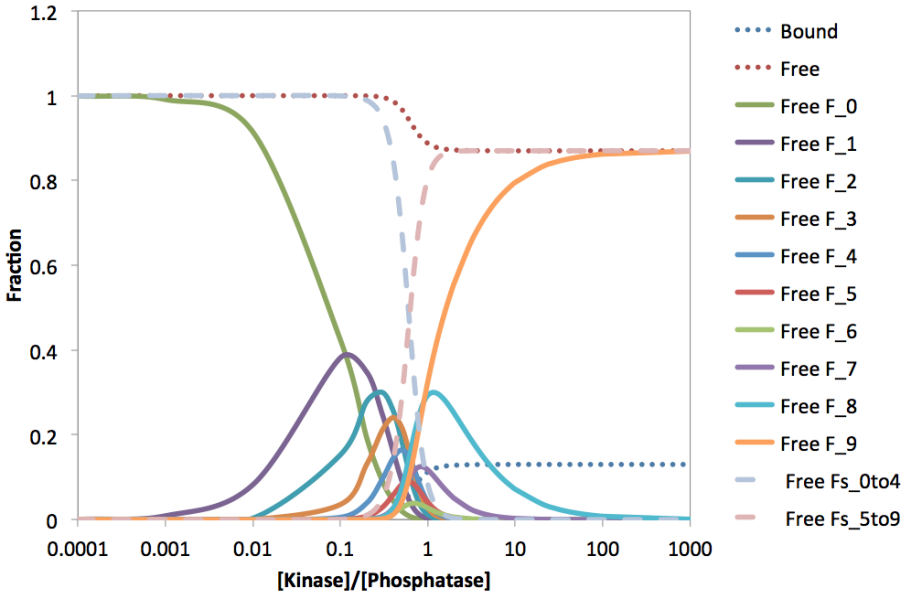

Figure 3.10: Simulated populations of phosphoforms at the saturated level of the kinase. The substrate has nine phosphorylation sites in total and binds to the partner protein upon phosphorylation on five sites. The graph shows the total amounts of substrate protein in free (Free) and bound (Bound) forms. It also shows the fraction of each free phosphoform. For example, "Free F−0" represents free phosphoform-0p. "Free Fs−0to4" represents the total amount of free phosphoforms with less than five phosphorylated sites. The total normalized amount of multisite substrate protein, the binding partner, and the phosphatase is set at 1, 2, and 1, respectively. The phosphorylation rate constant of phosphoforms with more than five phosphate groups is set four times greater than that of phosphoforms with zero to five phosphate groups (4 and 1, respectively). The association rate constant for the binding reaction from phosphoform-0 to phosphoform-9 is 0, 0, 0, 0, 0, 0.02, 0.04, 0.07, 0.08, 0.08 in order. All the dissociation and dephosphorylation rate constants are set at 1.

purified Cln2-Cdc28. However, other G1 cyclins, such as Cln1, in complex with Cdc28 may also contribute to phosphorylation of Sic1. As another example, Pho85, when complexed with Pcl1, a G1 cyclin homologue, can phosphorylate Sic1 *in vitro*, and Sic1 appears to be more stable in Pho85Δ cells [101]. CK2 phosphorylates Sic1 *in vivo* on Ser201 shortly after its *de novo* synthesis during late anaphase in glucose-grown cells [103, 126, 127].

In this work, we have shown that the steady-state Sic1-Cdc4 binding in response to the increasing activity of Cln2-Cdc28 in yeast G1 extract is ultrasensitive. The

apparent Hill coefficient of the wild-type response is about 3.2. The ultrasensitivity decreases as the number of phosphorylatable site decreases from nine to five ($n_H \simeq 1.0$). In our *in vitro* assays, mutant Sic1 proteins with four or less phosphorylatable sites do not bind to Cdc4. We also observed that the Cdc4-bound fraction of Sic1 at the saturated kinase level increases as the number of phosphorylatable sites increases. Our mass spectrometry analysis showed that the wild-type Sic1 is phosphorylated mostly on four or less sites in the initial lag phase of the binding curve, and the distribution shifts dramatically toward five and higher orders of phosphoforms as the concentration of Cln2-Cdc28 further increases. This work represents the first in-depth characterization of Sic1 in terms of its ultrasensitivity property and the role of multisite phosphorylation. The obtained experimental results, combined with our modeling analysis, suggest the mechanism through which Sic1's ultrasensitivity arises from multisite phosphorylation and provide hypotheses that can be tested in future work.

CHAPTER IV

Minimum Protein Oscillator Based on Multisite Phosphorylation and Dephosphorylation

4.1 Summary

We propose a novel minimum oscillator whereby a protein with multiple phosphorylation sites directly embedded in a negative feedback loop can exhibit oscillation. We demonstrate that if the fully phosphorylated substrate inhibits the first phosphorylation step in a cooperative manner, multisite substrates can exhibit oscillatory behavior at the presence of a kinase and phosphatase. With a fixed number of sites, the nonlinearity of the negative feedback and the substrate/enzyme ratio must be above certain threshold values to generate undamped oscillation. There is an inverse relationship between the number of phosphorylation sites and the minimum nonlinearity of the negative feedback required for oscillation; i.e., the ultrasensitivity and time delay rooted in multisite phosphorylation compensate for the explicit nonlinearity in the negative feedback. The period and amplitude of oscillation are mainly determined by the number of phosphorylation sites and the substrate/enzyme ratio. Our results suggest that a multisite protein can be exploited for the construction of a synthetic protein oscillator featuring simplicity, robustness and tunability.

4.2 Introduction

Biochemical oscillations arise in diverse biological processes related to metabolism, signaling and development [128, 129]. Well-studied examples include glycolysis [130–132], eukaryotic cell cycle control [133–135], and circadian rhythms [136]. Understanding the design principles of these rhythmic cellular behaviors has attracted tremendous interest in the past several decades due to their important biological roles and intriguing mathematical properties [137–139]. Combined theoretical and experimental study of natural systems has yielded increasing insights on the underlying mechanisms. Novak & Tyson [129] described four essential requirements of biochemical oscillators as (i) negative feedback to return the system to its initial state; (ii) time delay to prevent the reaction network settle on a stable steady state; (iii) nonlinear interactions to destabilize the steady state; and (iv) proper timescales of producing and consuming reactions to generate oscillations. An important class of biochemical oscillators arises in signaling pathways involving cascades of phosphorylation/dephosphorylation (P/D) reactions. A number of models have been proposed to investigate such oscillations such as coupled P/D cycles of Cdc25 and the marturation-promoting factor (MPF) [140], cyclin-dependent-kinase-related P/D cascades in eukaryotic cell cycle [133], and MAPK cascades [141, 142].

More recently, engineering of synthetic oscillators have emerged as an alternative way for exploring and testing the design principles of biomolecular oscillations. In addition, these synthetic oscillators can potentially be utilized in various biotechnology applications such as gene therapy. A number of designs with increasing robustness and tunability have been successfully demonstrated in bacteria [40, 41, 143, 144] or mammalian cells [145]. It is interesting to note that whereas natural oscillators occur with a wide spectrum of metabolic, signaling and gene regulation networks, all except one current synthetic oscillators have been constructed based on transcriptional regulations.

As previously noted [129], sufficient nonlinearity, often described as an ultrasensitive stimulus-response relationship, is critical for generating oscillation in a negative-feedback-containing network. The required ultrasensitivity can arise from a variety of mechanisms such as ligand cooperativity [3], operating in the zero-order region of enzymes [1], or positive feedback loops [146, 147]. Recently, it has been proposed that multisite phosphorylation, a common feature of many protein kinase substrates, could be another source for ultrasensitivity [17, 23]. On the other hand, we noticed an intriguing oscillatory system centered around KaiC, a protein with multiple phosphorylation sites that plays a critical role in enabling the circadian clock of cyanobacteria. KaiC interacts with two other proteins (KaiA and KaiB) and its phosphorylation level oscillates with a circadian period [148, 149]. Most remarkably, this three-protein clock can be reconstituted *in vitro* [150, 151]. Inspired by this natural oscillator and the aforementioned theory on multisite based ultrasensitivity, we hypothesize that embedding a single protein with multiple phosphorylation sites within a simple negative feedback loop could lead to well-sustained oscillations. Not only will the multistep P/D process create time delay, it will also enhance substantially the nonlinear interactions in the network. The objective of this chapter is to investigate systematically the condition under which P/D of a single multisite protein can generate undamped oscillation. It should be noted that Chickarmane *et al.* [152] analyzed a related specific case where a two-site protein exhibits oscillatory behavior when its fully phosphorylated form represses the production of the kinase. In this paper, we examine a general model featuring an alterable number of phosphorylation sites and a structurally simple negative feedback. We will show quantitatively how multisite phosphorylation compensate for nonlinearity in the negative feedback. Important parameters that affect the stability of the response and determine the oscillation amplitude and period will also be identified.

4.3 Methods

To explore the feasibility of creating a minimum protein oscillator based on multisite P/D of a single protein, we developed a detailed ordinary differential equation (ODE) model of the system and investigated systematically the effects of various parameters. The key components of the model include: multisite phosphorylation/dephosphorylation reactions; a negative feedback through the inhibition of the first phosphorylation step by the fully phosphorylated substrate protein; and initial condition specifications.

4.3.1 Model Description

We consider a protein substrate, S, with n phosphorylation sites in the presence of a kinase and a phosphatase in a closed system. We assume that P/D reactions proceed distributively, which means after substrate-enzyme association, at most one phosphate group can be added to or removed from the substrate before dissociation of the complex. Therefore, all partially phosphorylated forms of the protein are generated. The number of distinguishable phosphorylated species depends on how P/D reactions proceed. In two extreme cases, reactions might proceed fully randomly or fully sequentially. In this chapter, we focus on sequential P/D.

According to the Michaelis-Menten mechanism of enzymatic reactions, the substrate and enzyme react to form a substrate-enzyme complex which can in turn dissociate to form either the enzyme and substrate, or the enzyme and the product Figure 4.1. We consider these elementary reactions involving enzyme-substrate complexes in our model. This closed system contains $3n+1$ species and it can be described readily with a set of governing ODEs.

Assuming that ATP is abundant, the concentration of each form of the substrate

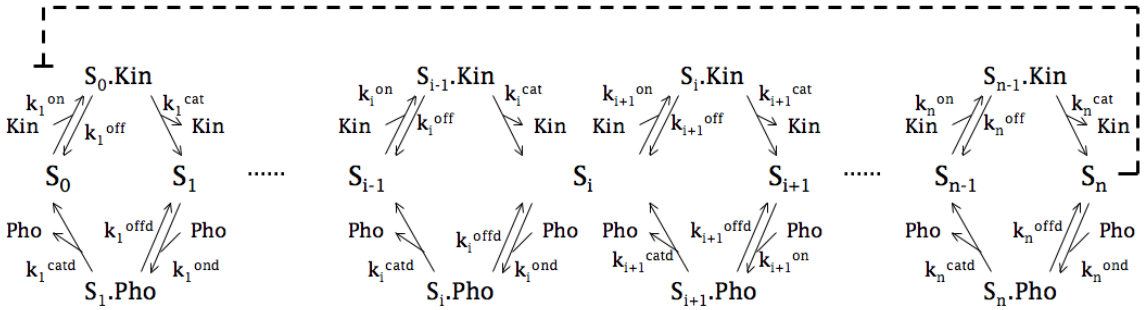

Figure 4.1: Sequential phosphorylation and dephosphorylation of an n-site protein with a negative feedback.

changes as follows:

$$\frac{d[S_0]}{dt} = -k_1^{on}[Kin][S_0] + k_1^{off}[S_0.Kin] + k_1^{catd}[S_1.Pho] \tag{4.1a}$$

$$\begin{aligned}\frac{d[S_i]}{dt} =& - k_{i+1}^{on}[Kin][S_i] + k_{i+1}^{off}[S_i.Kin] + k_{i+1}^{catd}[S_{i+1}.Pho] \\ & - k_i^{ond}[Pho][S_i] + k_i^{offd}[S_i.Pho] + k_i^{cat}[S_{i-1}.Kin], \quad i = 1, ..., n-1\end{aligned} \tag{4.1b}$$

$$\frac{d[S_n]}{dt} = -k_n^{ond}[Pho][S_n] + k_n^{offd}[S_n.Pho] + k_n^{cat}[S_{n-1}.Kin] \tag{4.1c}$$

$$\frac{d[S_{i-1}.Kin]}{dt} = k_i^{on}[Kin][S_{i-1}] - (k_i^{off} + k_i^{cat})[S_{i-1}.Kin], \quad i = 1, ..., n \tag{4.1d}$$

$$\frac{d[S_i.Pho]}{dt} = k_i^{ond}[Pho][S_i] - (k_i^{offd} + k_i^{catd})[S_i.Pho], \quad i = 1, ..., n \tag{4.1e}$$

where $[Kin]$, $[Pho]$ and $[S_i]$ represent concentrations of the kinase, the phosphatase and the substrate phosphorylated on i sites, respectively. k^{on}, k^{off} and k^{cat} stand for the rate constants of kinase-substrate association, dissociation and phosphorylation reactions, respectively. Similarly, k^{ond}, k^{offd} and k^{catd} are the corresponding

parameters for dephosphorylation. We assume that the total amounts of kinase and phosphatase remain constant in the system and thus their free forms can be determined as follows:

$$[Kin] = Kin_T - \sum_{i=0}^{n-1} [S_i.Kin] \tag{4.2a}$$

$$[Pho] = Pho_T - \sum_{i=1}^{n} [S_i.Pho] \tag{4.2b}$$

where Kin_T and Pho_T are the total amount of kinase and phosphatase, respectively.

4.3.2 Negative Feedback

To generate oscillation of the various species in the above phosphorylation and dephosphorylation chain, a negative feedback is required [129]. We propose a very simple network topology in which the negative feedback loop is formed by the fully phosphorylated species inhibiting the first phosphorylation step (see Figure 4.1). Furthermore, we assume that this inhibition of the association between S_0 and the kinase by S_n can be approximated by a Hill type function, which is widely used as a high-level description of nonlinear inhibitions in various processes such as transcription [40] and kinase signaling [141].

$$k_1^{on} = k_1^{on0} \frac{1}{1 + [S_n]^p} \tag{4.3}$$

where k^{on0} is the maximum rate constant for S_0-kinase association and p represents the nonlinearity of the negative feedback.

4.3.3 Initial Condition

We assume that initially the substrate protein is in the non-phosphorylated form and responds to sudden introduction of the kinases and phosphatase, which corresponds to the following initial conditions:

$$t = 0 : [S_0] = S_T, [Kin] = Kin_T, [Pho] = Pho_T$$
$$\text{Concentrations of all other species are zero.} \tag{4.4}$$

where S_T is the total concentration of the substrate protein in this closed system.

We have investigated systematically the above ODE model with numerical solvers in MATLAB 7.1. Each condition we have explored is described by a specific combination of values for four categories of parameters:
(i) the number of phosphorylation sites (n);
(ii) nonlinearity of the negative feedback (p);
(iii) kinetic parameters (k^{on}, k^{off}, k^{cat}; k^{ond}, k^{offd}, k^{catd}); and
(iv) total amounts of substrate and enzymes (S_T, Kin_T, Pho_T).

We focused on examining the dynamic profile of the various states of the substrate to identify conditions for generating sustainable oscillation. In addition, we were interested in what determine the period and amplitude of the oscillation when it occurs.

4.4 Results

4.4.1 Conditions for Sustainable Oscillation

We started with a single-site protein. We systematically explored a wide range of p values, kinetic parameters, as well as total amounts of substrate and enzymes.

The system always reached a steady state. We conjectured that adding more phosphorylation sites might cause oscillation as it would introduce time delay as well as nonlinearity in the response of the substrate to the enzymes. Therefore, we proceeded to the examination of multi-site proteins. For simplicity, we fixed the kinetic parameters using values reasonable for real biological systems [92] ($k^{on} = 10\mu M^{-1}s^{-1}$, $k^{off} = 10s^{-1}$, and $k^{cat} = 1s^{-1}$ for both phosphorylation and dephosphorylation).

Interestingly, our simulation results showed that adding phosphorylation sites could indeed make the system unstable. As an example, the oscillatory behavior of a nine-site protein is shown in Figure 4.2. We systematically explored a large parameter space by examining combinations of parameter values in wide ranges and found that concentrations of different phosphostates of the substrate are oscillatory under proper conditions. By "proper conditions", we mean i) the number of phosphorylation sites, n, is sufficiently large; ii) the nonlinearity of the negative feedback, p, is sufficiently high; and iii) the ratio between total substrate and total enzyme concentrations, S_T/E_T, is sufficiently large. The boundaries between the sustainable oscillation region and the stable steady state one in the parameter space, i.e. where bifurcation occurs, were determined numerically.

4.4.1.1 Nonlinearity in Feedback versus Number of Phosphorylation Sites

When there are enough phosphorylation sites, the degree of nonlinearity of the negative feedback, depicted by p, is the most important parameter in determining whether or not the system oscillates. As the number of phosphorylation sites increases, a smaller p value is required to generate oscillation, as summarized in Figure 4.3. For instance, p is required to be greater than seven for $n = 2$; whereas, for $n = 5$, a p value as low as three is enough. However, this effect of the number of phosphorylation sites on reducing the minimum nonlinearity requirement lessens when n is larger than six. At this point, the chain of the phosphorylation reaction is

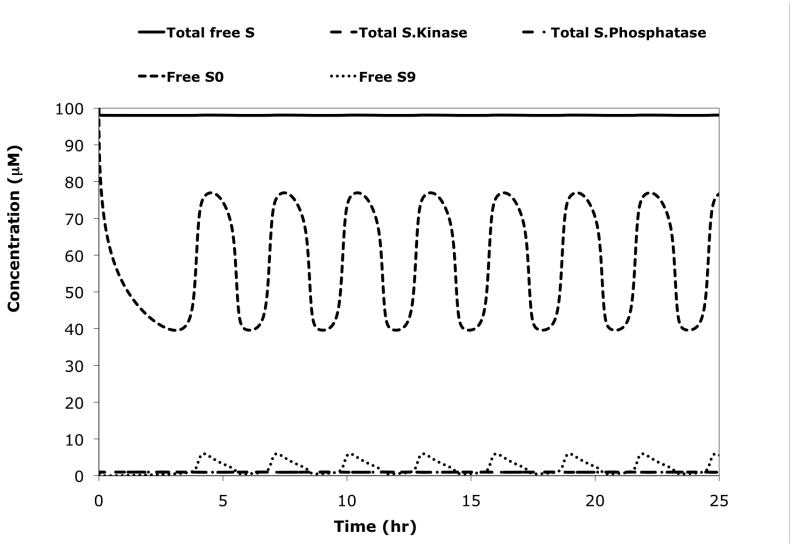

Figure 4.2: Oscillatory behavior of a nine-site protein.The concentrations of enzyme-substrate complexes are so small that they are almost unobservable in the graph. Parameters: $p = 3$; $S_T = 100\mu M, E_T = Kin_T = Pho_T = 1\mu M$.

long enough that increasing the number of intermediates will not affect the dynamics of the system.

It should be noted that although the fraction of the substrate bound to the enzymes is negligible compared to the fraction of free substrate when the concentration of the substrate is much larger than the concentration of the enzymes (Figure 4.2), omitting the steps of substrate-enzyme binding from the model affects the behavior of the system qualitatively. For instance, $n = 2$ does not show any oscillatory behavior under any condition and the minimum number of phosphorylation sites required for oscillation increases to three. This observation highlights the importance of appropriate modeling in investigating the dynamic behavior of a system.

4.4.1.2 Substrate/Enzyme Ratio versus Number of Phosphorylation Sites

The ratio of total substrate over total enzyme concentrations, which is specified by the initial condition in our model, is another important factor that determines whether or not the system is stable. This parameter, S_T/E_T , needs to be sufficiently large to generate oscillation. It has been observed that this minimum ratio is much

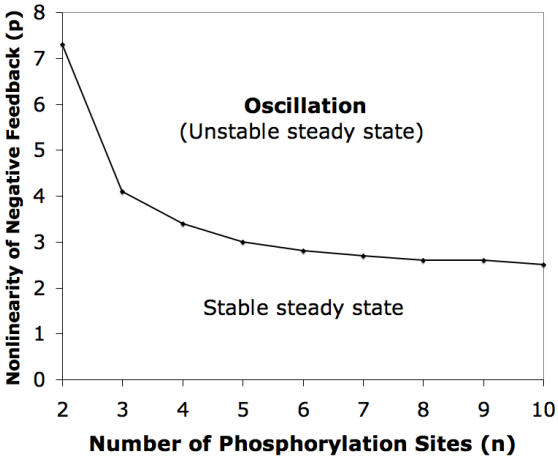

Figure 4.3: Nonlinearity of the negative feedback required for generating oscillatory behavior.

larger than one, which can be easily satisfied for almost all *in vitro* and many *in vivo* enzymatic reactions. Setting the concentration of kinase and phosphatase at 1 μM, we determined the minimum substrate concentration (within 5 μM error) required for generating oscillation with different numbers of phosphorylation sites for a negative feedback of $p = 4$ (Figure 4.4). The minimum substrate/enzyme ratio was not calculated for two-site and three-site proteins because they always reach steady state when $p = 4$ (Figure 4.3).

From four sites to six sites, the minimum substrate/enzyme ratio decreases sharply and then stays unchanged from $n = 6$ to $n = 9$ and then increases slowly. Having more sites means more intermediates and therefore more time-delay and more ultrasensitive responses of the substrate to the enzyme, which are in favor of oscillation. Thus, by increasing the number of phosphorylation sites, the system can oscillate in a larger space of the substrate concentration, i.e., the minimum decreases. On the other hand, increasing the number of sites and intermediate forms causes the amount of the fully phosphorylated substrate to decreases, which may never reach the threshold concentration for activating the negative feedback required for oscillation. Therefore, a larger amount of the substrate is required as n increases.

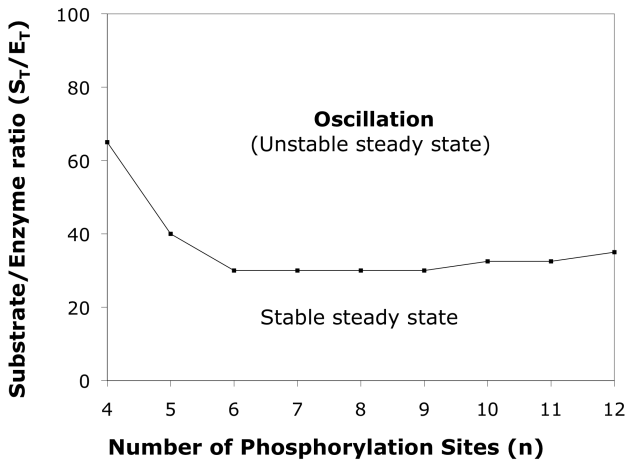

Figure 4.4: Minimum ratio of substrate/enzyme required for generating oscillatory behavior ($p = 4$).

Our simulation results also showed that the initial state of the substrate is not important. Starting with a non-phosphorylated substrate, or its fully phosphorylated form, or a combination of different phosphorylated forms all lead to the same results.

4.4.2 Period and Amplitude

In addition to conditions for sustainable oscillation, we also examined systematically two of the most important properties of oscillation when it occurs: period (or frequency) and amplitude. We define amplitude as the peak-to-valley concentration difference of the non-phosphorylated form of the substrate normalized by the total substrate concentration (i.e. $[S_0]/S_T$). We report here the effect of three parameters: (i) the number of phosphorylation sites (n); (ii) nonlinearity of the negative feedback (p), and (iii) substrate/enzyme ratio (S_T/E_T).

First, it was found that both the oscillation period and amplitude increases as the number of phosphorylation sites rises. As illustrated in Figure 4.5A, when $p = 3$ and $S_T/E_T = 1000$, a protein with five or more sites oscillates. The period lengthens from 12 hours for $n = 5$ to 444 hours for $n = 15$; while the amplitude enhances from 19% for $n = 5$ to 56% for $n = 15$. This qualitative overall trend is understandable with simple

intuition. As more phosphorylation sites are added, the reaction pathway becomes longer, which ultimately lengthens the period and boost the amplitude by allowing more time for the species to change their concentrations. However, it is worth noting that the ranges of period and amplitude obtained from quantitative simulation are remarkable. Second, interestingly, parameter p, representing the degree of nonlinearity of the negative feedback, has only a very minor effect on the period and amplitude (Figure 4.5B) even though it is a critical parameter determining whether oscillation occurs or not. Finally, the period of oscillation depends strongly on the ratio between the total substrate concentration and the total enzyme concentrations, S_T/E_T, while the amplitude is not affected significantly by this parameter (Figure 4.5C). For example, for $n = 5$ and $p = 3$, when the ratio is doubled from 750 to 1500, the period increases from 8 hours to 22 hours.

4.5 Discussion and Conclusion

Oscillations arising from phosphorylation and dephosphorylation in metabolic and signaling cascades have been studied previously [128]. However, P/D of a single protein has not been proposed as a potential source of oscillation to best of our knowledge. In this work we investigate theoretically the dynamic behavior of a multisite protein embedded in a negative feedback loop and show that different phosphorylated forms of a multisite substrate can oscillate under proper conditions.

In the proposed network for sustainable and tunable protein oscillations, one key component is the highly nonlinear negative feedback implemented through the inhibition of the first phosphorylation step by the fully phosphorylated substrate. Important features of this inhibition include: threshold in phosphorylated sites for functioning, nonlinearity or cooperativity in the negative feedback, and the effect on the first phosphorylation step. Each of these features can be found in known protein interaction processes. First, multisite phosphorylation is responsible for triggering various

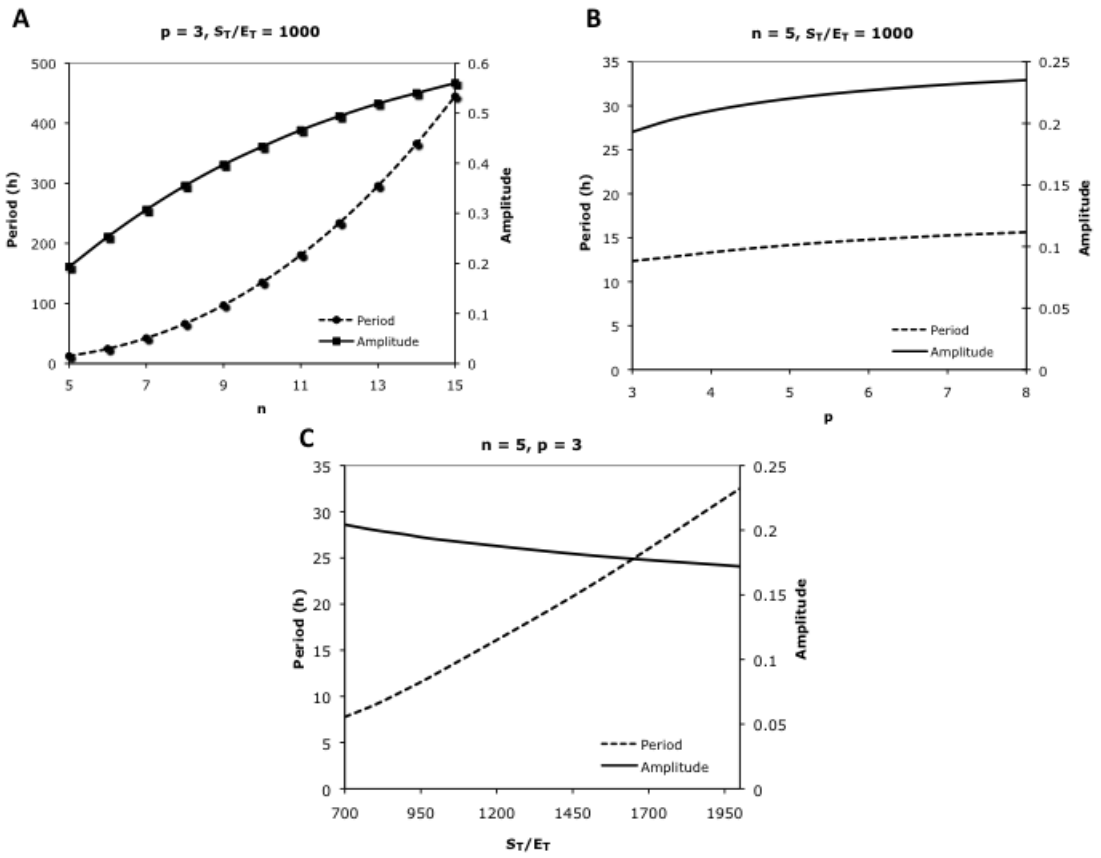

Figure 4.5: Dependency of oscillation period and amplitude on the number of phosphorylation sites, n (A), the nonlinearity of the negative feedback, p (B), and the substrate/enzyme ratio, S_T/E_T (C).

processes such as ubiquitination. For example, yeast protein Sic1 has nine phosphorylation sites and phosphorylation on six sites is required to be targeted by protein SCF^{Cdc4} for binding and subsequent ubiquitination [17, 109, 118, 153]. Second, with regard to nonlinearity or cooperativity, many proteins assemble as oligomers in functional forms. For example, protein KaiC in cyanobacteria forms a hexamer, which in turn binds to a dimer of another protein KaiA, to carry out autokinase activity [151, 154, 155]. The degree of cooperativity arising from a hexamer can be as high as six. Finally, it is possible to restrict the inhibitory effect to the first phosphorylation step if two kinases are involved and one introduces the first phosphate group as a requirement for further phosphorylation by the other kinase. This "priming" mech-

anism has been observed for protein substrates such as glycogen synthase [156, 157], β-Catenin [91], and insulin receptor substrate-2 [158]. Existing biomolecular processes such as those described above suggest that it might be feasible to construct experimentally the minimum protein oscillator studied in this work. However, it remains a challenge to identify suitable parts from nature or engineer proteins with desirable characteristics, and to assemble them into the proposed oscillator that does not rely on transcriptional regulation.

Proper modeling of biochemical reactions is very important for predicting system dynamics. For example, our results would be different if we disregard the intermediate enzyme-substrate complexes, although the fraction of the substrate bound to the enzymes is negligible compared to the fraction of free substrate when the concentration of the substrate is much larger than the concentration of enzymes (Figure 4.2). If we neglect this fraction, which is the case in many theoretical models, the number of intermediates will be smaller and a more nonlinear negative feedback will be required. Another characteristics of our model is the negative feedback exerted by the fully phosphorylated substrate on the first step of phosphorylation. We used a simple Hill function, Eq. (4.3), to represent the nonlinearity of this feedback without assuming specific underlying molecular mechanisms. The exact quantitative results we have obtained depend on this particular mathematical form. Nevertheless, the general qualitative conclusions, such as the relationship between the number of phosphorylation sites and the minimum feedback nonlinearity required for oscillation, are likely to hold for other mathematical forms and for inhibitions resulted from various molecular interactions.

We have focused on sequential phosphorylation and dephosphorylation. Random phosphorylation and dephosphorylation may also be utilized in biology as it provides more intermediate forms of the phosphorylated protein and allows more flexibility and evolvability for protein regulation. It can be shown that many of the qualitative

relationships describe above for sequential processes also apply to random systems. For example, as the total number of sites increases, the minimum nonlinearity of the negative feedback required for oscillation decreases. However, these relationships may be quantitatively different. For instance, with the same number of sites and feedback nonlinearity, the minimum substrate/enzyme ratio required for oscillation in a random process is larger than that for its sequential counterpart.

The sequential P/D system we have explored is topologically similar to a linear metabolic pathway, which could oscillate under certain conditions if the first enzyme is inhibited cooperatively by p molecules of the end product of the pathway [159]. However, there are also notable differences. Most importantly, the enzymes for consecutive reactions in a linear metabolic pathway are generally different, whereas the multi-step phosphorylation/dephosphorylation reactions are all catalyzed by the same kinase/phosphatase. Having the kinase and phosphatase exert effect on successive reactions leads to ultrasensitive response of the substrate, which could reduce the requirement of nonlinear interactions in other parts of the network. For instance, with a linear metabolic pathway, it was conjectured that the system cannot show sustainable oscillation when $n = 2$ unless $p > 8$ [160]; while in our sequential P/D system, the nonlinearity requirement on p is slightly lower for $n = 2$ (Figure 4.3).

In conclusion, our results suggest that a multisite protein in a negative feedback loop could potentially serve as a building block for generating oscillation. It remains to be seen whether such a simple network involving only a multisite protein and its kinase/phosphatase is employed by nature as a biochemical oscillator. On the other hand, it might be worth exploiting multisite proteins in constructing synthetic oscillators, which could not only shed lights on the functioning of natural oscillations, but also be utilized in bioengineering applications. The proposed oscillator features several desirable properties: (i) simplicity (no transcription involved); (ii) large parameter space for generating sustainable oscillations; and (iii) high tunability

in period and amplitude. Substantial knowledge on various protein interactions as well as creativity will be needed to design and construct the proposed circuitry.

CHAPTER V

Design of and Preliminary Experimentation with a Protein Degradation Switch Using Multiple Interaction Domains

5.1 Summary

Targeted protein degradation in eukaryotic cells requires recruitment of the target protein to proteasome which is usually triggered by ubiquitination of the target protein. One intriguing way to bypass the ubiquitination step is via artificial induction of target protein and proteasome dimerization. A natural dimerizing molecule, rapamycin, has been used to localize the target protein to the proteasome. In this design, the Rpn10 subunit of *Saccharomyces cerevisiae*'s proteasome is fused with Fpr1, and the target protein is fused with the Fpr1-rapamycin binding domain of Tor1. Upon adding rapamycin to the cell culture medium, Fpr1 and Tor1 domains come together and hence the target protein is localized to the proteasome and degrades. After conducting a brief theoretical study, we suggested that increasing the number of binding modules would lead to faster degradation. We constructed a series of differently tagged proteins to test our hypothesis. Various single, double, and triple tags with different combinations of wild-type and mutated Tor1 domains (14 combinations in total) were constructed and fused to a target protein Ura3. The temporal profile

of Ura3 in response to rapamycin has been measured in various constructs, and the half-life of the Ura3 protein has been estimated accordingly.

5.2 Introduction

Recent advances in synthetic biology have greatly increased our capability to manipulate intracellular processes. In particular, inducible targeted protein degradation, that has the potential for numerous biotechnological and medical applications, has attracted increasing attention for research [55, 161]. This approach aims to directly manipulate a target protein by specifically manipulating its stability, whereas alternative strategies such as promoter shutdown and RNA interface interference with the gene transcription and translation, respectively.

Protein degradation in eukaryotic cells requires recruitment of the target protein to the proteasome and is usually triggered by ubiquitination of the target protein [162]. A number of synthetic systems have been constructed to artificially recruit the target protein to the proteasome in an inducible and tunable manner [53, 56, 163, 164]. One intriguing way is through induced dimerization of the target protein and the proteasome using naturally occurring dimerizing molecules such as rapamycin [56]. In this method, both the target protein and the proteasome are fused to particular protein domains. Upon addition of a small molecule that can simultaneously bind to both domains, dimerization and consequently localization of the target protein to the proteasome occur.

Janse and colleagues [56] fused the Rpn10 subunit of *S. cerevisiae*'s 26S proteasome with an Fpr1 tag, and the target protein His3 with the ligand-binding domain of Tor1, $\text{Tor1}^{1883-2078}$ (hereafter called Tor). Addition of rapamycin to the cell culture medium leads to association of Fpr1 and Tor, and thus localization of Tor-His3 to the proteasome. This method was tested on other proteins and turned out to be ineffective for proteins that are inherently very stable. Inspired by recent works

employing tandem repeats of binding domains [49, 57], and the insights we have gained on the power of multiple sites, we propose to utilize multiple binding modules to improve the performance of the synthetic degradation system previously developed by Janse and colleagues [56].

We conjectured that faster degradation can be achieved by increasing the number of Tor domains fused to the target protein if we assume that per each Fpr1-rapamycin-Tor complex, the binding of the target protein and proteasome becomes stronger, i.e., there will be smaller probability in escaping form the proteasome. Consequently, a greater proportion of the target protein will be in bound (degradable) form. To explore this idea, we simulated the degradation of a Tor-fused protein in a Fpr1-Fpr1-Fpr1-fused proteasome background (Figure 5.1). We employed a simple reaction-limited model and used kinetic parameters of the dimerization process from well-studied mammalian systems. Rapamycin binds to FKBP, homolog of yeast Fpr1 in human, with a dissociation equilibrium constant of about 30 μM [165]. FKBP12-rapamycin in turn binds to the binding domain of mTor, homolog of yeast Tor1/2, more tightly with a dissociation constant of about 10 nM [165]. With these parameters, our modeled showed that induced degradation of a hypothetical target protein quickens as the number of Tor domains increases from one to three (Figure 5.2).

As an initial step of implementing the above design, we here examined the degradation of a reporter protein Ura3 fused to a varying number of Tor domains in yeast cells with triple-Fpr1 tagged proteasome. The temporal profile of Ura3 in response to rapamycin has been measured in various constructs and the half-lives have been estimated accordingly. Contrary to our expectations, we observed that addition of Tor domains did not shorten the half-life. Here, we summarize our experiments, discuss possible explanations for the observed behaviors, and propose potential solutions. This work exemplifies the complex nature of synthetic proteins and highlights the challenges involved in choosing the protein domains and linkers in modular design.

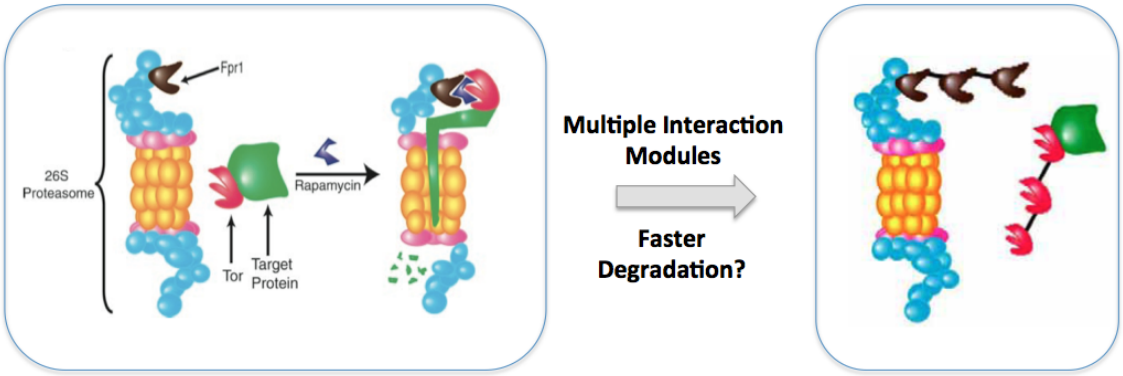

Figure 5.1: Do multiple interaction modules lead to faster degradation? The left picture is from Reference [56] and shows the design of the protein degradation device based on one interaction module for rapamycin. The cartoon on the right shows the new design where the proteasome is fused to three Fpr1 domains and the target protein is fused to three Tor domains.

5.3 Methods

5.3.1 Genomic Tagging of Proteasome

Rapamycin is toxic to *S. cerevisiae* cells and arrests them at G1 phase through interaction with Fpr1 and the Tor1/Tor2 enzymes. Mutations in Fpr1 and Tor1/2 alleviate the toxicity effect of rapamycin [166]. Thus, all the experiments were performed in a derivative of rapamycin-resistant mutant DY001 to ensure that the components of the heterodimerization system would minimally interact with endogenous proteins to prevent cell cycle arrest and mislocalization of the reporter upon addition of rapamycin [166]. The proteasome subunit Rpn10 of parent strain DY001 was triple tagged with Fpr1 by homologous recombination as described previously [56]. FPR1 was amplified by PCR from the strain FY4 [167]. The final structure at the cloning site was 5'- RPN10 C-term-FPR1-FPR1-FPR1-RPN10 UTR-3'.

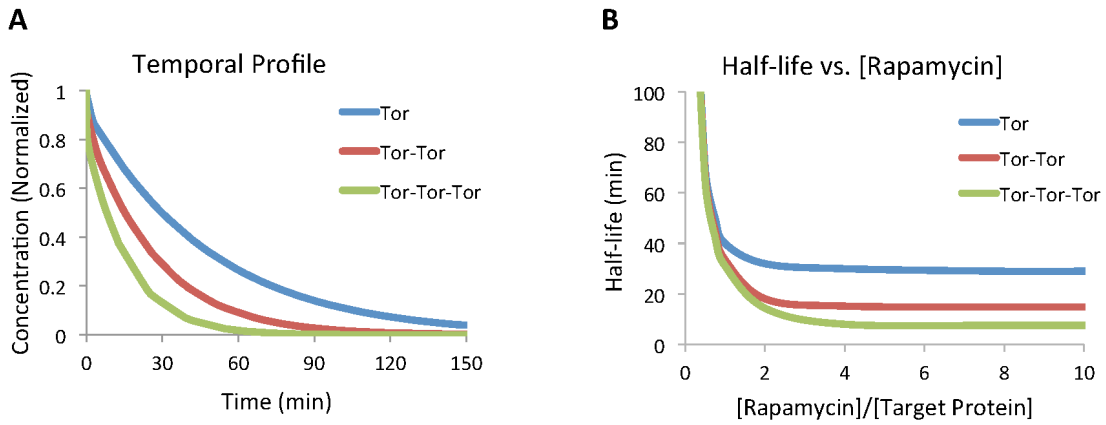

Figure 5.2: Modeling results of rapamycin-induced degradation of a hypothetical target protein. (A) Temporal profile of target protein fused with one, two, and three Tor domains at [rapamycin]/[target protein] = 10. (B) Half-life of target protein fused with one, two, and three Tor domains at various concentrations of rapamycin.

5.3.2 Construction of Reporter Plasmids

All versions of the Ura3 reporter were derivatives of the vector pRS415. Tor1^{S1972R} is an allele of Tor1 that has a severely impaired binding affinity to Fpr1-rapamycin [168, 169]. The sequence corresponding to amino acids 1883-2078 of both Tor1 and Tor1^{S1972R} were amplified and inserted into the vector pRS415 along with URA3 amplified from strain FY4. The reporter plasmids had the hemagglutinin epitope (HA) fused to the to URA3 C-terminal. A short linker, CubR, was used between the TOR module and the URA3 module. The linker(s) between TOR units was very similar. It had 20 amino acids, of which two were different from one linker to another as an artifact of a unique restriction enzyme site engineered at these positions to allow assembly via multiple ligations. The final structure at the cloning site was 5'- [1-3 TOR1/TOR1^{S1972R}]-CubR-URA3 C-term-HA-URA3 UTR-3'. 14 various combinations (two single modules, four double modules, and eight triple modules) have been constructed. The constructs are expressed under the constitutively active yeast ADH promoter. The parent strain DY001 used in this study does not have a chromoso-

mal copy of URA3 and therefore requires exogenous expression of functional Ura3 for growth. Expression of URA3 is used as a selection marker for transformation in synthetic medium lacking uracil.

5.3.3 Cell Cultures and Protein Assays

Transformed yeast cells were grown in liquid synthetic media supplemented with uracil at 30°C. At early log phase, cycloheximide was added to a final concentration of 30 μg/ml to halt protein synthesis. Then culture was split into two parts after 30 min. In one part, rapamycin dissolved in DMSO was added. The other part was used as a negative control, and the same volume of DMSO, but with no rapamycin, was added to it. Cells were harvested at fixed time points and whole-cell extracts were prepared using glass beads and CelLytic Y Cell Lysis reagent (Sigma-Aldrich). The total amount of protein was measured by Bradford assay and Nanodrop. About 25 μg of total protein from each sample was used for electrophoresis and immunoblotted with anti-HA (3F10) primary antibody (Roche Applied Science) and then HP-conjugated anti-rat secondary antibody.

5.3.4 Data Analysis and Curve Fitting

The amount of HA-fused Ura3 was estimated by measuring the band size of the blot using the ImageJ package. To measure the protein half-life, we assumed protein concentration decays exponentially. Data were plotted in logarithmic scale against time and fitted to a linear equation. The half-life was measured through dividing Log(2) by the absolute value of the slope of the fitted line.

5.3.5 Modeling and Simulation

We considered a hypothetical target protein with one to three Tor domains, and proteasome with three Fpr1 domains. The rapamycin binds to any Fpr1 domain

with a dissociation constant (K_D) of 30 μM. Fpr1-rapamycin binds to the Tor domain in a free target protein with K_D of 10 nM. We assumed the second and third Fpr1-rapamycin-Tor associations occur more tightly, by assigning smaller dissociation constants (half) per each pre-existed Fpr1-rapamycin-Tor module. Furthermore, we assumed the protein degrades with a first order kinetics when at least one Fpr1-rapamycin-Tor exists. The model was formulated by mass action kinetics and the set of ordinary differential equations was solved with MATLAB 7.1.

5.4 Results

To test our hypothesis about improved efficiency of protein degradation via additional binding domains of Tor, we fused the Rpn10 subunit of *S. cerevisiae*'s 26S proteasome with three Fpr1 tags. On the other hand, we fused the target protein, Ura3, with a varying number of Fpr1-rapamycin binding domain of Tor1 and/or a mutant version of it. Tor1^{S1972R} is an allele of Tor1 that has a severely impaired binding affinity to Fpr1-rapamycin [168, 169] and used as a non-heterodimerizing control. Upon addition of rapamycin to the cell culture medium, we expected that Fpr1 and Tor1 form a dimer and hence Ura3 be translocated to the proteasome and degrades. Ura3, encoded by URA3, is an orotidine 5-phosphate decarboxylase and is involved in the *de novo* synthesis of pyrimidine ribonucleotides including uracil [170]. Loss of Ura3 activity leads to a lack of cell growth unless uracil or uridine is added to the media [171]. Hence, the synthetic cell culture medium used for our degradation assays was supplemented with uracil.

5.4.1 Rapamycin-Induced Degradation of Ura3

The strain Rpn10-Fpr1-Fpr1-Fpr1 was transformed with plasmids that expressed Tor- or Tor^{S1972R}-Ura3-HA. The transformants were grown in liquid culture supplemented with uracil to early log phase, whereupon cycloheximide was added to halt

protein translation. Each culture was then split into two parts, and rapamycin was added to one part. Samples were collected at various times, and whole-cell protein extracts were made, quantified, and used for Western blot analysis (Figure 5.3). As we expected, upon addition of rapamycin, the amount of HA-fused Ura3 dropped rapidly. The half-life is estimated to be about 10 min. The control sample, Ura3-HA fused to the malfunctional Tor domain was very stable with a half-life of about 90 min (Figure 5.4).

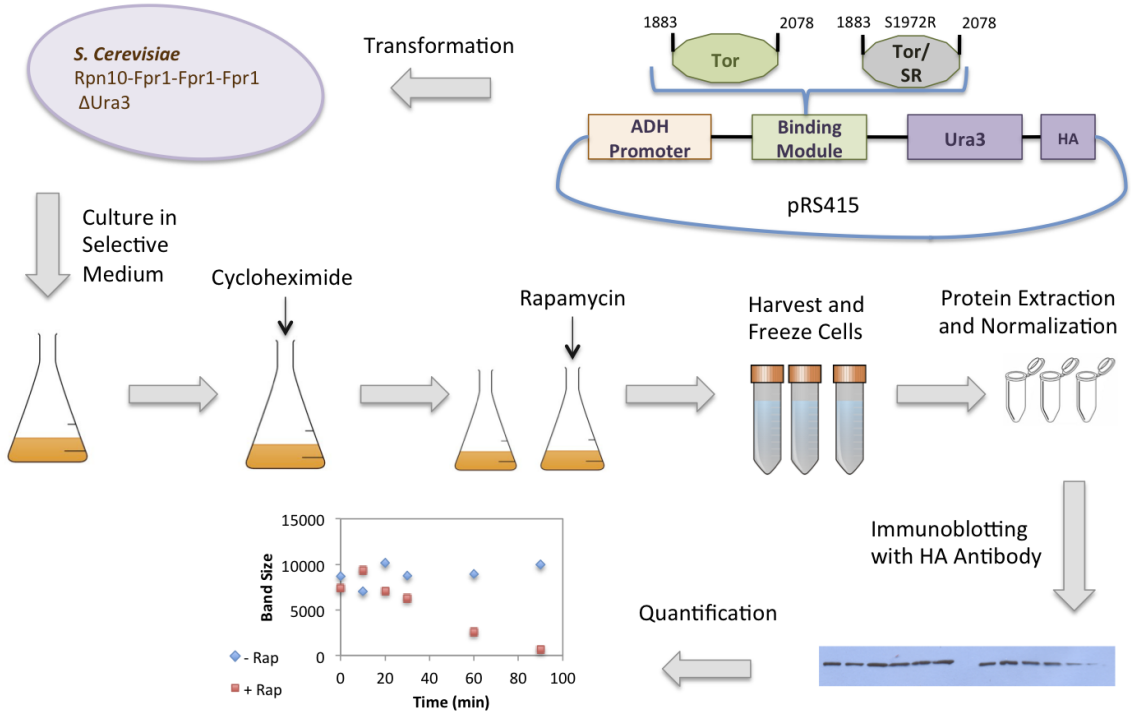

Figure 5.3: Experimental procedure for testing the performance of the degradation device.

5.4.2 Degradation of Ura3 Fused to Multiple Binding Domains of Tor

Our modeling predicted that increasing the number of binding modules would lead to faster degradation. To test this prediction, we constructed double and triple tags with wild-type and mutated Tor domains fused each of them to Ura3-HA.

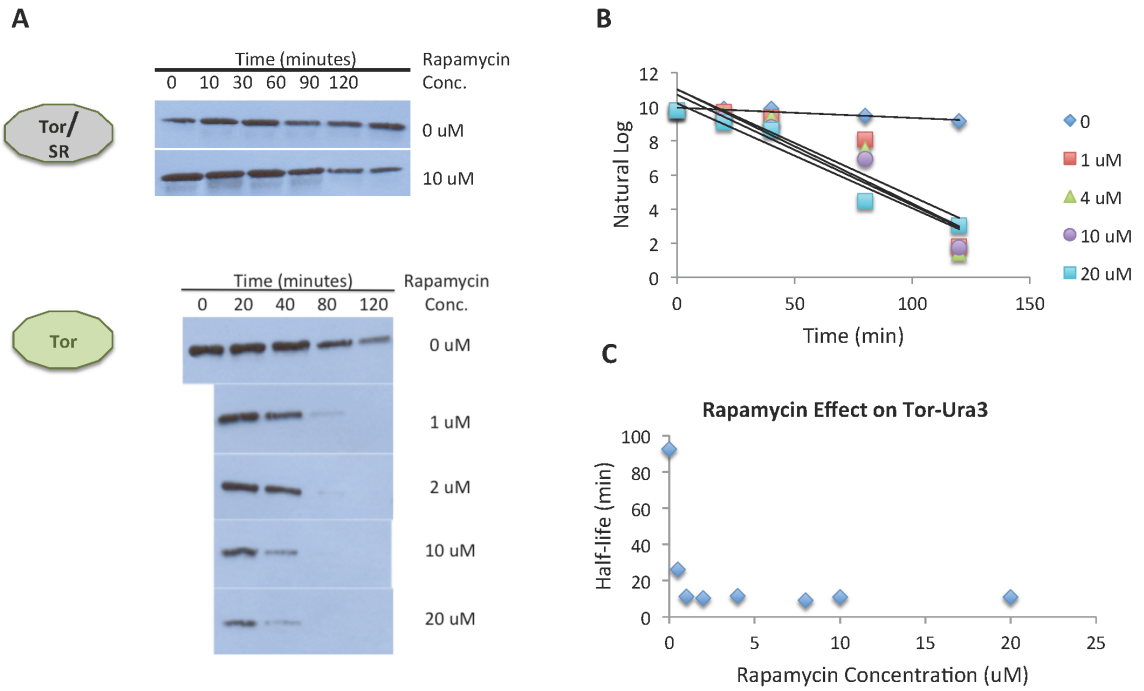

Figure 5.4: Degradation of single-Tor-tagged Ura3-HA. (A) Cells expressing Tor^{S1972R}-Ura3-HA and Tor-Ura3-HA were harvested over a 120-min period after rapamycin induction. The total protein of each sample was extracted and immunoblotted against the HA antibody. (B) The amount of HA-fused Ura3 was quantified in samples taken at different time points and the natural Log of the data was fitted to a linear equation in order to estimate the half-life. (C) The half-life of Tor-Ura3 at various concentrations of rapamycin.

We examined the degradation profile of Tor-Tor-Ura3 at various concentrations of rapamycin. Surprisingly, the protein's half-life did not decrease, instead it increased to about 30 min (Figure 5.5). The control strain, expressing Tor^{S1972R}-Tor^{S1972R}-Ura3-HA still showed a half-life of 90 min. Thus we speculated that the second Tor added to the construct decreased the binding of the initial Tor to the Fpr1-rapamycin complex.

Similarly, the construct with three Tor domains, Tor-Tor-Tor-Ura3-HA, degrades with a half-life of 30 min (Figure 5.6). Because no appreciable difference was observed between the double- and triple-Tor-fused Ura3, we conjectured that the additional Tor domain is not accessible to the Fpr1-rapamycin complex. To test this hypothesis,

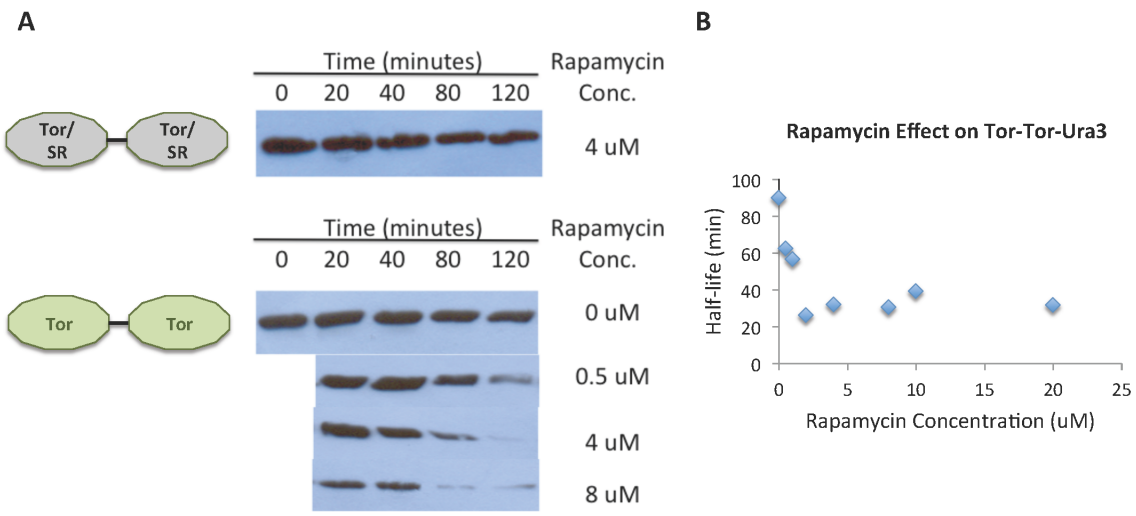

Figure 5.5: Degradation of double-Tor-tagged Ura3-HA. (A) Western blot of double-Tor- and -Tor^{S1972R}-tagged Ura3-HA samples with the HA antibody. (B) The half-life of Tor-Tor-Ura3 at various concentrations of rapamycin.

we set out to closely examine the half-life of Ura3 fused to Tor at different positions by exploiting Tor^{S1972R} domain as a null binding component.

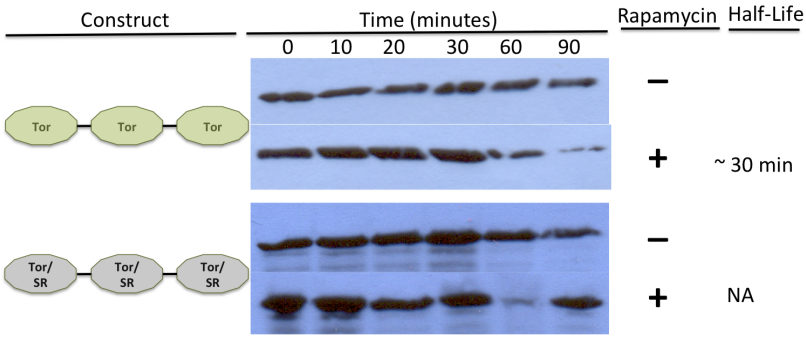

Figure 5.6: Degradation of triple-Tor-tagged Ura3-HA. Western blot of triple-Tor- and Tor^{S1972R}-tagged Ura3-HA samples with the HA antibody.

5.4.3 Position Effects

First, we looked at the double-tag constructs with one functional Tor domain. The half-life of Ura3 with an intact Tor at the N-terminus is comparable to that of the Ura3 construct with two functional Tor (Figure 5.7A). Switching the positions of

the functional Tor and the mutant one dramatically decreased Ura3's degradability and increased its half-life to about 100 min. This observation indicates that the Tor domain at the N-terminus is effective and the Tor domain in the middle does not enhance degradation.

We also examined the position effect in the triple modules. The constructs Tor-Tor^{S1972R}-Tor^{S1972R}-Ura3-HA and Tor-Tor-Tor^{S1972R}-Ura3-HA had degradation profiles similar to that of Tor-Tor-Tor-Ura3-HA as we expected (Figure 5.7B). Tor^{S1972R}-Tor-Tor-Ura3-HA was stable, similar to Tor^{S1972R}-Tor-Ura3-HA and Tor^{S1972R}-Ura3-HA. At this point it became clear to us that only the Tor domain at the N-terminus is accessible to the Fpr1-rapamycin complex. Tor domains in the middle of the constructs are not accessible and even have negative effects on the binding of the N-terminus Tor and thus the half-life of the reporter protein Ura3.

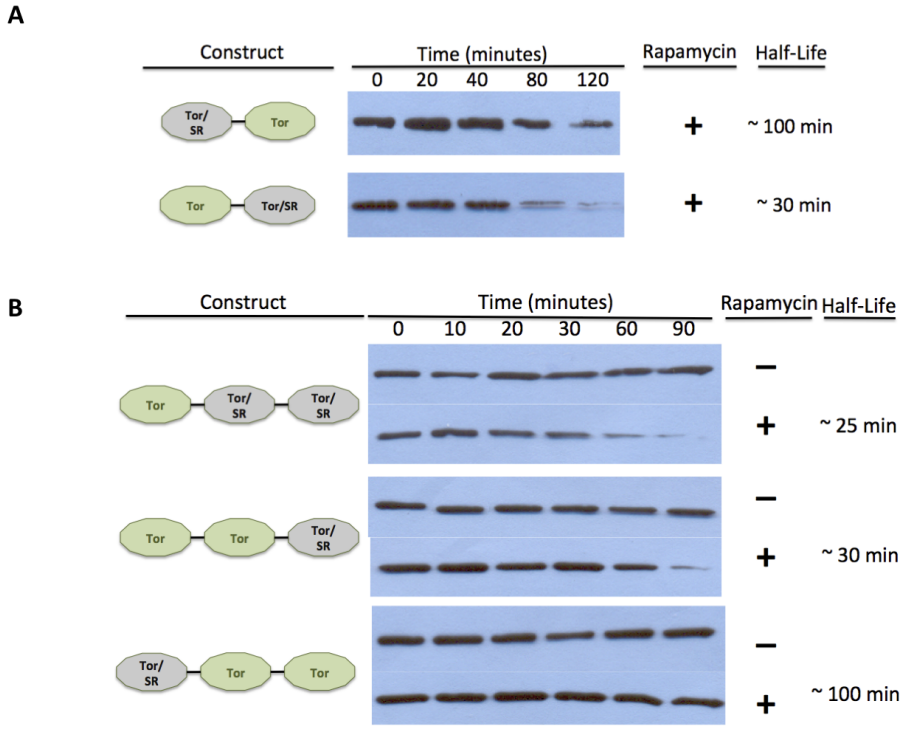

Figure 5.7: Position effects in double and triple modules. (A) Double modules with two different orientations of Tor and Tor^{S1972R} fused to Ura3-HA. (B) Triple modules with three various combinations of Tor and Tor^{S1972R} fused to Ura3-HA.

5.5 Discussion and Conclusion

In this study, we employed a dimerizing molecule, rapamycin, to induce artificial association of the reporter protein, Ura3, with the proteasome in *S. cerevisiae*. The rapamycin-induced half-life of the reporter protein, fused to one Tor domain, in the strain Rpn10-Fpr1-Fpr1-Fpr1 was $\sim$ 10 min. Previously, this approach was demonstrated with another reporter protein, His3. Upon addition of rapamycin, half of the HA-tagged His3 protein degraded in $\sim$ 20 min [56]. Two successful examples of implementation enhance the generalizability potential of this modular design. Fusing the Tor module to endogenous proteins of choice in an Fpr1 fused proteasome strain background allows rapamycin-dependent control of degradation in an effective way.

We then attempted to improve the performance of this synthetic protein degradation device by increasing the number of modular binding domains of Tor. However, the rapamycin-induced degradation of double- and triple-Tor-tagged Ura3 observed to be slower than that of single-Tor tagged Ura3. Examination of other constructs, with a mixed combination of Tor and a mutant that can not bind to Fpr1-rapamycin, suggested that the additional Tor domain is not effective and imposes negative effects on the binding affinity of the N-terminus domain.

We further hypothesize that the additional Tor domain imposes steric inhibition on the Fpr1-rapamycin and Tor association due to its comparatively large size. The Tor tag used in our design is about 200 amino acid residues. The minimal binding module in mTor, mammalian Tor, is about 100 amino acids which is smaller than the one we used in our design [165, 172]. We may be able to overcome the physical blocking effects imposed by additional Tor domains by using the small mammalian Tor domains. We do not think that the Fpr1 domains impose any steric inhibition on binding due to its small size (about 12 kDa). This can be confirmed by comparing the rapamycin-induced degradation of Tor-Ura3 in two strains with Rpn10-Fpr1 and Rpn10-Fpr1-Fpr1-Fpr1 background.

Another plausible reason may be the sequence and length of the linker used to connect the Tor domains or the Fpr1 domains. Rigid linkers do not allow the required topological rearrangements of the rapamycin-bound Fpr1 and Tor happen for binding. We do not suspect the linker between Tor and Ura3 to be an issue; because the Tor-Ura3 construct degrades well and almost the same linker has been used in all other constructs. Using other flexible linkers like a 20-amino-acid-long-poly-serine/glycine peptide, which is commonly used for connecting SH3 domains [50] might resolve this problem.

Finally, there might exist a threshold distance at which the proteasome can access the target protein for unfolding and destruction. Particularly that it is known that an optimal topological arrangement exists for presenting substrates to the proteasome [56]. Additional Tor domains might lead to the increase of distance between the Ura3 moiety and the Rpn10 subunit, and hence, in spite of formation of the Fpr1-rapamycin-Tor complex, the proteasome can not reach Ura3 for destruction.

Any of the three issues discussed above, or a combination of them, might have caused the ineffectiveness of our proposed design. Further investigations will be needed to identify the exact problem and eventually to achieve the proposed degradation switch.

CHAPTER VI

Concluding Remarks and Future Directions

"[Science] never solves a problem without creating ten more."

George Bernard Shaw (1856–1950)

6.1 Summary

In this thesis we employed a hybrid experimental/theoretical approach to better understand switch-like responses arising from multisite protein phosphorylation. We made unintuitive verifiable predictions in correlating the number of phosphorylation sites to the ultrasensitivity of response through mathematical modeling and simulation. We partially confirmed our simulation results by close examination of the model protein Sic1 and its mutants with varying numbers of phosphorylation sites. Furthermore, by comparing the experimental and simulation results we made new hypotheses about Sic1 phosphorylation mechanism, which can be tested by further measurements. We also sought to capitalize on the insights we gained from our mechanistic study by utilizing multisite phosphorylation and the broader design principle of multisite protein domains in synthetic biology application. More specifically, we designed a minimum oscillator using protein components with multiple phosphorylation sites that features high nonlinearity. We also attempted to improve the performance of a protein degradation switch based on the similar concept of multiple protein binding

domains and we learned valuable lessons about modular design of synthetic proteins. In this chapter, I summarize the main findings and discuss the possible areas for further investigation.

6.2 Switch-Like Responses Arising from Multisite Protein Phosphorylation

6.2.1 Theoretical Investigation of The Role of Multisite Phosphorylation in Switch-Like Protein Degradation

Inspired by the fact that natural destruction of numerous proteins including Sic1 is controlled by the degree of phosphorylation, we aimed to model and investigate phosphorylation-triggered protein degradation in a systematic manner. Our simulation results show that while a single-site protein does not degrade in an switch-like manner, multisite phosphorylation can lead to thresholding for degradation and a switch-like elimination. Generally, as the number of phosphosites increases, a more switch-like temporal response can be achieved. The steepness of the temporal response is also affected by the number of phosphosites required for degradation and the kinetics of phosphorylation reactions. The steepness is at maximum when protein degrades after becoming phosphorylated on about half of its total sites if phosphorylation and dephosphorylation reactions proceed fully randomly. When phosphorylation and dephosphorylation proceed sequentially, the maximum ultrasensitivity reaches the highest level if nearly but not exactly fully phosphorylated protein is targeted for destruction. The elimination curve of a multisite protein phosphorylated sequentially is more switch-like than that of a protein phosphorylated randomly.

It is worthy to note the difference between switch-like responses in a temporal response process and those observed for a steady-state stimulus-response curve. In dynamic processes, we look at the temporal profile of the output over time upon

introduction of a stimulus. The extent to which a temporal profile is switch-like is determined by the two time points at which the output reaches 10% and 90% of its final or initial value. The shape of the temporal response is drastically influenced by the temporal profile of the stimulus. A more switch-like stimulus leads to a more switch-like response, while the degree to which the temporal profile is switch-like is increased upon conversion of stimulus to response. In steady-state analysis, the steady-state level of output is examined at various levels of stimulus strength (e.g. kinase activities). The ultrasensitivity is determined by the two stimulus values at which the output reaches 10% and 90% of its saturated or unstimulated value. Alternatively, the Hill coefficient (n_H) can be used as a measurement of ultrasensitivity in sigmoidal stimulus-response curves.

Generally, multisite modification provides a precise mechanism for regulating the speed and sharpness of the output in response to an input of stimulus. Other kinds of modification such as ubiquitination, hydroxylation, acetylation, methylation, and glycosylation which are involved in tuning macromolecules' stability, activity and translocation can also be accounted for by the model presented in this work. Through multisite modification, a gradually changing input signal can be converted into a switch-like output signal. These macromolecular information processors serve as building blocks for higher-level functional modules such as oscillators and toggle switches.

6.2.2 Experimental Exploration of Ultrasensitive Steady-State Response of Sic1 to Cln2-Cdc28 Kinase

To elucidate the exact mechanism of ultrasensitivity arising from multisite phosphorylation, we closely examined the model protein Sic1. Sic1 has nine Ser/Thr phosphorylation sites and its degradation is triggered by multisite phosphorylation during G1/S transition. Phosphorylated Sic1 is recruited to the proteasome for degradation through binding to Cdc4. Although Sic1 is a relatively well studied

protein and Sic1-Cdc4 binding has been the focus of many studies, very little is known about the Sic1 phosphorylation process. We reconstituted the Sic1 phosphorylation/dephosphorylation/binding processes *in vitro* and measured the Cdc4-bound fraction of Sic1 (output) in presence of various amounts of Cln2-Cdc28 kinase complex (input).

We found that binding of phosphorylated Sic1 to Cdc4 in response to increasing activity of Cln2-Cdc28 kinase increases in a switch-like fashion with a Hill coefficient (n_H) of ~ 3.2. Employing Sic1 mutants with various numbers of phosphorylable sites allowed us to directly investigate the role of multiple sites. Two main features were observed: First, the response of Sic1 to the kinase Cln2-Cdc28 becomes less ultrasensitive as the number of phosphorylable sites decreases. In fact, the Hill coefficient decreases to ~ 1.0 as the number of phosphorylable sites decreases to five, representing a typical hyperbolic response. Second, the Sic1 proteins with more phosphorylable sites binds in larger amounts to Cdc4 at saturated levels of kinase and Sic1 proteins with less than five phosphorylable sites do not bind appreciably.

These results agree well with our theoretical study, which suggested that ultrasensitivity arises from a combination of multistep phosphorylation and increasing "affinity" along the phosphorylation chain. In particular, the empirical Sic1-Cdc4 binding curves can be reproduced theoretically if the following two conditions are met: (i) the equilibrium constants of phosphorylation/dephosphorylation are larger for the phosphoforms that are phosphorylated on more than four sites, (ii) the Sic1-Cdc4 association rate constant increases as the number of phosphorylated sites on Sic1 increases. The first condition enhances the ultrasensitivity of the response by promoting the multistep phosphorylation reaction as it proceeds. Our mass spectrometry analysis show that the wild-type Sic1 is phosphorylated mostly on less than five sites in the initial lag phase of the binding curve. Interestingly, the distribution shifts dramatically toward six and higher orders of phosphorylated states as the

concentration of Cln2-Cdc28 increases. This observation partially supports our hypothesis. The second condition is essential for generating different levels of saturation for various mutants and the wild-type Sic1. Actual measurements of dissociation rate constants for various Sic1 peptides partially support this hypothesis [109].

This work represents one of the few experimental studies on ultrasensitivity arising from multisite protein phosphorylation. In particular, the ultrasensitivity of Sic1 protein in binding to Cdc4 in response to increasing activity of kinase is measured for the first time. Our results highlight the important role of multisite protein phosphorylation in converting a graded input (Cln2-Cdc28 activity) to an ultrasensitive output (binding to Cdc4) and thereby generating a switch-like cellular behavior such as the G1/S transition in *S. cerevisiae*.

6.2.3 Future Research Directions

Two areas worthy of further investigation and closely related to this project would be (i) measurement of Sic1 phosphorylation parameters, and (ii) *in vivo* temporal and spatial profiling of Sic1 degradation.

6.2.3.1 Sic1 Phosphorylation Kinetics

For a thorough comparison of experimental and modeling results, the kinetic parameters of Sic1 phosphorylation, dephosphorylation and binding to Cdc4 need to be incorporated into the mathematical model. Sic1-Cdc4 binding has been studied with various methods and the apparent association constants of various synthetic Sic1 peptides and Cdc4 have been measured previously [75, 109]; however, no information is available on Sic1 phosphorylation and dephosphorylation kinetics.

We are collaborating with Professor Kristina Håkansson's lab in the Department of Chemistry at the University of Michigan to develop an isotope-free mass spectrometry protocol for quantitative analysis of Sic1 phosphorylation. In our bottom-

up approach, the Sic1 protein is digested by protease trypsin prior to HPLC and mass spectrometry. Synthetic peptides are being designed as internal standards to calibrate the amount of each phosphorylated/unphosphorylated peptide, containing Ser/Thr-Pro residues. Each standard peptide has one Val to Ile/Leu or Ile/Leu to Val mutation, so it is distinct from its counterpart peptide resulting from the sample protein's digestion due to its different mass-to-charge (m/z) ratio.

As an initial step, we examined the mutant Sic1 with two phosphorylable sites: Thr45 and Ser76. Each of these sites is on a distinct peptide. Preliminary results for Sic1-2p samples, exposed to kinase for varying time period, are shown in Figure 6.1. It is clear that the phosphorylation kinetics of these two sites are different; however, the total amount of each peptide is not conserved and decreases over time. One possible explanation is the phosphorylation of other sites besides Thr45 and Ser76, which leads to the existence of doubly phosphorylated peptides currently not accounted for. This project is in progress and we hope to investigate the phosphorylation kinetics of the wild-type Sic1 eventually.

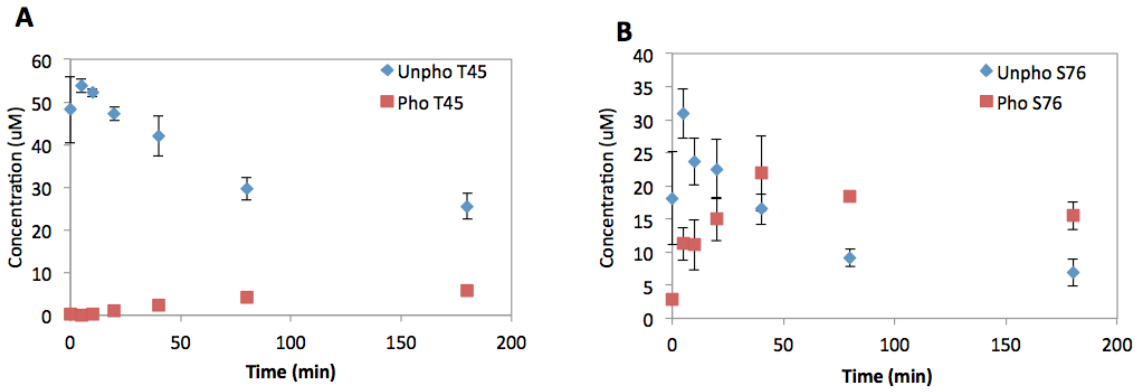

Figure 6.1: Mass spectrometry bottom-up analysis on Sic1-2p samples collected at various time points. (A) Phosphorylated (Pho) and unphosphorylated (Unpho) Thr45 in peptide $Sic1^{33-50}$. (B) Phosphorylated (Pho) and unphosphorylated (Unpho) Ser76 in peptide $Sic1^{54-79}$.

There are two challenges in regards with extension of this approach to the wild-

type Sic1. The first one is that two of the peptides resulting from trypsin digestion of wild-type Sic1 will have two phosphorylation sites. Thereby additional steps should be taken to identify which site is phosphorylated in singly phosphorylated peptides for these two particular peptides. Treatment of the samples with an additional protease with different cleavage sites such as chymotrypsin might be a solution. Tandem mass spectrometry may address this problem as well.

The second and main challenge is the difficulty in utilizing the concentration of phosphosites(peptides) to determine the concentration of phosphoproteins. In bottom-up analysis, a protein is digested into peptides and the degree of phosphorylation at one site represents the overall abundance of the peptides containing this site. For the wild-type Sic1 which has nine phosphorylation site, partially phosphorylated Sic1 corresponds to a maximum of $2^9 = 512$ different phosphorylated states of the protein, whereas even in the ideal case (assuming each peptide contains only one phosphorylation site) merely $2 \times 9 = 18$ concentrations of the phosphorylated/unphosphorylated sites can be obtained from mass spectrometry analysis. This problem can potentially be addressed by combining information from complementary methods such as top-down mass spectrometry analysis, isoelectric focusing, and examining Sic1 mutants with smaller number of sites.

One dimensional isoelectric focusing (IEF) can be used to separate and semi-quantify phosphoforms. However, IEF technique does not provide any information on the identity of phosphorylated sites and can not be used as a sensitive and high-throughput method. Theoretically, isoelectronic point of 0p-Sic1 to 9p-Sic1 spans a wide range from 7.89 to 5.24 [174] and thereby separation of different phosphoforms to some extent on the IEF gel is possible; however, in our preliminary attempt, the resolution of the gel was not high enough to differentiate various phosphoforms. Further exploration of this technique is needed. For example, we stained the gel by Silver stain. Other staining procedures such as SYPRO Ruby which is based on

fluorescence might produce the sensitivity we need.

After experimental data are generated with above approaches, kinetic parameters of phosphorylation reactions can be estimated. By comparing the measured kinetic parameters, it would be possible to determine how phosphorylation of one site affects the affinity of substrate for the kinase. It would be interesting to check if phosphorylation of a single site positively affects subsequent phosphorylation of other sites as we predicted. Information obtained at this stage increases our basic knowledge on the Sic1 protein and can be used for further refinement of the theoretical model.

6.2.3.2 Temporal Profile of Sic1 Degradation

In this study we did not reconstitute the ubiquitination and proteolysis systems. In yeast, association of Sic1 with Cdc4 promotes Sic1 ubiquitination by the E2 (Cdc34) ligase and multiubiquitinated Sic1 is degraded by the 26S proteasome. Additional factors other than multisite phosphorylation may contribute to switch-like elimination of Sic1 *in vivo*. The most important one is the positive feedback exerted by liberated Clb5,6-Cdc28. Another factor might be the involvement of kinases other than Cln2-Cdc28. Sic1 is phosphorylated by multiple kinases, which can differentially affect the stability of Sic1 and consequently progression through G1. All these factors may lead to a different behavior *in vivo*, compared to our *in vitro* experiments.

Examination of the *in vivo* temporal profile of Sic1 during the cell cycle at single-cell resolution can provide us with a vivid picture of related intracellular events. We have done some preliminary studies on profiling Sic1 concentration *in vivo*. Sic1 is labeled with green fluorescent protein (GFP) and using inverted fluorescence microscopy, live-cell imaging is performed. We set up a system to keep cells viable and fixed through mounting them in a synthetic medium on a thin agarose layer (Figure 6.2A). Images are taken every five minutes during a five-hour time course (Figure 6.2B). We used a MATLAB code to process the stacks of images and quan-

tify the green fluorescence signal. Figure 6.2C demonstrates the change in fluorescence intensity during the different phases of the cell cycle over five hours.

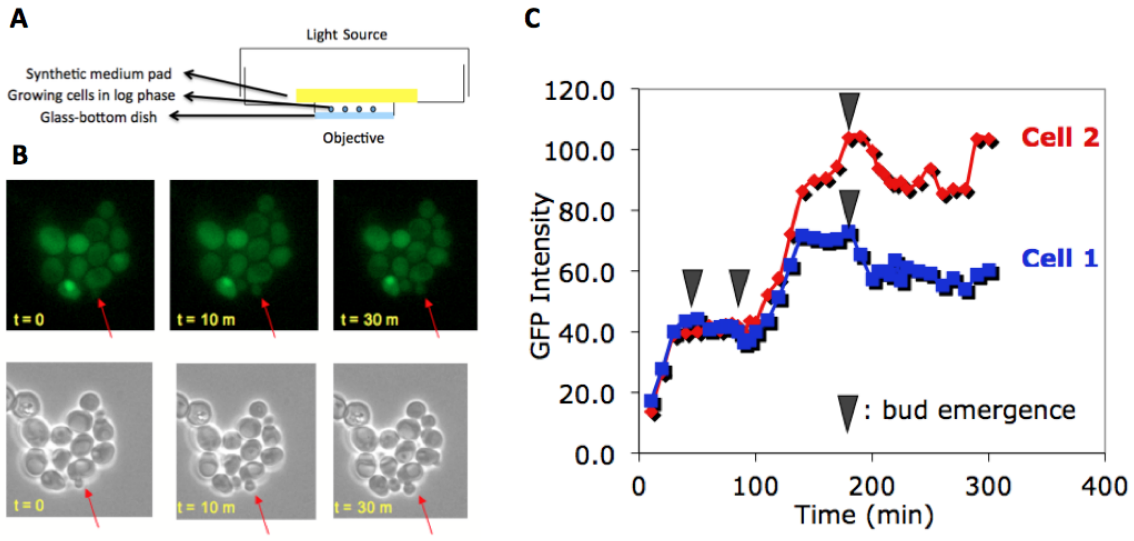

Figure 6.2: Temporal profile of GFP labeled Sic1 in *S. cerevisiae*. (A) Sample setup for live cell imaging. (B) 100x Images taken by inverted fluorescence microscope. The arrows indicate the same cell at three various time points. (C) Green fluorescence signal of two cells is quantified and tracked over a five-hour course.

We have observed a sharp decrease of the GFP signal due to Sic1 elimination at the budding time. The major obstacle for further in-depth analysis is image processing. Auto-detection of newly budded cells and recording of the pedigree demands advanced image processing. Currently, segmentation and labeling are carried out manually. In order to examine more cells to obtain statistically meaningful results, image processing programs (e.g. using MATLAB) need to be developed for automatic edge detection and tracing of mother and daughter cells.

Besides the Sic1 protein, it is very important to examine other proteins involved in the Sic1 degradation process, particularly the Cln2 subunit of the Cln2-Cdc28 kinase. Labeling Cln2 with a second fluorescent protein such as mCherry makes it possible to track two proteins simultaneously. Microscopic visualization will not only enable us to monitor temporal changes of the proteins, but also provide information of the

changes in their localization.

6.3 Protein-Based Synthetic Devices

6.3.1 Multisite Phosphorylation and Oscillation

Non-linearity is an essential ingredient for constructing oscillatory biological systems such as circadian clocks. Since multisite phosphorylation can potentially generate ultrasensitive (highly non-linear) responses, we proposed to construct a protein oscillator based on multisite phosphorylation and dephosphorylation. We investigated for the first time the conditions under which a single-level protein phosphorylation and dephosphorylation could generate oscillation.

Our design features a multisite protein embedded in a negative feedback loop formed through the inhibition of the first step of phosphorylation by the fully phosphorylated substrate. Our computational results demonstrated that if the phosphorylated substrate inhibits substrate-kinase association in a cooperative (i.e. nonlinear) manner, substrates with more than one site can show oscillatory behavior. Interestingly, an inverse relationship exists between the number of phosphorylation sites and the minimum cooperativity in the negative feedback required for driving the system into the oscillatory regime. When the ratio of substrate/enzyme is increased, the period of oscillation increases, but the amplitude does not change significantly. Increasing the number of phosphorylation sites increases both the oscillation period and amplitude.

Theoretical modeling in this work proposes that multisite protein phosphorylation and dephosphorylation could be potentially considered in designing synthetic oscillators. The main advantage of this synthetic oscillator is its simplicity. In addition, the period and amplitude can be readily tuned. The frequency of oscillation can be adjusted by tuning the ratio of enzyme and substrate. The amplitude of oscillation

can be modified by changing the number of phosphorylation sites.

To our knowledge, no natural multisite protein exists that show the negative feedback with a high cooperativity. Thereby, the specific design and construction of this protein-based oscillator will rely on further exploration to combine existing protein modules and new engineered protein domains.

6.3.2 Design and Preliminary Construction of a Protein Degradation Switch

Generalizing from the concept of the multiple phosphorylation sites, multiple binding domains can enhance the response of a protein to a given stimulus. In both cases, if the degree of modification determines the property of the protein, the protein's response to the stimulus will be affected by the number of phosphate groups/binding interactions. We employed this concept to design and construct a protein degradation switch.

We designed a degradation switch by utilizing a naturally occurring dimerizing molecule, rapamycin, to artificially localize a target protein to the S26 proteasome in *S. cerevisiae*. We fused the Rpn10 subunit of *S. cerevisiae*s proteasome with multiple Fpr1 tags. On the other hand, we fused a target protein Ura3 with multiple Fpr1-rapamycin binding Tor domains. We expected that upon addition of rapamycin to the cell culture medium, rapamycin binds to Fpr1 and Fpr1-rapamycin in turn binds to Tor domains, hence Ura3 will be localized to the proteasome and degrades swiftly.

Simulation results predicted that the more binding domains exist on the target protein, the faster its degradation happens. To test this idea, we made a series of constructs with varying numbers of Tor domains. Contrary to our prediction, not only was the rapamycin-induced degradation of double- and triple-Tor tagged Ura3 not faster than single-Tor tagged Ura3, but the degradation actually slowed down. Examination of other constructs, containing Tor and its mutant with impaired affinity

for Fpr1-rapamycin, suggested that the additional Tor domain interfered with binding of other domains. We conjecture that steric inhibition caused by the large size of Tor and/or the rigidity of linkers between Tor or Fpr1 binding modules might be two causes that should be considered in further investigation.

Although this project turned out to be more challenging than previously thought and the results we obtained are not as good as we expected, we learned valuable lessons about designing synthetic proteins. This work highlights the complexity involved in choosing the protein domains and linkers in modular design.

6.3.3 Future Research Directions

The second half of this thesis was mostly about the design and construction of synthetic protein devices. Here I discuss how the hypothetical oscillator presented in Chapter 4 can be constructed. I also propose possible solutions to overcome the challenges associated with the design of the protein degradation switch presented in Chapter 5.

6.3.3.1 Synthetic Protein-Based Oscillator

In the proposed network for sustainable and tunable protein oscillations, one key component was the highly nonlinear negative feedback formed through the inhibition of the first phosphorylation step by the fully phosphorylated substrate. Important features of this inhibition include: threshold in phosphorylated sites for inhibition, nonlinearity or cooperativity in the negative feedback, and the effect on the first phosphorylation step. To our knowledge, no existing natural system has all these features. Nevertheless, with recent advances in synthetic biology, it is possible to engineer a system with all the required features.

Each of these features can be found in known protein interaction processes. For example, Sic1 or any other well-studied small multisite protein such as Pho4 can be

used as the base of the synthetic substrate. With regard to nonlinearity or cooperativity, many proteins assemble as oligomers in functional forms. For example, protein KaiC in cyanobacteria forms a hexamer, which in turn binds to a dimer of another protein KaiA, to carry out autokinase activity [154, 155]. The degree of cooperativity arising from a hexamer can be as high as six. Alternatively, tandem repeats of an inhibitory binding domain can lead to the required ultrasensitive inhibition. Finally, it is possible to restrict the inhibitory effect to the first phosphorylation step if two kinases are involved and one introduces the first phosphate group as a requirement for further phosphorylation by the other kinase. This "priming" mechanism has been observed for protein substrates such as glycogen synthase [156, 157], β-Catenin [91], and insulin receptor substrate-2 [158].

Existing biomolecular processes such as those described above suggest that it is feasible to construct experimentally the minimum protein oscillator studied in this thesis.

6.3.3.2 Synthetic Protein Degradation Switch

In order to achieve the protein degradation switch proposed in Chapter 5, first the source of problem need to be diagnosed. To find out whether the problem is rooted in Fpr1 modules and/or Tor modules, background strains with single- and triple-Fpr1 fused Rpn10 can be used. If the degradation of single-Tor fused Ura3 be slower in the triple Fpr1 fused Rpn10, then the Fpr1 modules and particularly the linkers (little flexibility is provided in the Fpr1 domain design) should be redesigned. Similarly, if the problem is rooted in the Tor modules, the Tor domains and/or the linkers need to be re-examined.

Our main hypothesis is that the additional Tor domain imposes steric inhibition on Fpr1-rapamycin and Tor association due to its comparatively large size. Smaller Tor domains, for example mammalian Tor, which is about 11 kDa, might resolve the

problem. The other plausible cause of problem is the sequence and length of the linker used to connect Tor domains. Using other well known flexible linkers like a 20-amino acid long poly serine/glycine peptide, which is commonly used for connecting SH3 domains, might resolve this problem [49, 57].

None of the efforts suggested above will be trivial. Hence, it might be very helpful to perform structure-based computational analysis to model binding of the single, double, and triple modules, and also to design new parts. *In vitro* reconstitution of the system and analyzing the binding of various modules may also provide insights about the underlying problem and suggest more effective designs of the switch.

APPENDICES

APPENDIX A

Non-Dimensionalization

In this note, we describe how the ODE system presented in Chapter 2 is non-dimensionalized to simplify the analysis. As described in the main text, the substrate protein contains n sites and degrades after being phosphorylated on m sites. The concentration of each phospho-state is a function of the concentrations of the upstream and downstream phospho-states, the kinase and phosphatase, and the kinetic parameters. For illustration purpose, consider the governing equations for the sequential system.

$$\frac{d[S_0]}{dt} = k_0^{-1}[pho][S_1] - k_0[kin][S_0] - k_0^d[S_0] \tag{A.1a}$$

$$i = 1, ..., n-1 \tag{A.1b}$$

$$\frac{d[S_i]}{dt} = k_{i-1}[kin][S_{i-1}] + k_i^{-1}[pho][S_{i+1}] - k_i[kin][S_i] - k_{i-1}^{-1}[pho][S_i] - k_i^d[S_i]$$

$$\frac{d[S_n]}{dt} = k_{n-1}[kin][S_{n-1}] - k_{n-1}^{-1}[pho][S_n] - k_n^d[S_n] \tag{A.1c}$$

where k_i, k_i^{-1} and k_i^d stand for kinetic rate constants of phosphorylation, dephosphorylation and degradation, respectively. $[kin]$, $[pho]$ and $[S_i]$ represent concentrations of the kinase, phosphatase and the substrate with i sites phosphorylated, respectively. $k_i^d = 0$ for $i = 0, ..., m-1$ and $k_i^d \neq 0$ for $i = m, ..., n$.

Let us look at the general case represented by Eq. (A.1b). To non-dimensionalize this equation, we use the initial concentration of the substrate, S_{Ini}, to normalize the dependent variable $[S_i]$:

$$[\bar{S}_i] \equiv \frac{[S_i]}{S_{Ini}} \tag{A.2}$$

For non-dimensionalization of the independent variable t, let us choose the time scale associated with the degradation reaction.

$$\bar{t} \equiv \frac{t}{1/k^d_{ave}} \tag{A.3}$$

where k^d_{ave} is average of the degradation rate constants:

$$k^d_{ave} = \frac{1}{n+1-m}\sum_{i=m}^{n} k^d_i \tag{A.4}$$

Substituting $[S_i]$ and t with the new set of dimensionless variables $[\bar{S}_i]$ and $\bar{t}$ gives the following non-dimensionalized equation:

$$\frac{d[\bar{S}_i]}{d\bar{t}} = \frac{k_{i-1}}{k^d_{ave}}[kin][\bar{S}_{i-1}] + \frac{k_i^{-1}}{k^d_{ave}}[pho][\bar{S}_{i+1}] - \frac{k_i}{k^d_{ave}}[kin][\bar{S}_i] - \frac{k_{i-1}^{-1}}{k^d_{ave}}[pho][\bar{S}_i] - \frac{k^d_i}{k^d_{ave}}[\bar{S}_i] \tag{A.5}$$

Now we define three sets of new dimensionless parameters:

$$\alpha_i \equiv \frac{k_i}{k^d_{ave}}[kin] \tag{A.6a}$$

$$\beta_i \equiv \frac{k_i^{-1}}{k^d_{ave}}[pho] \tag{A.6b}$$

$$\gamma_i \equiv \frac{k_i^d}{k_{ave}^d} \tag{A.6c}$$

and eventually end up with

$$\frac{d[\bar{S}_i]}{d\bar{t}} = \alpha_{i-1}[\bar{S}_{i-1}] + \beta_i[\bar{S}_{i+1}] - \alpha_i[\bar{S}_i] - \beta_{i-1}[\bar{S}_i] - \gamma_i[\bar{S}_i] \tag{A.7}$$

In this work, we assume that the degradation rate constants are the same for all the phospho-states with m or more sites phosphorylated. In this case, the system reduces from five types of parameters in the original system ($k_i, k_i^{-1}, k_i^d, [kin], [pho]$) to two sets in the dimensionless space (α_i, β_i). Equivalently, we can simply set the degradation rate constants k_i^d to 1 and change $k_i[kin]$ and $k_i^{-1}[pho]$ as whole groups in the original system when exploring the effect of parameters.

It should also be noted that the concentration of kinase may change over time and also needs to be expressed as a function of the dimensionless time while we work in the non-dimensionalized space:

$$[kin] = f(t) = \bar{f}(\bar{t}) \tag{A.8}$$

APPENDIX B

Explored but Ineffective Approaches in Quantifying Sic1-Cdc4 Binding

Before choosing the current set-up for experimenting Sic1-Cdc4 binding (described in Chapter 3), we had explored other protein fusions of Sic1 and Cdc4 and various binding set-ups.

NiNTA Column to Immobilize His-Cdc4 for Pulling Down Gst-Sic1. We initially examined the binding of phosphorylated Gst-Sic1 to His-tagged Cdc4. Gst-Sic1 was incubated with the Cln2-Cdc28 kinase. Phosphorylation was confirmed by mass spectrometry and gel electrophoresis. The reaction mixture (containing Gst-Sic1 and Cln2-Cdc28) was incubated with 6x-His-tagged truncated Cdc4 in complex with Gst-Skp1, and was incubated at 4°C for 1 hour. At this temperature the phosphorylation reaction can not proceed, so the equilibrium does not change after binding a fraction of phosphorylated Sic1 to the Cdc4. The final solution (containing Gst-Sic1 and Cln2-Cdc28, and His-Cdc4/Skp1-GST complex) was run through Ni-NTA columns (Qiagen 30600). Thus, the His6-tagged Cdc4 and proteins in complex with it (Skp1 and Sic1) should supposedly remain in the column, the remaining proteins (unbound Sic1 and Cln2-Cdc28) should be removed from the column in the first and second washing steps. The Cdc4-bound fraction was pulled down in the elution buffer

and visualized using the anti-Sic1 antibody. The immunoblotting of this sample and a control sample without Cdc4 indicated that Sic1 bound to NiNTA resins nonspecifically. In an attempt to solve this issue, a smaller size of column (Qiagen31014) and a greater number of washing steps were tried. The unspecific binding was still significant. Thus, we decided to take attempt a different approach and instead of using NiNTA column used glutathione columns.

Glutathione Column to Immobilize Gst-Cdc4 for Pulling Down His-Sic1. To switch to glutathione for the immobilization step, we had to use a Gst-tagged Cdc4 protein and a His-tagged Sic1. We phosphorylated His-tagged Sic1 and immobilized Gst-Cdc4 on glutathione-sepharose column (Pierce 21516). A similar procedure as the one described above was repeated. This time the setup worked and a significant difference was observed between the phosphorylated and unphosphorylated samples, but the sensitivity of method was low. Thus, we decided to attempt a more sensitive detection method based on ELISA instead of Western Blot.

Glutathione Coated Plate to Immobilize Gst-Cdc4 for Collecting His-Sic1. We used 96-well pre-coated glutathione plates (Pierce 15140). Glutathione is immobilized on the plate through its central sulfhydryl, and we used an ELISA based detection strategy. In principle, Cdc4 binds to glutathione, and phosphorylated Sic1 binds to the Cdc4 protein. An HRP-conjugated Sic1 antibody was used to detect the bound Sic1. A QuantaBlu Fluorogenic Peroxide Substrate kit (Pierce 15169) was used for the detection of peroxidase activity. This method had the main advantage of being high-throughput. However, it was very sensitive to the type of the buffer used for the protein storage and washing steps. Moreover, the Sic1 antibody showed a very high level of unspecific binding to the wells. Cdc4 showed no effect on the Sic1-His signal; either because it did not bind to Sic1 or its effect was overshadowed by the nonspecific binding of the antibody. Thereby, we returned to the conventional method based on batch assays and Western Blotting.

Glutathione Sepharose Beads to Immobilize Gst-Cdc4 for Collecting His-Sic1. Glutathione sepharose 4B (GE Healthcare) was used for immobilizing Gst-fused Cdc4. Most of the Cdc4 appeared in unbound form and were washed before reaching the elution step. The measurement of Cdc4 in the elution buffer indicated that very little Gst-fused Cdc4 was bound to the glutathione beads and therefore the result was not quantitative enough. We did not pursue this method further and instead we decided to use a Flag tagged version of Cdc4. This approach worked and is described in Chapter 3.

APPENDIX C

Sic1 Calibration

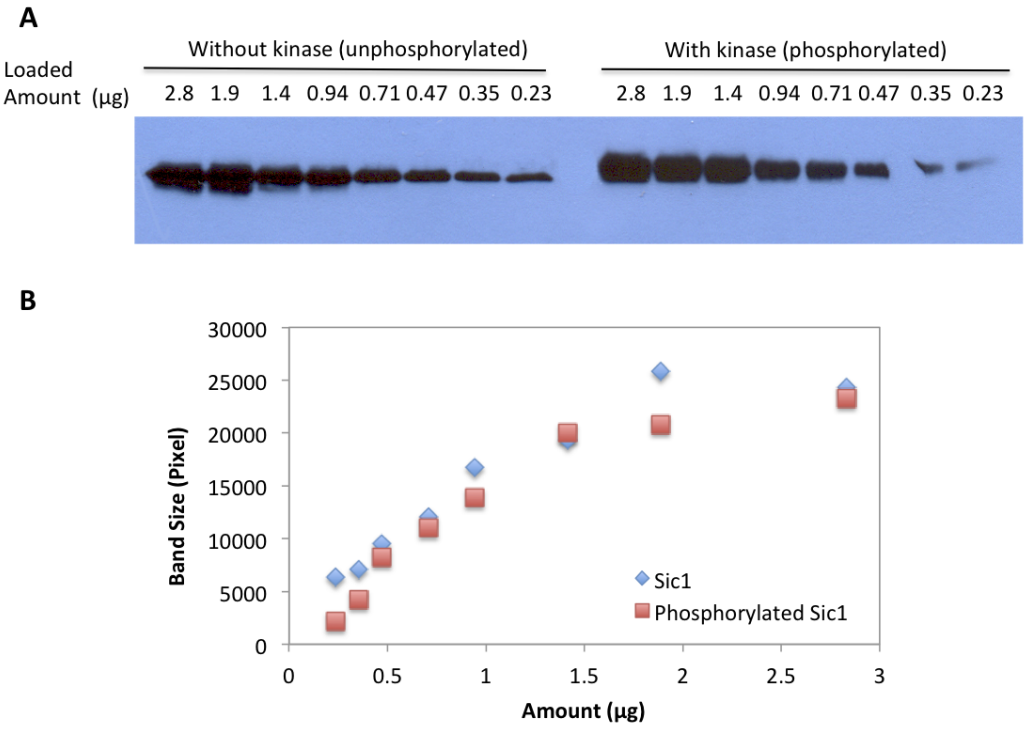

Figure C.1: Different amounts of 6x-His-Sic1, in two forms of incubation (with/without the Cln2-Cdc28 kinase), were loaded into 12.5% SDS-polyacrylamide gel (Bio-rad) and immunoblotted against the C-terminus Sic1 antibody (A). The band sizes were quantified using ImageJ and plotted against the loaded amount (B). The analysis of the graph indicates that the samples loaded with less than about 1 μg are proportionally correlated to their blot size.

Bibliography

[1] Goldbeter A, Koshland DE (1981) An amplified sensitivity arising from covalent modification in biological systems. Proc Natl Acad Sci U S A 78: 6840-1981.

[2] Olson JS, Gibson QH, Nagel RL, Hamilton HB (1972) The ligand-binding properties of hemoglobin Hiroshima. J Biol Chem 247(23): 7485-7493.

[3] Hill A (1910) The possible effects of the aggregation of the molecule of haemoglobin on its dissociation curves. J Physiol 40: iv-vii.

[4] Goodey NM, Benkovic SJ (2008) Allosteric regulation and catalysis emerge via a common route. Nat Chem Biol 4(8): 474-482.

[5] Meinke MH, Bishop JS, Edstrom RD (1986) Zero-order ultrasensitivity in the regulation of glycogen phosphorylase. Proc Natl Acad Sci U S A 83(9): 2865-2868.

[6] Becskei A, Seraphin B, Serrano L (2001) Positive feedback in eukaryotic gene networks: cell differentiation by graded to binary response conversion. EMBO J 20(10): 2528-2535.

[7] Kim SY, Ferrell JE Jr (2007) Substrate competition as a source of ultrasensitivity in the inactivation of Wee1. Cell 128(6): 1133-1145.

[8] Chock PB, Stadtman ER (1977) Superiority of interconvertible enzyme cascades in metabolic regulation: Analysis of multicyclic systems. Proc Natl Acad Sci U S A 74(7): 2766-2770.

[9] Ferrell JE Jr (1996) Tripping the switch fantastic: how a protein kinase cascade can convert graded inputs into switch-like outputs. Trends Biochem Sci 21: 460.

[10] Brown GC, Hoek JB, Kholodenko BN (1997) Why do protein kinase cascades have more than one level. Trends Biochem Sci 22(8): 288.

[11] Goldbeter A, Koshland DE (1984) Ultrasensitivity in biochemical systems controlled by covalent modification. Interplay between zero-order and multistep effects. J Biol Chem 259(23): 14441-14447.

[12] Huang CYF, Ferrell JE Jr (1996) Ultrasensitivity in the mitogen-activated protein kinase cascade. Proc Natl Acad Sci U S A 93: 10078-10083.

[13] Ferrell JE Jr, Bhatt RR (1997) Mechanistic studies of the dual phosphorylation of mitogenactivated protein kinase. J Biol Chem 272(30): 19008-19016.

[14] Ferrell JE Jr, Machleder EM (1998) The biochemical basis of an all-or-none cell fate switch in *Xenopus oocytes*. Science 280(5365): 895-898.

[15] Verma R, Annan RS, Huddleston MJ, Carr SA, Reynard G, et al. (1997) Phosphorylation of Sic1p by G1 Cdk required for its degradation and entry into S phase. Science 278(5337): 455-460.

[16] Verma R, Feldman RM, Deshaies RJ (1997) SIC1 is ubiquitinated *in vitro* by a pathway that requires CDC4, CDC34, and cyclin/CDK activities. Mol Biol Cell 8(8): 1427-1437.

[17] Nash P, Tang X, Orlicky S, Chen Q, et al (2001) Multi-site phosphorylation of a CDK inhibitor sets a threshold for the onset of DNA replication. Nature 414 (29): 514-521.

[18] Schwob E, Bohm T, Mendenhall MD, Nasmyth K (1994) The B-type cyclin kinase inhibitor p40-SIC1 controls the G1 to S transition in *S. cerevisiae*. Cell 79(2): 233-244.

[19] Schneider BL, Yang QH, Futcher AB (1996) Linkage of replication to start by the Cdk inhibitor Sic1. Science 272: 560-562.

[20] Deshaies RJ, Ferrell JE Jr (2001) Multisite Phosphorylation and the Countdown to S Phase. Cell 107(28): 819-822.

[21] Welcker M, Singer J, Loeb KR, Grim J, Bloecher A, et al. (2003) Multisite phosphorylation by Cdk2 and GSK3 controls cyclin E degradation. Mol Cell 12(2): 381-392.

[22] Salazar C, Hofer T (2003) Allosteric regulation of the transcription factor NFAT1 by multiple phosphorylation sites: a mathematical analysis. J Mol Biol 327(1): 31-45.

[23] Gunawardena J (2005) Multi-site protein phosphorylation makes a good threshold but can be a poor switch. Proc Natl Acad Sci U S A 102 (41): 14617-14622.

[24] Lin X, Gao Y, Shi Y, Church GM. Achieving ultrasensitivity through single protein multisite modification. In revision (2011).

[25] Vlach J, Hennecke S, Amati B (1997) Phosphorylation-dependent degradation of the cyclin-dependent kinase inhibitor $p27^{Kip1}$. EMBO J 16(17): 5334-5344.

[26] Tsvetkov LM, Yeh KH, Lee SJ, Sun H, Zhang H (1999) $p27^{Kip1}$ ubiquitination and degradation is regulated by the SCF^{Skp2} complex through phosphorylated Thr187 in p27. Curr Biol 9(2):661-664.

[27] Barberis M, De Gioia L, Ruzzene M, Sarno S, Coccetti P, et al. (2005) The yeast cyclin-dependent kinase inhibitor Sic1 and mammalian $p27^{Kip1}$ are functional homologues with a structurally conserved inhibitory domain. Biochem J 387: 639-647.

[28] Vermeulen K, Van Bockstaele DR, Berneman ZN (2003) The cell cycle: a review of regulation, deregulation and therapeutic targets in cancer. Cell Prolif 36: 131-149.

[29] Chu I, Arnaout A, Kahn H, Hanna W, Narod S, et al (2007) p27 Phosphorylation by Src regulates inhibition of cyclin E-Cdk2. Cell 128: 281-294.

[30] Moore DD, Sefton BM, Shaw RJ, Turk BE (2010) Analysis of Protein Phosphorylation. Current Protocols in Molecular Biology 92:18.0.1-18.0.3.

[31] Campbell DG, Morrice NA (2002) Identification of protein phosphorylation sites by a combination of mass spectrometry and solid phase Edman sequencing. J Biomol Tech 13(3): 119-130.

[32] Czernik AJ, Girault JA, Nairn AC, Chen J, Snyder G, et al. (1991) Production of phosphorylation state-specific antibodies. Methods Enzymol 201: 264-283.

[33] Ballif RA, Roux PP, Gerber SA, MacKeigan JP, Blenis J, Gygi SP (2005) Quantitative phosphorylation profiling of the ERK/p90 ribosomal S6 kinase-signaling cassette and its targets, the tuberous sclerosis tumor suppressors. Proc Natl Acad Sci U S A 112(3): 667-672.

[34] Zappacosta F, Collingwood TS, Huddleston MJ, Annan RS (2006) A quantitative results-driven approach to analyzing multisite protein phosphorylation. Mol Cell Proteom 5: 2019-2030.

[35] Zhang X, Jin QK, Carr SA, Annan RS (2002) N-terminal peptide labeling strategy for incorporation of isotopic tags: a method for the determination of site-specific absolute phosphorylation stoichiometry. Rapid Commun Mass Sp 16: 2315-2332.

[36] Hegeman AD, Harms AC, Sussman MR, Bunner AE, Harper JF (2004) An isotope labeling strategy for quantifying the degree of phosphorylation at multiple sites in proteins. J Am Soc Mass Spec 15: 647-653.

[37] Olsen JV, Blagoev B, Gnad F, Macek B, Kumar C, et al. (2006) Global, *in vivo*, and site-specific phosphorylation dynamics in signaling networks. Cell 127: 635-648.

[38] Steen H, Jebanathirajah JA, Springer M, Krischner MW (2005) Stable isotope-free relative and absolute quantitation of protein phosphorylation stoichiometry by MS. Proc Natl Acad Sci U S A 102: 3948-3953.

[39] Gardner TS, Cantor CR, Collins JJ (2000) Construction of a genetic toggle switch in Escherichia coli. Nature 403(6767): 339-342.

[40] Elowitz MB, Leibler S (2000) A synthetic oscillatory network of transcriptional regulators. Nature 403: 335-338.

[41] Atkinson MR, Savageau MA, Myers JT, Ninfa AJ (2003) Development of genetic circuitry exhibiting toggle switch or oscillatory behavior in *Escherichia coli*. Cell 113(5): 597-607.

[42] Grunberg R, Ferrar TS, van der Sloot AM, Constante M, Serrano L (2010) Building blocks for protein interaction devices. Nucleic Acids Res 38(8): 2645-2662.

[43] Golynskiy MV, Koay MS, Vinkenborg JL, Merkx M (2011) Engineering protein switches: sensors, regulators, and spare parts for biology and biotechnology. Chembiochem 12(3): 353-3561.

[44] Ostermeier M (2009) Designing switchable enzymes. Curr Opin Struct Biol 19(4): 442-448.

[45] Koide S (2009) Generation of new protein functions by nonhomologous combinations and rearrangements of domains and modules. Curr Opin Biotechnol 20(4): 398-404.

[46] Pawson T, Nash P (2003) Assembly of cell regulatory systems through protein interaction domains. Science 300: 445-452.

[47] Grunberg R, Serrano L (2010) Strategies for protein synthetic biology. Nucleic Acids Res 38(8): 2663-2675.

[48] Lim WA (2002) The modular logic of signaling proteins: building allosteric switches from simple binding domains. Curr Opin Struct Biol 12(1): 61-68.

[49] Dueber JE, Yeh BJ, Chak K, Lim WA (2003) Reprogramming control of an allosteric signaling switch through modular recombination. Science 301(5641): 1904-1908.

[50] Dueber JE, Wu GC, Malmirchegini GR, Moon TS, Petzold CJ, et al. (2009) Synthetic protein scaffolds provide modular control over metabolic flux. Nat Biotechnol 27(8): 753-759.

[51] Robinson CR, Sauer RT (1998) Optimizing the stability of single-chain proteins by linker length and composition mutagenesis. Proc Natl Acad Sci U S A 95(11): 5929-5934.

[52] Lorenz MC, Heitman J (1995) TOR mutations confer rapamycin resistance by preventing interaction with FKBP12-rapamycin. J Biol Chem 270(46): 27531-27537.

[53] Banaszynski LA, Chen LC, Maynard-Smith LA, Ooi AG, Wandless TJ (2006) A rapid, reversible, and tunable method to regulate protein function in living cells using synthetic small molecules. Cell 126: 995-1004.

[54] Iwamoto M, Bjorklund T, Lundberg C, Kirik D, Wandless TJ (2010) A general chemical method to regulate protein stability in the mammalian central nervous system. Chem Biol 17(9): 981-988.

[55] Stankunas K, Crabtree GR (2007) Exploiting protein destruction for constructive use. Proc Natl Acad Sci U S A 104(28):11511-11512.

[56] Janse DM, Crosas B, Finley D, Church GM (2004) Localization to the proteasome is sufficient for degradation. J Biol Chem 279(20): 21415-21420.

[57] Dueber JE, Mirsky EA, Lim WA (2007) Engineering synthetic signaling proteins with ultrasensitive input/output control. Nat Biotechnol 25(6): 660-662.

[58] Cohen P (2000) The regulation of protein function by multisite phosphorylation - a 25 year update. TIBS 25: 596-600.

[59] Patwardhan P, Miller WT (2007) Processive phosphorylation: Mechanism and biological importance. Cell Signal 19: 2218-2226.

[60] Skowyra D, Craig KL, Tyers M, Elledge SJ, Harper JW (1997) F-box proteins are receptors that recruit phosphorylated substrates to the SCF ubiquitin-ligase complex. Cell 91: 209-219.

[61] Patton EE, Willems AR, Tyers M (1998) Combinatorial control in ubiquitin-dependent proteolysis: don't Skp the F-box hypothesis. TIG 14(6): 236-243.

[62] Deshaies RJ (1997) Phosphoryation and proteolysis: partners in the regulation of cell division in budding yeast. Curr Opin Genetics Dev 7: 7-16.

[63] Ang XL, Harper JW (2005) SCF-mediated protein degradation and cell cycle control. Oncogene 24: 2860-2870.

[64] Hunter T (2007) The age of crosstalk: phosphorylation, ubiquitination, and beyond. Mol Cell 28: 730-738.

[65] Roach PJ (1991) Multisite and hierarchal protein phosphorylation. J Biol Chem 266 (22): 14139-14142.

[66] Buchkovich K, Duffy LA, Harlow E (1989) The retinoblastoma protein is phosphorylated during specific phases of the cell cycle. Cell 58:1097-1105.

[67] Knudsen ES, Wang JY (1996) Differential regulation of retinoblastoma protein function by specific Cdk phosphorylation sites. J Biol Chem 271(14): 8313-8320.

[68] Ezhevsky SA, Ho A, Becker-Hapak M, Davis PK, Dowdy SF (2001) Differential regulation of retinoblastoma tumor suppressor protein by G1 cyclin-dependent kinase complexes in vivo. Mol Cell Biol 21(14): 4773-4784.

[69] Kim SY, Song EJ, Lee KJ, Ferrell JE Jr (2005) Multisite M-phase phosphorylation of Xenopus Wee1A. Mol Cell Biol 25(23): 10580-10590.

[70] Nugroho TT, Mendenhall MD (1994) An inhibitor of yeast cyclin-dependent protein kinase plays an important role in ensuring the genomic integrity of daughter cells. Mol Cell Bio 14: 3320-3228.

[71] Lengronne A, Schwob E (2002) The yeast CDK inhibitor Sic1 prevents genomic instability by promoting replication origin licensing in late G1. Mol Cell 9: 1067-1078.

[72] Cross FR, Schroeder L, Bean JM (2007) Phosphorylation of the Sic1 inhibitor of B-type cyclins in *Saccharomyces cerevisiae* is not essential but contributes to cell cycle robustness. Genetics 176: 1541-1555.

[73] Klein P, Pawson T, Tyers M (2003) Mathematical modeling suggests cooperative interactions between a disordered polyvalent ligand and a single receptor site. Curr Biol 13:1669-1678.

[74] Borg M, Mittag T, Pawson T, Tyers M, Forman-Kay JD, et al. (2007) Polyelectrostatic interactions of disordered ligands suggest a physical basis for ultrasensitivity. Proc Natl Acad Sci U S A 104: 9650-9655.

[75] Mittag T, Orlicky S, Choy WY, Tang X, Lin H, et al. (2008) Dynamic equilibrium engagement of a polyvalent ligand with a single-site receptor. Proc Natl Acad Sci U S A 105: 17772-17777.

[76] Mittag T, Marsh J, Grishaev A, Orlicky S, Lin H, et al. (2010) Structure/function implications in a dynamic complex of the intrinsically disordered Sic1 with the Cdc4 subunit of an SCF ubiquitin ligase. Structure 18: 494-506.

[77] Koshland DE, Goldbeter A, Stock JB (1982) Amplification and adaptation in regulatory and sensory systems. Science 217: 220-225.

[78] Qian H, Cooper JA (2008) Temporal cooperativity and sensitivity amplification in biological signal transduction. Biochemistry 47: 2211-2220.

[79] Thron CD (1997) Bistable biochemical switching and the control of the events of the cell cycle. Oncogene 15: 317-325.

[80] Bhalla US, Iyengar R (1999) Emergent properties of networks of biological signaling pathways. Science 283: 381-387.

[81] Ferrell JE Jr, Xiong W (2001) Bistability in cell signaling: How to make continuous processes discontinuous, and reversible processes irreversible. Chaos 11: 227-236.

[82] Xiong W, Ferrell JE Jr (2003) A positive-feedback-based bistable 'memory module' that governs a cell fate decision. Nature 426: 460-465.

[83] Hooshangi S, Thiberge S, Weiss R (2005) Ultrasensitivity and noise propagation in a synthetic transcriptional cascade. Proc Natl Acad Sci U S A 102: 3581-3586.

[84] Salazar C, Hofer T (2007) Versatile regulation of multisite protein phosphorylation by the order of phosphate processing and protein-protein interactions. FEBS J 274: 1046-1061.

[85] Krishnamurthy S, Smith E, Krakauer D, Fontana W (2007) The stochastic behavior of a molecular switching circuit with feedback. Biology Direct 2:13-30.

[86] Liu X, Bardwell L, Nie Q (2010) A combination of multisite phosphorylation and substrate sequestration produces switchlike responses. Biophys J 98(8):1396-407.

[87] Chen KC, Csikasz-Nagy A, Gyorffy B, Val J, Novak B, et al. (2000) Kinetic analysis of a molecular model of the budding yeast cell cycle. Mol Biol Cell 11: 369-391.

[88] Cross FR, Archambault V, Miller M, Klovstad M (2002) Testing a mathematical model of the yeast cell cycle. Mol Biol Cell 13: 52-70.

[89] Chen KC, Galzone L, Csikasz-Nagy A, Cross FR, Novak B, Tyson JJ (2004) Integrative analysis of cell cycle control in budding yeast . Mol Biol Cell 15: 3841-3862.

[90] Barberis M, Klipp E, Vanoni M, Alberghina L (2007) Cell size at S phase initiation: an emergent property of the G1/S network. PLOS Comp Biol 3(4): e64.

[91] Liu C, Li Y, Semenov M, Han C, et al (2002) Control of β-catenin phosphorylation/degradation by a dual-kinase mechanism. Cell 108(6): 837-847.

[92] Jeffery DA, Springer M, King DS, OShea EK (2001) multisite phosphorylation of Pho4 by the cyclin-CDK Pho80-Pho85 is semi-processive with site preference. J Mol Biol 306: 997-1010.

[93] Bean JM, Siggia ED, Cross FR (2006) Coherence and timing of cell cycle start examination at single cell resolution. Mol Cell 21: 3-14.

[94] Pierce NW, Kleiger G, Shan SO, Deshaies RJ (2009) Detection of sequential polyubiquitylation on a millisecond timescale. Nature 462(7273): 615-619.

[95] Marino S, Hogue IB, Ray CJ, Kirschner DE (2008) A methodology for performing global uncertainty and sensitivity analysis in systems biology. J Theor Biol 254(1): 178-196.

[96] Markevich NI, Hoek JB, Kholodenko BN (2004) Signaling Switches and Bistability Arising from Multisite Phosphorylation in Protein Kinase Cascades. JCB 164(3): 353-359.

[97] Benito J, Martn-Castellanos C, Moreno S (1998) Regulation of the G1 phase of the cell cycle by periodic stabilization and degradation of the p25rum1 CDK inhibitor. EMBO J 17(2): 482-497.

[98] Wang S, Zhang Y, Soosairajah J, Kraft AS (2007) Regulation of RUNX1/AML1 during the G2/M transition. Leuk Res 31(6): 839-851.

[99] Bao MZ, Shock TR, Madhani HD (2010) Multisite phosphorylation of the *S. cerevisiae* filamentous growth regulator Tec1 is required for its recognition by the E3 ubiquitin ligase adaptor Cdc4 and its subsequent destruction *in vivo*. Eukaryot Cell 9(1): 31-36.

[100] Park HJ, Ding L, Dai M, Lin R, Wang H (2008) Multisite phosphorylation of *Arabidopsis* HFR1 by casein kinase II and a plausible role in regulating its degradation rate. J Biol Chem 283(34): 23264-23273.

[101] Nishizawa M, Kawasumi M, Fujino M, Toh-e A (1998) Phosphorylation of Sic1, a cyclin-dependnet kinase (Cdk) inhibitor, by Cdk including Pho85 kinase is required for its prompt degradation. Mol Biol Cell 9: 2393-2405.

[102] Wysocki R, Javaheri A, Kristjansdottir K, Sha F, Kron SJ (2006) CDK Pho85 tergets CDK inhibitor Sic1 to relieve yeast G1 checkpoint arrest after DNA damage. Nature Struct & Mol Biol 13(10): 908-914.

[103] Coccetti P, Zinzalla V, Tedeschi G, Russo GL, Fantinato S ,et al (2006) Sic1 is phosphorylated by CK2 on Ser201 in budding yeast cells. Biochem Biophys Res Commun 346: 786-93.

[104] Sedgwick C, Rawluk M, Decesare J, Raithatha S, Wohlschlegel J, et al (2006) Saccharomyces cerevisiae Ime2 phosphorylates Sic1 at multiple PXS/T sites but is insufficient to trigger Sic1 degradation. Biochem J 399: 151-160.

[105] Escote X, Zapater M, Clotet J, Posas F (2004) Hog1 mediates cell-cycle arrest in G1 phase by the dual targeting of Sic1. Nature Cell Biotech 6(10): 997-1002.

[106] Elsasser S, Chi Y, Yang P, Campbell JL (1999) Phosphorylation controls timing of Cdc6p destruction: A biochemical analysis. Mol Biol Cell 10(10): 3263-3277.

[107] Lanker S, Valdivieso MH, Wittenberg C (1996) Rapid Degradation of the G1 Cyclin Cln2 Induced by CDK-Dependent Phosphorylation. Science 271(5255): 1597-1601.

[108] Jallepalli PV, Brown GW, Muzi-Falconi M, Tien D, Kelly TJ (1997) Regulation of the replication initiator protein $p65^{cdc18}$ by CDK phosphorylation. Genes Dev 11(21): 2767-2779.

[109] Hao B, Oehlmann S, Sowa ME, Harper JW, Pavletich NP (2007) Structure of a Fbw7-Skp1-Cyclin E complex: Multisite-phosphorylated substrate recognition by SCF ubiquitin ligases. Mol Cell 26: 131-143.

[110] Jin J, Shirogane T, Xu L, Nalepa G, et al (2003) $SCF^{\beta-TRCP}$ links Chk1 signaling to degradation of the Cdc25A protein phosphatase. Genes Dev 17(24): 3062-3074.

[111] Hansen DV, Loktev AV, Ban KH, Jackson PK (2004) Plk1 regulates activation of the anaphase promoting complex by phosphorylating and triggering $SCF^{\beta TrCP}$-dependent destruction of the APC Inhibitor Emi1. Mol Biol Cell 15(12): 5623-5634.

[112] Chi Y, Huddleston MJ, Zhang X, Young RA, et al (2001) Negative regulation of Gcn4 and Msn2 transcription factors by Srb10 cyclin-dependent kinase. Genes Dev 15(9): 1045-1050.

[113] Hübner A, Barrett T, Flavell RA, Davis RJ (2008) Multisite phosphorylation regulates Bim stability and apoptotic activity. Mol Cell 30(4): 415-425.

[114] Weinreich M, Liang C, Chen HH, Stillman B (2001) Binding of cyclin-dependent kinases to ORC and Cdc6p regulates the chromosome replication cycle. Proc Natl Acad Sci U S A 98(20): 11211-11217.

[115] Orlando DA, Lin CY, Bernard A, et al (2008) Global control of cell-cycle transcription by coupled CDK and network oscillators. Nature 453: 944-947.

[116] Hodge A, Mendenhall M (1999) The cyclin-dependent kinase inhibitory domain of the yeast Sic1 protein is contained within the C-terminal 70 amino acids. Mol Gen Genet 262(1): 55-64.

[117] Brocca S, Testa L, Samalikova M, Grandori R, Lotti M (2011) Defining structural domains of an intrinsically disordered protein: Sic1, the cyclin-dependent kinase inhibitor of *Saccharomyces cerevisiae*. Mol Biotechnol 47(1): 34-42.

[118] Orlicky S, Tang X, Willems A, Tyers M, Sicheri F.(2003) Structural basis for phosphodependent substrate selection and orientation by the SCF^{Cdc4} ubiquitin ligase. Cell 12(2): 243-256.

[119] Salazar C, Brummer a, Alberghina L, Thomas Hofer (2010) Timing control in regulatory networks by multisite protein modifications. Trends Cell Biol 20(11): 634-641.

[120] Petroski MD, Deshaies RJ (2005) *In vitro* reconstitution of SCF substrate ubiquitination with purified proteins. Methods Enzymol 398: 143-158.

[121] Visintin R, Craig K, Hwang ES, Prinz S, Tyers M, Amon A (1998) The phosphatase Cdc14 triggers mitotic exit by reversal of Cdk-dependent phosphorylation. Mol Cell 2(6): 709-718.

[122] Wasch R and Cross FR (2002) APC-dependent proteolysis of the mitotic cyclin Clb2 is essential for mitotic exit. Nature 418(6897): 556-562.

[123] Trunnell NB, Poon AC, Kim SY, Ferrell JE Jr (2011) Ultrasensitivity in the Regulation of Cdc25C by Cdk1. Mol Cell 41(3): 263-274.

[124] Serber Z, Ferrell JE Jr (2007) Tuning bulk electrostatics to regulate protein function. Cell 128(3): 441-444.

[125] Verma R, McDonald H, Yates JR 3rd, Deshaies RJ (2001) Selective degradation of ubiquitinated Sic1 by purified 26S proteasome yields active S phase cyclin-Cdk. Mol Cell 8(2): 439-448.

[126] Coccetti P, Rossi RL, Sternieri F, Porro D, Russo GL, et al. (2004) Mutations of the CK2 phosphorylation site of Sic1 affect cell size and S-Cdk kinase activity in *Saccharomyces cerevisiae*. Mol Microbiol 51(2): 447-460.

[127] Barberis M, Pagano MA, Gioia LD, Marin O, Vanoni M, et al. (2005) CK2 regulates in vitro the activity of the yeast cyclin-dependent kinase inhibitor Sic1. Biochem Biophys Res Commun 336(4): 1040-1448.

[128] Goldbeter A (1996) Biochemical oscillations and cellular rhythms: The molecular bases of periodic and chaotic behaviour. Cambridge University Press, Cambridge.

[129] Novak L, Tyson JJ (2008) Design principles of biochemical oscillators. Nature Rev 9: 981-991.

[130] Termonia Y, Ross J (1981) Oscillations and control features in glycolysis: numerical analysis of a comprehensive model. Proc Natl Acad Sci U S A 78(5): 2952-2956.

[131] Bier M, Teusink B, Kholodenko BN, Westerhoff HV (1996) Control analysis of glycolytic oscillations. Biophys Chem 62: 15-24.

[132] Nielsen K, Sorensen PG, Hynne F, Busse HG (1998) Sustained oscillations in glycolysis: an experimental and theoretical study of chaotic and complex periodic behavior and of quenching of simple oscillations. Biophys Chem 72: 49-62.

[133] Gonze D, Goldbeter A (2000) A model for a network of phosphorylation-dephosphorylation cycles displaying the dynamics of dominoes and clocks. J Theor Biol 210: 167-186.

[134] Tyson JJ, Csikasz-Nagy A, Novak B (2002) The dynamics of cell cycle regulation. Bioessays 24(12): 1095-1109.

[135] Csikasz-Nagy A, Battogtokh D, Chen KC, Novak B, Tyson JJ (2006) Analysis of a generic model of eukaryotic cell-cycle regulation. Biophys J 90(12): 4361-4379.

[136] Dunlap JC (1999) Molecular bases for circadian clocks. Cell 96: 271-290.

[137] Tyson JJ, Othmer HG (1978) The Dynamics of Feedback Control Circuits in Biochemical Pathways. In R Rosen and F M Snell (Eds.): Progress in Theoretical Biology, 5, 1. New York: Academic Press.

[138] Goldbeter A (2002) Computational approaches to cellular rhythms. Nature 420: 238-245.

[139] Roenneberg T, Chua E, Bernardo R, Mendoza E (2008) Modelling biological rhythms. Curr Biol 18(17): R826-R835.

[140] Aguda BD (1999) Instabilities in phosphorylation-dephosphorylation cascades and cell cycle checkpoints. Oncogene 18: 2846-2851.

[141] Kholodenko BN (2000) Negative feedback and ultrasensitivity can bring about oscillations in the mitogen-activated protein kinase cascades. Eur J Biochem 267(6): 1583-1588.

[142] Wang X, Hao N, Dohlman HG, Elston TC (2006) Bistability, stochasticity, and oscillations in the mitogen-activated protein kinase cascade. Biophys J 90: 1961-1978.

[143] Fung E, Wong WW, Suen JK, Bulter T, Lee SG, Liao JC (2005) A synthetic genemetabolic oscillator. Nature 435: 118-122.

[144] Stricker J, Cookson S, Bennett MR, Mather WH, Tsimring LS, Hasty J (2008) A fast, robust and tunable synthetic gene oscillator. Nature 456: 516-519.

[145] Tigges M, Marquez-Lago TT, Stelling J, Fussenegger M (2009) A tunable synthetic mammalian oscillator. Nature 15: 309-312.

[146] Kholodenko BN (2006) Cell-signalling dynamics in time and space. Nat Rev Mol Cell Biol 7(3): 165-176.

[147] Tsai TY, Choi YS, Ma W, Pomerening JR, Tang C, Ferrell JE Jr (2008) Robust, tunable biological oscillations from interlinked positive and negative feedback loops. Science 321(5885): 126-129.

[148] Iwasaki H, Nishiwaki T, Kitayama Y, Nakajima M, Kondo T (2002) KaiA-stimulated KaiC phosphorylation in circadian timing loops in cyanobacteria. Proc Natl Acad Sci U S A 99(24): 15788-15793.

[149] Tomita J, Nakajima M, Kondo T, Iwasaki H (2005) No Transcription-Translation Feedback in Circadian Rhythm of KaiC Phosphorylation. Science 307: 251-254.

[150] Nakajima M, Imai K, Ito H, Nishiwaki T, Murayama Y, Iwasaki H, Oyama T, Kondo T (2005) Reconstitution of circadian oscillation of cyanobacterial KaiC phosphorylation *in vitro*. Science 308: 414-415.

[151] Rust MJ, Markson JS, Lane WS, Fisher DS, O'Shea EK (2007) Ordered phosphorylation governs oscillation of a three-protein circadian clock. Science 318(5851): 809-812.

[152] Chickarmane V, Kholodenko BN, Sauro HM (2007) Oscillatory dynamics arising from competitive inhibition and multisite phosphorylation. J Theor Biol 244: 68-76.

[153] Tang X, Orlicky S, Lin Z, Willems A, Neculai D, et al. (2007) Suprafacial orientation of the SCF^{Cdc4} dimer accommodates multiple geometries for substrate ubiquitination. Cell 129(6): 1165-1176.

[154] Johnson CH, Egli M, Stewart PL (2008) Structural insights into a circadian oscillator. Science 322: 697-701.

[155] Kim YI, Dong G, Carruthers CW, Golden SS, Wang AL (2008) The day/night switch in KaiC, a central oscillator component of the circadian clock of cyanobacteria. Proc Natl Acad Sci U S A 105: 12825-12830.

[156] Roach PJ (1990) Control of glycogen synthase by hierarchal protein phosphorylation. FASEB J 4: 2961-2968.

[157] Chu B, Soncin F, Price BD, Stevenson MA, Calderwood SK (1996) Sequential phosphorylation by mitogen-activated protein kinase and glycogen synthase kinase 3 represses transcriptional activation by heat shock factor-1. JBC 271: 30847-30857.

[158] Sharfi H, Eldar-Finkelman H (2008) Sequential phosphorylation of insulin receptor substrate-2 by glycogen synthase kinase-3 and c-Jun NH2-terminal kinase plays a role in hepatic insulin signaling. Am J Physiol Endocrinol Metab 294: E307-E315.

[159] Morales M, Mckay D (1967) Biochemical oscillations in controlled systems. Biophys J 7(5): 621-625.

[160] Griffith JS (1968) Mathematics of cellular control processes. J Theor Biol 20: 202-208.

[161] Schrader EK, Harstad KG, Matouschek A (2009) Targeting proteins for degradation. Nat Chem Biol 5(11): 815-822.

[162] Prakash S, Inobe T, Hatch AJ, Matouschek A (2009) Substrate selection by the proteasome during degradation of protein complexes. Nat Chem Biol 5: 29 - 36.

[163] Stankunas K, Bayle JH, Gestwicki JE, Lin YM, Wandless TJ, Crabtree GR (2003) Conditional protein alleles using knockin mice and a chemical inducer of dimerization. Mol Cell 12: 1615-1624.

[164] Pratt MR, Schwartz EC, Muir TW (2007) Small-molecule-mediated rescue of protein function by an inducible proteolytic shunt. Proc Natl Acad Sci USA 104: 11209-11214.

[165] Banaszynski LA, Liu CW, Wandless TJ (2005) Characterization of the FKBP.rapamycin.FRB ternary complex. J Am Chem Soc 127(13): 4715-4721.

[166] Heitman J, Movva NR, Hall MN (1991) Targets for cell cycle arrest by the immunosuppressant rapamycin in yeast. Science 253: 905-909.

[167] Winston F, Dollard C, Ricupero-Hovasse SL (1995) Construction of a set of convenient *Saccharomyces cerevisiae* strains that are isogenic to S288C. Yeast 11: 53-55.

[168] Cafferkey R, Young PR, McLaughlin MM, Bergsma DJ, Koltin Y, et al. (1993) Dominant missense mutations in a novel yeast protein related to mammalian phosphatidylinositol 3-kinase and VPS34 abrogate rapamycin cytotoxicity. Mol Cell Biol 13(10): 6012-6023.

[169] Helliwell SB, Wagner P, Kunz J, Deuter-Reinhard M, Henriquez R, Hall MN (1994) TOR1 and TOR2 are structurally and functionally similar but not identical phosphatidylinositol kinase homologues in yeast. Mol Biol Cell 5(1): 105-118.

[170] Umezu K, Amaya T, Yoshimoto A, Tomita K (1971) Purification and properties of orotidine-5'-phosphate pyrophosphorylase and orotidine-5'-phosphate decarboxylase from baker's yeast. J Biochem 70(2): 249-262.

[171] Jones ME (1992) Orotidylate decarboxylase of yeast and man. Curr Top Cell Regul 33: 331-342.

[172] Choi J, Chen J, Schreiber SL, Clardy J (1996) Structure of the FKBP12-rapamycin complex interacting with the binding domain of human FRAP. Science 273(5272): 239-242.

[173] Van der Sloot AM, Kiel C, Serrano L, Stricher F (2009) Protein design in biological networks: from manipulating the input to modifying the output. PEDS 22(9): 537-542.

[174] Bjellqvist B, Hughes GJ, Pasquali C, Panquet N, et al. (1993) The focusing positions of polypeptides in immobilized pH gradients cab be predicted from their amino acid sequences. Electrophoresis 14: 1023-1013.